Title
AN EXPERIMENTAL INVESTIGATION OF THE STATE OP A HIGHLY IONIZED DECAYING HYDROGEN PLASMA

Author
Cooper, William Samuel

Publication Date
1963-06-17

UCRL-10849

University of California

Ernest O. Lawrence Radiation Laboratory

AN EXPERIMENTAL INVESTIGATION OF THE STATE OF A HIGHLY IONIZED DECAYING HYDROGEN PLASMA

DISCLAIMER

UCRL-10849
UC-20 Controlled
Thermonuclear Processes
TID-4500 (19th Ed.)

UNIVERSITY OF CALIFORNIA

Lawrence Radiation Laboratory
Berkeley, California

Contract No. W-7405-eng-48

AN EXPERIMENTAL INVESTIGATION OF THE STATE OF A HIGHLY IONIZED DECAYING HYDROGEN PLASMA

William Samuel Cooper III
(Ph. D. Thesis)

June 17, 1963

Printed in USA. Price $2.50. Available from the
Office of Technical Services
U. S. Department of Commerce
Washington 25, D.C.

AN EXPERIMENTAL INVESTIGATION OF THE STATE OF A HIGHLY IONIZED DECAYING HYDROGEN PLASMA

Contents

AN EXPERIMENTAL INVESTIGATION OF THE STATE OF A HIGHLY IONIZED DECAYING HYDROGEN PLASMA

William Samuel Copper III

Lawrence Radiation Laboratory
University of California
Berkeley, California

June 14, 1963

ABSTRACT

The atomic processes governing the decay of an initially highly ionized, dense, recombining hydrogen plasma are discussed qualitatively. The dominant process is three-body recombination. We show that the upper excited states of neutral hydrogen atoms in such a recombining plasma are essentially in equilibrium with the free electrons, and estimate the lowest excited state for which this is true. We derive the theory necessary for determination of the plasma properties (electron density and temperature) from a spectroscopic analysis of the emitted radiation in the visible and ultraviolet regions of the spectrum.

We give experimental details of the formation of a highly ionized hydrogen plasma in a strong magnetic field by a hydromagnetic ionizing wave. The plasma typically has an electron density of about 3×10^{15} cm^{-3} and a temperature of about 10^4 °K, and is observed to decay in several hundred μsec.

The electron density and temperature in the decaying plasma were measured by the observations of the Stark broadening of the H_β line and by absolute measurements of the intensity of the H_β line and of the intensity of the continuum radiation at two wavelengths, one in the visible region of the spectrum and one in the ultraviolet. A carbon arc was used as a radiation standard. Side-on and end-on observations show that the plasma is probably uniform along magnetic field lines to ±10%, but has a strong radial variation. These measurements and end-on framing camera pictures show conclusively that the plasma is not lost by motion across the magnetic field. The plasma is not lost by motion along the magnetic field either; it decays by volume recombination.

Accurate (approaching ±5%) measurements of the electron density and temperature as a function of time by end-on observations at one radius yield decay rates that agree very well with those calculated by Bates, Kingston, and McWhirter for a plasma opaque to the lines of the Lyman series. Finally, we show that the plasma in most of the volume must initially be nearly completely ionized. The plasma then cools essentially in local thermodynamic equilibrium (LTE) until the temperature drops below about 1.2×10^4 °K. After this, the temperature is too low for detailed balancing to apply in the rates of collisional processes determining the population of the ground state, and the plasma departs in a reasonable way from the LTE cooling curve.

I. INTRODUCTION

This thesis describes the experimental investigation of the rate of decay of an initially highly ionized, dense hydrogen plasma and departures of the state of the plasma from thermodynamic equilibrium. A decaying plasma provides a readily available and easily observable example of a nonequilibrium plasma state; the very fact that the plasma is decaying implies a lack of thermodynamic equilibrium.

One of the first observations of a decaying hydrogen plasma was made by Lord Rayleigh,[1] who in 1944 observed that the Balmer lines in the spectrum of an electrodeless discharge in hydrogen persisted some 10 μsec after the termination of the current pulse. Observations of afterglows in gases other than hydrogen were already plentiful, but will not be discussed in this thesis. Craggs and Meek,[2] who had observed similar afterglows lasting about 3 μsec in spark discharges in hydrogen, and later Zanstra[3] suggested that the afterglow observed by Lord Rayleigh was caused by recombination of electrons and hydrogen ions, accompanied by emission of radiation. It was thought that the recombination was predominantly due to the two-body process

$$H^+ + e \rightarrow H^* + h\nu, \tag{1}$$

and it became customary to describe the recombination rate by a recombination coefficient $\alpha(T_e)$ defined by

$$\frac{dN_i}{dt} = -\alpha(T_e)N_iN_e, \tag{2}$$

where N_i is the density of positive ions in the plasma, N_e is the density of free electrons, and T_e is the electron temperature.

Recombination in plasmas was of considerable interest not only to those working in the field of gaseous discharges, but also to astrophysicists and upper-atmosphere physicists. Using the results of calculations by Chillié,[4] who was interested in the emission spectrum of gaseous nebulae, Zanstra calculated values of α for radiative recombination.[3] Several experiments were performed by Craggs and coworkers in 1946 and 1947 to determine experimental values of α by

observing the decay of the plasma produced by a spark discharge in hydrogen.[5-7] They obtained values of α ranging from 2×10^{-12} to 10^{-11} cm^3 sec^{-1}, with initial ion densities around 3×10^{17} cm^{-3} and electron temperatures estimated to be between 10,000 and 15,000 °K. These values of α were about a factor of 10 larger than those calculated by Zanstra. Experiments reported by Fowler and Atkinson yielded a very rough value for α of 1 to 2×10^{-12} cm^3 sec^{-1}, based on observations of the decay of a hydrogen plasma (ion density $\sim 6 \times 10^{16}$ cm^{-3}, electron temperature ~4500 °K) produced in a "T" shock tube.[8] This value of α was also somewhat higher than the value predicted for radiative recombination.

D'Angelo showed in 1961 that another process, "three-body" recombination could contribute significantly to recombination rates in dense plasmas.[9] This process is simply the inverse of electron collisional ionization, and is described by

$$H^+ + e + e \rightarrow H(n) + e, \qquad (3)$$

where H(n) denotes a hydrogen atom in the nth quantum level. Giovanelli had also considered this process in 1948 in the study of stellar atmospheres,[10] and Craggs and Meek had even suggested it in 1945 as possibly being important in recombination in dense plasmas.[2] Smith had estimated the cross section for the process quantum-mechanically in 1936,[11] and had concluded (erroneously) that three-body recombination would be unimportant in plasmas with ion densities less than about 10^{18} cm^{-3}. If diffusion losses are negligible, three-body recombination is the dominant process in governing the decay of most highly-ionized laboratory plasmas. Although a three-particle process is involved, the problem is sufficiently complicated by the presence of radiative transitions that the recombination rate is not simply proportional to $N_i N_e^2$. It is most convenient to continue to express the recombination rate by an equation of the form of Eq. (2), but to allow α to be a function of the electron density as well as the electron temperature, i.e.,

$$\frac{dN_i}{dt} = -\alpha(N_e, T)N_iN_e . \qquad (4)$$

Several recent works by Bates and Kingston,[12,13] McWhirter,[14] Bates, et al.[15,16] Stubbs, et al.,[17] Byron, et al.[18] and Hinnov and Hirshberg[19] have dealt with theoretical aspects of the problem. In addition, Hinnov and Hirshberg give experimental results for α which agree well with their theory. They used as a source of plasma the H or He discharge of the B-1 Stellarator, which yielded a low-temperature ($T \leq 3{,}000$ °K), low-density ($N_i \leq 5 \times 10^{13}$ cm^{-3}) decaying plasma. Observations of the decay of this plasma by spectroscopic and microwave means gave values of α from 4×10^{-11} to 1.4×10^{-9} cm^3 sec^{-1}, depending on the state of the plasma.

In the study of a recombining plasma, one is led to the question of departures of the plasma from thermodynamic equilibrium. Naturally, the plasma cannot be in complete thermodynamic equilibrium. However, it is not unreasonable to expect that the ion- and electron-velocity distributions may be very nearly Maxwellian at any point in the plasma, especially in dense, relatively cool plasmas, and that the distributions may be characterized by a kinetic electron temperature T_e. Also, frequently the distributions of the various excited states of a given ion and the various ionization states of a given species may be very close to those predicted from equilibrium arguments by Boltzmann's and Saha's equations, respectively, using the kinetic temperature T_e. A system satisfying all these conditions is said to be in local thermodynamic equilibrium (LTE). A plasma may be in LTE even though it is spatially nonuniform and changing in time. A knowledge of the departures of the plasma from LTE is especially necessary in interpreting spectroscopic observations.

A number of authors[20-24] have generalized Saha's equation to include various steady-state nonequilibrium plasma systems. These generally involve solving for steady-state conditions such that the rates of two competing but essentially different processes (such as radiative recombination and electron collisional ionization) balance. In the case of a recombining plasma, the assumption of even

quasi-steady-state conditions is frequently not justified, especially in treating the ground state.

Analysis of non-steady-state, nonequilibrium plasmas is more difficult. McWhirter et al. give theoretical and experimental results pertaining to the closely related nonequilibrium problem of the formation, rather than the decay, of a plasma.[25] They calculate the distribution of excited states at the time of 50% ionization during the formation of a deuterium discharge in Zeta by estimating the rates of all pertinent collisional and radiative processes serving to populate and depopulate the excited states. A strikingly non-Maxwellian distribution of excited states is observed. Similar effects in an rf discharge had been observed by Harrison and Craggs[26] and also recently by Hinnov and Hirshberg.[19] McWhirter,[14] Bates, Kingston, and McWhirter,[15, 16] and Bates and Kingston[13] have applied the same method to the calculation of recombination rates and distribution of excited states in recombining hydrogenic plasmas. The process consists of simply writing down the rate equations of all processes populating and depopulating the excited states and the ground state, using known or assumed cross sections for the various collisional and radiative processes, and solving them simultaneously. The results yield both the recombination rate and the distribution of excited states, with an accuracy determined by the uncertainties in cross sections and calculational approximations.

The present work was begun for several reasons. First, there seemed to be a general lack of precise experimental measurements of the recombination rate of dense hydrogen plasmas ($N_i > 10^{14}$ cm^{-3}), and of the departures of such a system from thermal equilibrium. Both can now be treated reasonably well by existing theories. Second, there was a need to know the properties of the plasma in an experiment already existing in this laboratory. This was the plasma used in the study of Alfvén waves reported previously.[27, 28] The Alfvén waves are induced in a decaying hydrogen plasma. Preliminary studies of this plasma indicated an initial ion density of about 5×10^{15} cm^{-3} and an electron temperature of 10,000 to 20,000 °K, with a decay time of

several hundred μsec.[29] The plasma was of considerable length, 86 cm, and was created in a strong magnetic field -- both factors tending to reduce losses due to diffusion. The experimental apparatus seemed well suited to the study of recombination in a decaying hydrogen plasma. Third, quantitative plasma spectroscopy (reviewed recently by several authors[30-32]) had reached the point where it seemed possible to make time- and space-resolved measurements of ion densities and electron temperatures with accuracies of 5 to 10%. Measurements of the electron temperature, in particular, in a decaying plasma should be as precise and accurate as possible, as the recombination rate for dense plasmas is a strong function of the electron temperature.

For these reasons a careful study of the plasma was begun, using spectroscopic diagnostic techniques. The study was designed to measure as accurately as possible the recombination rate of this hydrogen plasma to observe the spatial variations of the ion density and electron temperature during the decay period, and, if possible, any departures of the state of the plasma from LTE.

II. THEORY

A. Recombination in Highly Ionized Plasmas

1. Qualitative Discussion of the State of a Recombining Plasma

A careful analysis of recombination in plasmas, even hydrogenic ones, is very difficult. (A general review of the subject is given by Bates and Dalgarno.[33]) It is relatively easy, however, to gain a qualitative picture of the recombination. We assume initially a completely ionized hydrogen plasma, populated by ions and electrons with arbitrary energy distributions. We also assume that no particles enter or leave the plasma. The electron-energy distribution very rapidly approaches a Maxwellian. Spitzer[34] derives an expression for the characteristic time in seconds for a group of particles interacting with themselves to approach a Maxwellian energy distribution, starting from an arbitrary distribution, but assumed to have a "temperature" T. This time is

$$t = \frac{11.4A^{1/2}T^{3/2}}{NZ^4 \ell n\Lambda}. \tag{5}$$

Here A is the mass of the particle (1 for hydrogen), T is in °K, N is the number of particles per cubic centimeter, Z is the charge of each particle in electron units, and $\ell n\Lambda$ is a slowly varying function of density and temperature, of the order of 10. Substituting numbers appropriate for electrons into Eq. (5), we get

$$t_e \cong \frac{2\times 10^{-2}T^{3/2}}{N_e}. \tag{6}$$

We see that for any plasma with $T < 10^6$ °K and $N_i > 10^{14}$ cm^{-3}, the relaxation time t_e for the electrons to reach a Maxwellian distribution will be considerably less than 1 μsec. Provided the decay time of the plasma is much longer than this, we may assume the electrons always to have a Maxwellian energy distribution and a temperature T_e. For the plasma investigated in this thesis, assuming $T = 2\times 10^4$ °K

and $N_e = 5 \times 10^{15}$ cm^{-3}, we get $t_e = 10^{-11}$ sec. The observed decay time is much longer, about 10^{-4} sec. We assume a Maxwellian distribution of electron energies and velocities in all further calculations. Although it is not particularly important to the present discussion, we might point out that (again following Spitzer) the time for both the electrons and the ions to reach a common temperature T is about m_i/m_e times t_e, or about 2×10^{-8} sec, again much shorter than the observed decay time.

Provided there are no sources of energy in the plasma, it will begin to cool by radiation. Electrons begin to recombine with ions to form excited neutrals in quantum level n by the following reactions:

$$H^+ + e \rightleftarrows H(n) + h\nu \qquad (7)$$

$$H^+ + e + e \rightleftarrows H(n) + e \, . \qquad (8)$$

The rate of the first process, radiative recombination, is proportional to $N_i N_e$ and decreases with increasing principal quantum number.[20] The rate of the second process, three-body recombination, is proportional to $N_i N_e^2$, and increases rapidly with increasing principal quantum number.[20] Therefore the upper levels of the atom are rapidly filled by three-body recombination in the case of dense plasmas, forming a "reservoir" of electrons in excited states essentially in equilibrium with the continuum of free electrons. Two further processes, spontaneous radiative transitions and transitions between bound states due to electron collisions are also important. These processes correspond to the equations

$$H(n) \rightleftarrows H(p) + h\nu, \text{ and} \qquad (9)$$

$$H(n) + e \rightleftarrows H(p) + e \, . \qquad (10)$$

As in the case of Eqs. (7) and (8), the rates of radiative transitions are much smaller than the rates of collision-induced transitions for large principal quantum numbers. It is very probable that the principal quantum number changes by only ± 1 in the reaction given by

Eq. (10) [see Eq. (21)]. It is also much more probable in any given collision that the bound electron goes to another bound state than to a free state (collisional ionization). Therefore electrons reach the "reservoir" of bound electrons primarily by three-body recombinations, then rapidly random-walk in single steps through the bound states in the reservoir. They only infrequently reach the continuum of free electrons (reionization) or the ground state (recombination). The populations of excited states in the "reservoir" are related to the temperature and density of free electrons by Saha's equation, to a very good approximation.

The "reservoir" extends down to the lowest bound state for which detailed balance still holds for the collisional processes populating and depopulating the state. Below this level, the levels are populated primarily by radiative or collision-induced transitions from higher levels, and are depopulated primarily by radiative or collision-induced transitions to lower levels. Detailed balance does not exist, and the populations of the levels below the reservoir is generally less than the equilibrium populations calculated from Saha's equation. For very low levels in optically thin plasmas, the rate coefficients of the radiative processes tending to depopulate the state become much larger than the rate coefficients of the collisional processes tending to populate the state, and the population of the state is then far below the equilibrium value.

Usually, all levels except the ground state may be considered to be in a quasi-steady state, as the flux of electrons into and out of any level is much greater than the time rate of change of the number of electrons in the level. If the electron density and temperature are high enough, even the ground state may be treated in this approximation. The "reservoir" of electrons essentially in thermal equilibrium with the free electrons then includes the ground state. In such a case the numbers of excited atoms in all states may be calculated from Saha's equation, and the rate at which the plasma recombines is determined entirely by the time rate of change of the electron temperature and Saha's equation.

2. Numerical Solutions

If all pertinent cross sections are known, the problem can be solved to any desired accuracy by use of modern high-speed computers. (Approximate solutions by various authors are discussed in Appendix B.) This is the approach adopted by Bates et al.[15, 16] and by Stubbs et al.[17]

We first discuss the work of Bates et al. They set up rate equations governing the population and depopulation of a given quantum level. Such a rate equation determining the density of excited atoms in the pth quantum level (principal quantum number p) has the form (changing their notation somewhat)

$$\dot{N}_p = - N_p [N_e K(p) + A(p)] + N_e \sum_{q \neq p} N_q K(q, p) + \sum_{q>p} N_q A(q, p)$$

$$+ N_i N_e [K(c, p)] + \beta(p) . \qquad (11)$$

The K's, A's, and β's are rate coefficients for the various processes given by Eqs. (7) through (10). The first term on the right is the rate of depopulating the pth level by collisional ionization and collisionally induced transitions to other bound states [K(p)] and by radiative transitions to lower bound states [A(p)]. The second term is the rate of populating the pth level by collisionally induced transitions from other bound states. The third term populates the pth level by radiative transitions from higher states, and the last term populates the level by three-body recombinations [K(c, p)] and radiative recombinations [β(p)]. Terms corresponding to photoionization and photoexcitation have been omitted. There are as many such equations as there are bound states. The set of equations may be greatly simplified by the assumptions $N_p \ll N_1$, $N_p \ll N_e$, and $p \neq 1$. These assumptions are justified for most laboratory plasmas. They imply that $\dot{N}_p \cong 0$ and $p \neq 1$, so the left side of all the equations but the first may be set equal to zero without introducing much error. Further simplification results from the assumption that the upper states -- those with principal quantum number n greater than some number s, where s will

be defined more precisely in a later section -- are in equilibrium with the free electrons (justified by physical arguments given earlier). Then the populations of these states may be calculated from Saha's equation. This assumption is checked during the course of the calculations by requiring that the calculated densities of excited states approach the equilibrium value as $p \to s$.

Bates et al. first consider optically thin plasmas.[13] They calculate as a function of electron density and temperature a collisional-radiative decay coefficient γ defined by

$$\dot{N}_1 = \gamma N_i N_e . \tag{12}$$

For hydrogen the coefficient γ may be written

$$\gamma = \alpha_{cr} - S \frac{N_1}{N_e}, \tag{13}$$

where α_{cr} is the collisional-radiative recombination coefficient, S is the collisional-radiative ionization coefficient, and N_1 is the density of atoms in the ground state (n = 1). Usually, in recombining laboratory plasmas practically all electrons that disappear from the continuum of free electrons reappear in the ground state, and the recombination coefficient α as defined by Eq. (4) becomes identical with the coefficient γ defined by Eq. (12).

The dependence of α_{cr} and S, the collisional-radiative decay and ionization coefficients calculated by Bates et al. on the electron density and temperature is shown in Figs. 1 and 2. From Fig. 1 we see that in the limit of very low electron densities or very high temperatures, collisional effects become unimportant and α_{cr} approaches α_{rad} (independent of N_e), corresponding to purely radiative recombination. This case has recently been treated by Seaton[35] and Burgess.[36] In the limit of very high electron densities or very low temperatures, the collisional processes dominate, and α_{cr} becomes proportional to N_e, corresponding to purely three-body recombination.

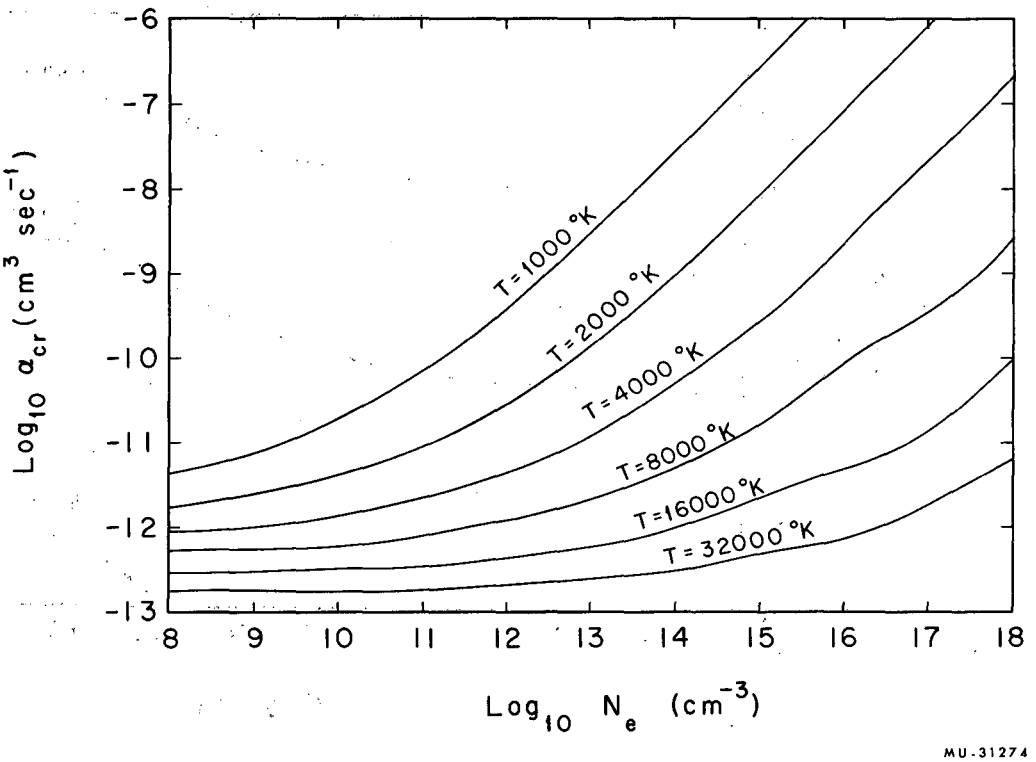

Fig. 1. Collisional-radiative decay coefficient a_{cr} as a function of electron density, for several temperatures.

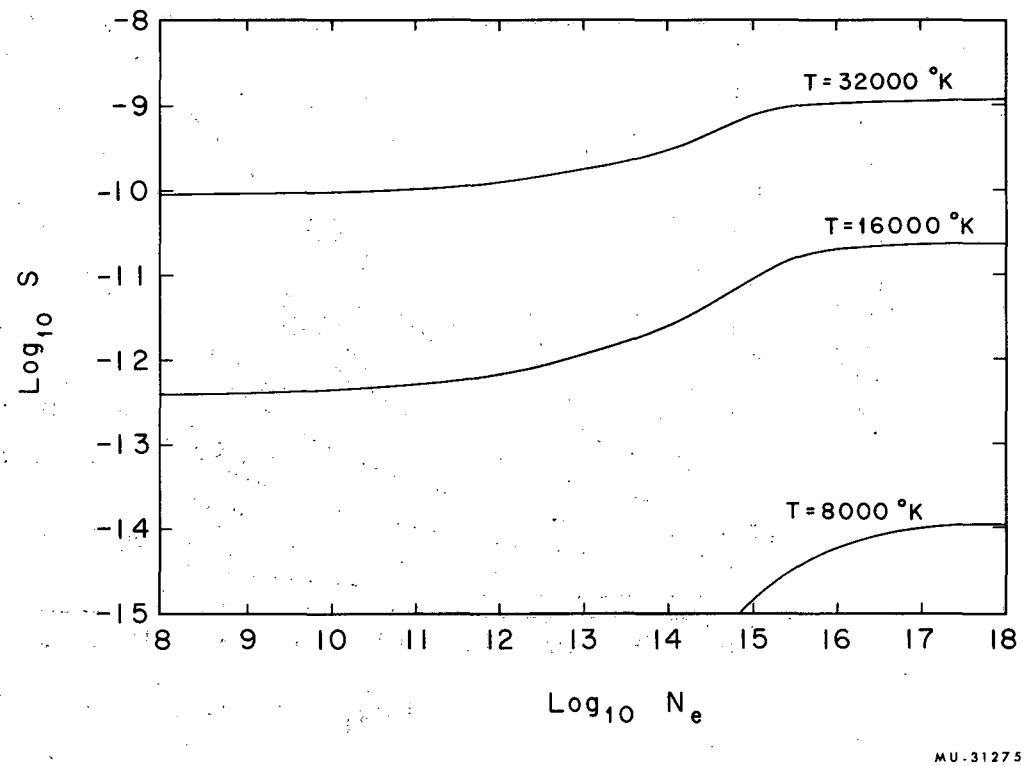

Fig. 2. Collisional-radiative ionization coefficient S as a function of electron density, for several temperatures.

Comparing Figs. 1 and 2, we see that for any given electron density there is a temperature above which S is greater than α_{cr}. Because N_1 approximates N_e in a recombining highly ionized plasma, above this temperature the rate of depopulation of the ground state by electron collisional excitation and ionization becomes comparable to the rate of population of the ground state through collisional and radiative processes. In the limit of large electron densities, radiative effects become negligible, and the rates of the collisional processes exactly cancel (detailed balance); then in Eq. (13) γ goes to 0 and we have

$$N_1 = \frac{\alpha_{cr}}{S} N_e , \tag{14}$$

which is just Saha's equation (α_{cr} is proportional to N_e in this limit).

Figure 3 shows the locus of points such that $\alpha_{cr} = S$ on an electron density vs temperature diagram (solid line). Plasmas to the left of this line recombine at a rate determined by the electron density and temperature and independent of the ground-state neutral density. Plasmas to the right of this line are essentially in thermal equilibrium, and recombine at a rate determined by the rate at which they cool. Very dense plasmas can scarcely be expected to be optically thin to the hydrogen resonance lines. The conditions under which a recombining highly ionized hydrogen plasma will be opaque to L_α, the first member of the hydrogen Lyman series, are given in Appendix A. The electron-density-temperature diagram is then divided by the dashed lines into four regions (for plasmas of three different dimensions: 1, 10, and 100 cm). Plasmas below these lines will be optically thin, and the decay coefficients given in Figs. 1 and 2 may be used. Plasmas located above these lines will be opaque at least to L_α, and a modification of the theory is required to take into account the trapping of resonance radiation. For future reference, the four regions are designated by Roman numerals, as follows:

I. Opaque at least to L_α; populations of upper states related to N_e and T_e by Saha's equation; recombining at a rate determined by N_e and T_e, and independent of N_1.

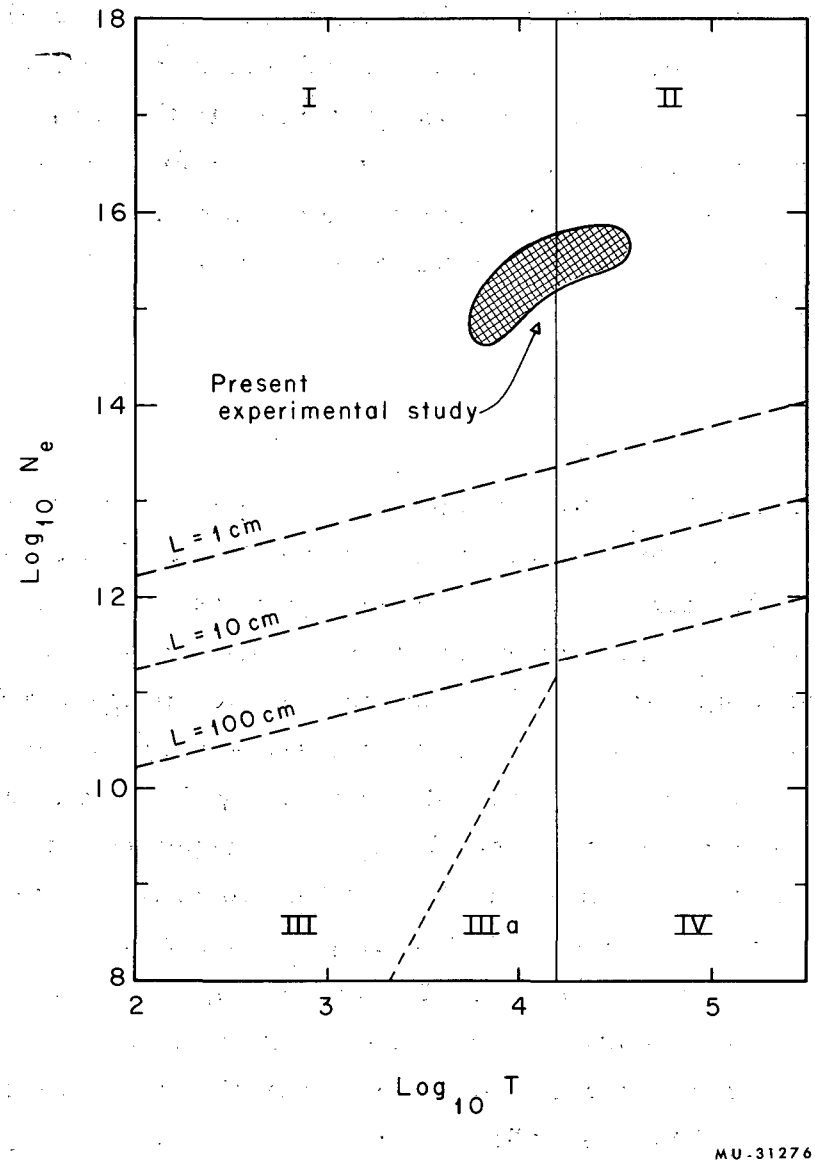

Fig. 3. Electron-density vs temperature diagram, showing several regions of interest in a recombining, highly ionized hydrogen plasma: Region I: Opaque at least to L_α, recombining. Region II: Opaque at least to L_α, recombining at a rate determined by the time rate of change of T; nearly in LTE. Region III: Transparent, recombining. Region IIIa: Transparent, recombining by radiative recombination. Region IV: Transparent, recombining at a rate determined by the time rate of change of T; nearly in LTE.

II. Opaque at least to L_α; populations of all states given very nearly by Saha's equation; recombining at a rate determined by the time rate of change of T_e.

III. Transparent to all radiation; populations of upper states related to N_e and T_e by Saha's equation; recombining at a rate determined by N_e and T_e, and independent of N_1.

IV. Transparent to all radiation; populations of all states given very nearly by Saha's equation; recombining at a rate determined by the time rate of change of T_e.

The location of the dashed lines separating opaque from transparent plasmas is approximately correct for recombining plasmas with $N_1 \cong N_e$. Very early in the decay period, of course, any "fully" ionized plasma will be transparent to all radiation, unless the electron density is so enormously high that the Bremsstrahlung radiation from the plasma is comparable to black-body radiation at the same temperature at some wavelength in the spectrum.

The cross-hatched area in Fig. 3 shows the region of the electron-density-temperature diagram occupied by the plasma studied in this thesis. Within the region labeled "IIIa," recombination is predominantly radiative (i.e., the recombination rate as calculated by Bates et al. is not more than about 30% greater than the "pure" radiative recombination rate). The region is bounded on the right by the condition that electron collisional excitation from the ground state be negligible. Considering the limited area of Region IIIa, it seems improbable that radiative recombination has ever been observed in a partially ionized laboratory plasma.

In Ref. 16, Bates et al. consider recombination in optically thick plasmas. The general problem is extremely complex, depending not only on the electron density and temperature of the plasma, but also on the dimensions of the plasma and the mechanisms broadening the spectral emission lines. They consider a number of special cases: (1) absorption of all lines of the Lyman series, (2) absorption of all line radiation of all series, (3) absorption of Lyman lines and continuum, and (4) absorption of all line radiation plus the Lyman

continuum. Of these, the first is of primary importance in the present work. In this case, the rates of population and depopulation of the ground-state due to emission and absorption of the Lyman lines exactly balance. The situation may be treated by removing all terms corresponding to emission of Lyman line radiation from the initial rate equations, Eq. (11). Bates et al. find it necessary to express the approximate solutions of the new rate equations in terms of both N_1 and N_2, rather than only N_1 as in the case of optically thin plasmas. They define six new rate coefficients, such that

$$\dot{N}_1 = a_1 N_i N_e + P_{21} N_2 N_e - R_1 N_1 N_e \qquad (15)$$

and

$$\dot{N}_2 = a_2 N_i N_e + P_{12} N_1 N_e - R_2 N_2 N_e , \qquad (16)$$

and tabulate numerical values of a_1, a_2, P_{12}, P_{21}, R_1, and R_2. Equations (15) and (16) can usually be simplified considerably by making approximations appropriate to conditions in the plasma under study. For instance, $\dot{N}_2$ is almost always much smaller than any of the terms on the right of Eq. (16), and may be set equal to zero. Equation (16) may then be solved for N_2, now a quasi-steady-state density, and that value substituted into Eq. (15). As will be shown in a later section, often all terms involving N_1 may be neglected also.

The trapping of resonance radiation decreases the recombination rate of a decaying plasma. This must always be the case, as it introduces an additional mechanism for depopulating the ground state. The decrease may be a factor of 10 or more in laboratory plasmas.

The decay rates calculated by Bates et al. are probably the most accurate available.[37] The accuracy of their numerical calculations is limited primarily by the accuracy of the cross sections needed in calculating the rates of collisional processes. They used quantum-mechanical and semiclassical cross sections derived by various authors, and estimated an uncertainty of a factor of 2 or 3 in the calculated rates. They did not estimate the extent to which this uncertainty

is reflected in the recombination rates; these may also be uncertain by a factor of 2.

B. Populations of Excited States in a Dense Recombining Hydrogen Plasma

1. The Lowest Level in the Reservoir

We have already stated that we may expect all levels with principal quantum number $n > s$ to be essentially in thermal equilibrium with the free electrons, where s is the principal quantum number of the lowest level for which detailed balance approximately holds. The densities of excited states with $n > s$ (or more likely, $n > s + 2$ or $n > s + 3$) may then be calculated from Saha's equation, by using the electron density and temperature.

To estimate s in a recombining optically thin plasma, we may use the following model: Consider all levels with $n > s$ to be in thermal equilibrium with the free electrons. We define $\rho(n)$ to be the ratio of the density of atoms in the nth level in the recombining plasma to the density of atoms in that level if equilibrium conditions were to hold

$$\rho(n) \equiv \frac{N_n}{N_n^{eq}} . \tag{17}$$

We now assume $\rho(s) \simeq 1$ and $\rho(s-2) \ll 1$. With these assumptions, the most important processes determining the population of the $(s-1)$th level are (1) collision-induced transitions between the levels s and $s-1$, (2) collision-induced transitions from $s-1$ to $s-2$, and (3) radiative transitions from $s-1$ to lower levels. These processes are shown schematically in Fig. 4, together with their rates. The rates of collisional ionization of and three-body recombination to $s-1$ are negligible, as are the rates of collision-induced transition to the levels with $n < s-2$ or $n > s+2$. The assumption $\rho(s-2) \ll 1$ guarantees that the rate of collision-induced transition to $s-1$ from $s-2$ is also negligible.

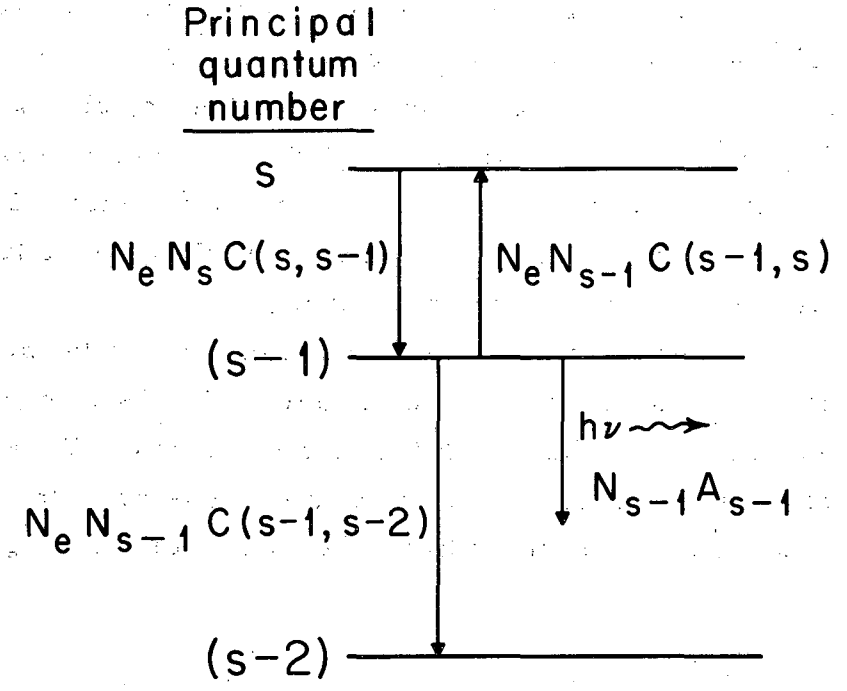

Fig. 4. Energy-level diagram, showing rates of processes important in recombination.

The rate coefficients for collision-induced transitions between level n and level p ($p < n$) have been calculated by Byron et al.[18] from Gryziński's cross sections.[38] Their expression for the rate coefficient $C(n, p)$ is

$$C(n, p) = \frac{8\pi e^2 a_0^2}{\hbar} \frac{k_{np}^2 p^7}{n^5} \left[1 + \frac{8k_{np} + 6}{15(\pi\beta_p)^{1/2}}\right] \left[\frac{5\beta_p}{1+5\beta_p}\right], \qquad (18)$$

where

$$k_{np} \equiv \frac{|E_p|}{|E_p - E_n|}$$

and

$$\beta_p \equiv \frac{|E_p|}{kT}.$$

If we let $p = n - 1$, for hydrogen this expression becomes approximately

$$C(n, n-1) \cong 1.37 \times 10^{-7} \frac{(n-1)^7}{n(2n-1)^2} \left[1 + \frac{2n(2n+3)}{15(\pi x)^{1/2}}\right] \left[\frac{\frac{5x}{(n-1)^2}}{1 + \frac{5x}{(n-1)^2}}\right] \qquad (19)$$

for $n \geq 3$, where $x = \chi_1/kT$, and χ_1 is the ionization potential of the hydrogen atom from the ground state. The population of the $s-1$ level is then determined by the rate equation

$$C(s, s-1)N_s = N_{s-1}\left[C(s-1, s-2) + C(s-1, s) + \frac{A_{s-1}}{N_e}\right], \qquad (20)$$

where A_{s-1} is the reciprocal of the lifetime of the $s-1$ level. Using detailed balance to eliminate $C(s-1, s)$ and rearranging, we have for Eq. (20)

$$\left[\frac{\rho(s)}{\rho(s-1)} - 1\right] = \frac{N_{s-1}{}^{eq} C(s-1, s-2)}{N_s{}^{eq} C(s, s-1)} + \frac{N_{s-1}{}^{eq} A_{s-1}}{N_s{}^{eq} N_e C(s, s-1)} . \qquad (21)$$

Since all rate coefficients in Eq. (21) are strong functions of the principal quantum number, we expect $\rho(n)$ to be a strong function of n around $n = s$. We have already specified $\rho(s) \cong 1$. A reasonable value of $\rho(s-1)$ is 0.5; this is then the definition of s. We expect $\rho(n)$ to behave qualitatively as shown in Fig. 5. The solution of Eq. (21) with the left side equal to 1 then gives s for any specified N_e and T. Because $C(n, n-1)$ is not a strong function of T, and the ratio $C(s-1, s-2)/C(s, s-1)$ even less so, we expect that for sufficiently large N_e we may neglect the second term, and s will be independent of N_e and will depend on T alone, primarily through the ratio $N_{s-1}{}^{eq}/N_s{}^{eq}$. This is just the condition that the rate of collision-induced transitions from the level n to the level $n-1$ have a minimum at $n = s$, as pointed out by Byron et al.[18] (see Appendix B). In the limit of very low N_e, we may neglect the first term with respect to the second; then s is roughly independent of temperature [because $C(s, s-1)$ is only a weak function of temperature] but depends on N_e. In this case s is determined by the equality of the rate of collision-induced transitions from the level s to the level $s-1$ and the rate of radiative transitions from $s-1$ to lower levels.

If we approximate $C(s-1, s-2)/C(s, s-1)$ by the ratio of the factors $(n-1)^7/n(2n-1)^2$ [the functions contained in the brackets in Eq. (18) are comparatively weak functions of n and x] and let $\rho(s)/\rho(s-1) = 2$, Eq. (21) may be written

$$F(s) + \frac{G(s)}{N_e} = e^{-xH(s)} , \qquad (22)$$

where

$$F(s) \equiv \left(\frac{s-2}{s-1}\right)^7 \left(\frac{s-1}{s}\right) \left(\frac{2s-1}{2s-3}\right), \qquad (23)$$

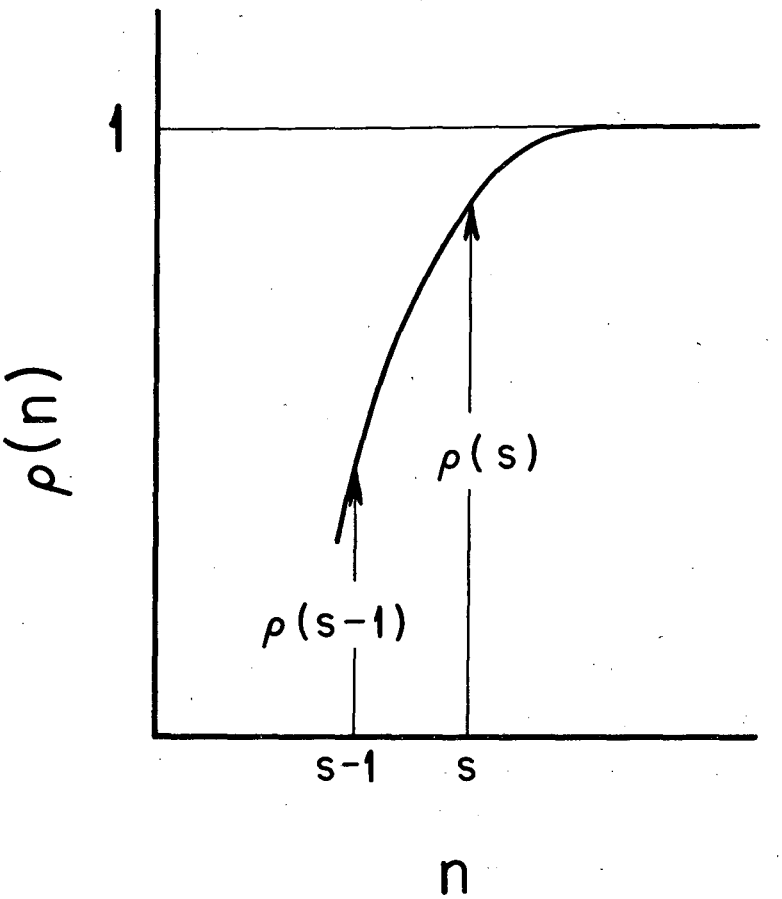

Fig. 5. Plot of ρ(n) as a function of n.

$$G(s) \equiv \frac{A_{s-1}}{C(s,\ s-1)} \left(\frac{s-1}{s}\right)^2, \tag{24}$$

and

$$H(s) \equiv \frac{2s-1}{[s(s-1)]^2}. \tag{25}$$

We have neglected the weak temperature dependence of $C(s,\ s-1)$. The functions $F(s)$, $G(s)$, and $H(s)$ are shown in Figs. 6, 7, and 8. $C(s,\ s-1)$ was evaluated for a temperature of 8,000 °K in Fig. 7. Given an electron density and temperature, we can solve Eq. (25) graphically to obtain an estimate of s.

Byron et al. state that s (equivalent to their n^*) is either the quantum number of the level at which $A_s = N_e C(s,\ s-1)$ or $s \cong (x/3)^{1/2}$, whichever is larger.[18] Both statements can be justified in view of the preceding discussion. The expression $s \cong (x/3)^{1/2}$ results from determining n such that $N_n^{eq} C(n,\ n-1)$ is proportional to n^4 (true for large n). Griem derives from simple physical estimates of the collision cross section an expression for s that is correct if radiative decay is important.[39]

All these values of s become too large either if the plasma is opaque to the resonance lines or if the temperature is high enough (> 16,000 °K) that excitation from the ground state becomes important.

2. Numerical Results

Bates and Kingston in a recent paper present detailed results of calculations of the distribution of excited states in a decaying hydrogen plasma as a function of the electron temperature and density for two cases:[13] (a) the plasma is optically thin, and (b) the plasma is opaque to Lyman-line radiation. The results follow from computer solutions of Eq. (11), and are as exact as the knowledge of the necessary cross sections. They calculate $\rho(p)$ [defined by Eq. (17)] by defining three population coefficients such that

$$\rho(p) = r_0(p) + r_1(p)\rho(1) + r_2(p)\rho(2). \tag{29}$$

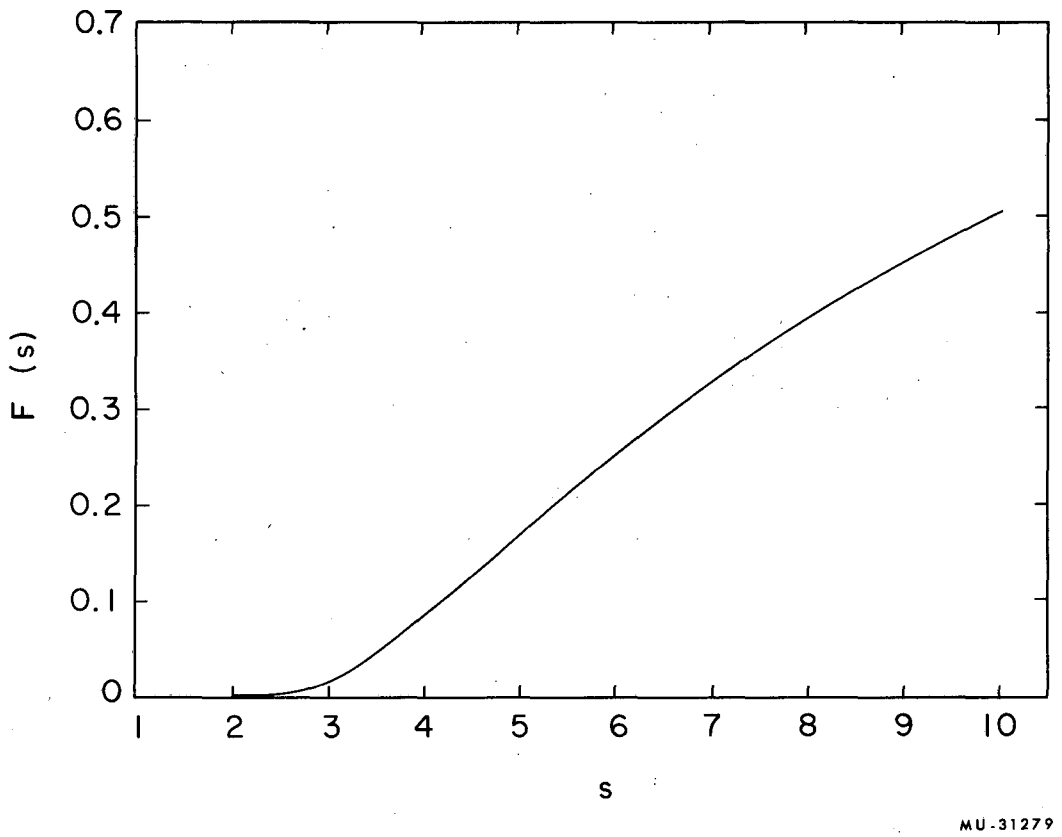

Fig. 6. Plot of F(s) as a function of s.

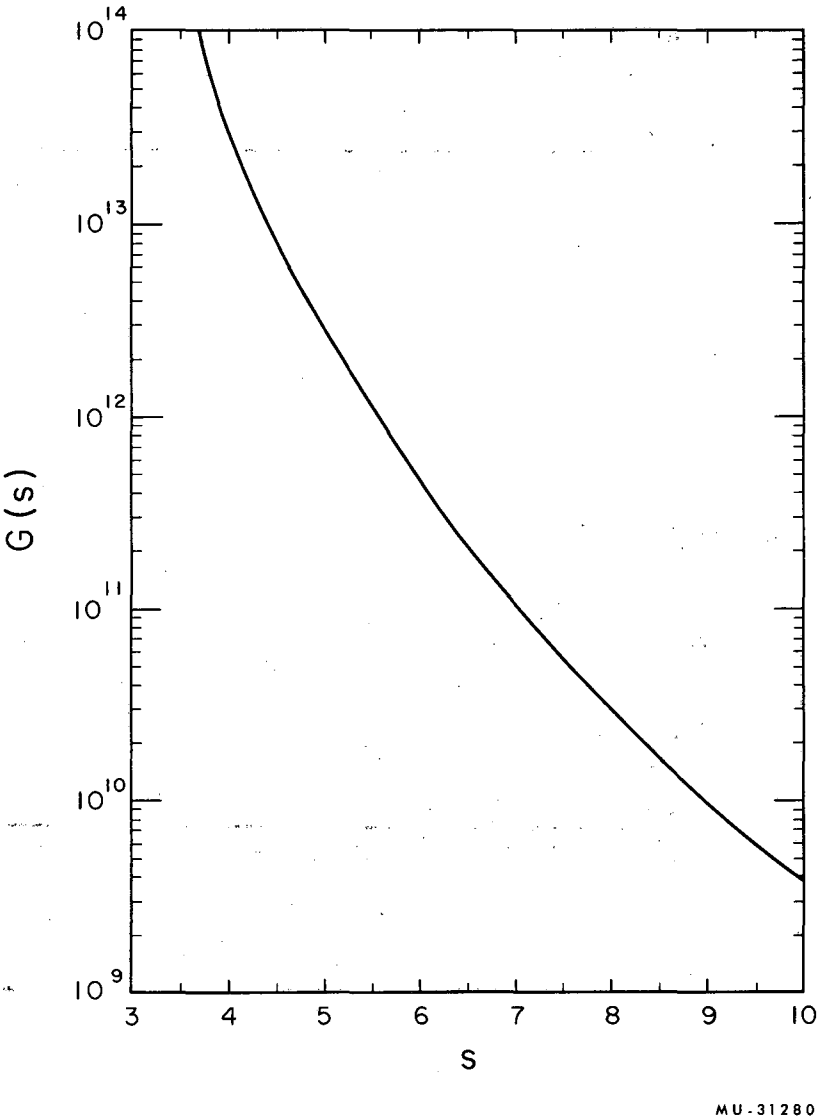

Fig. 7. Plot of G(s) as a function of s.

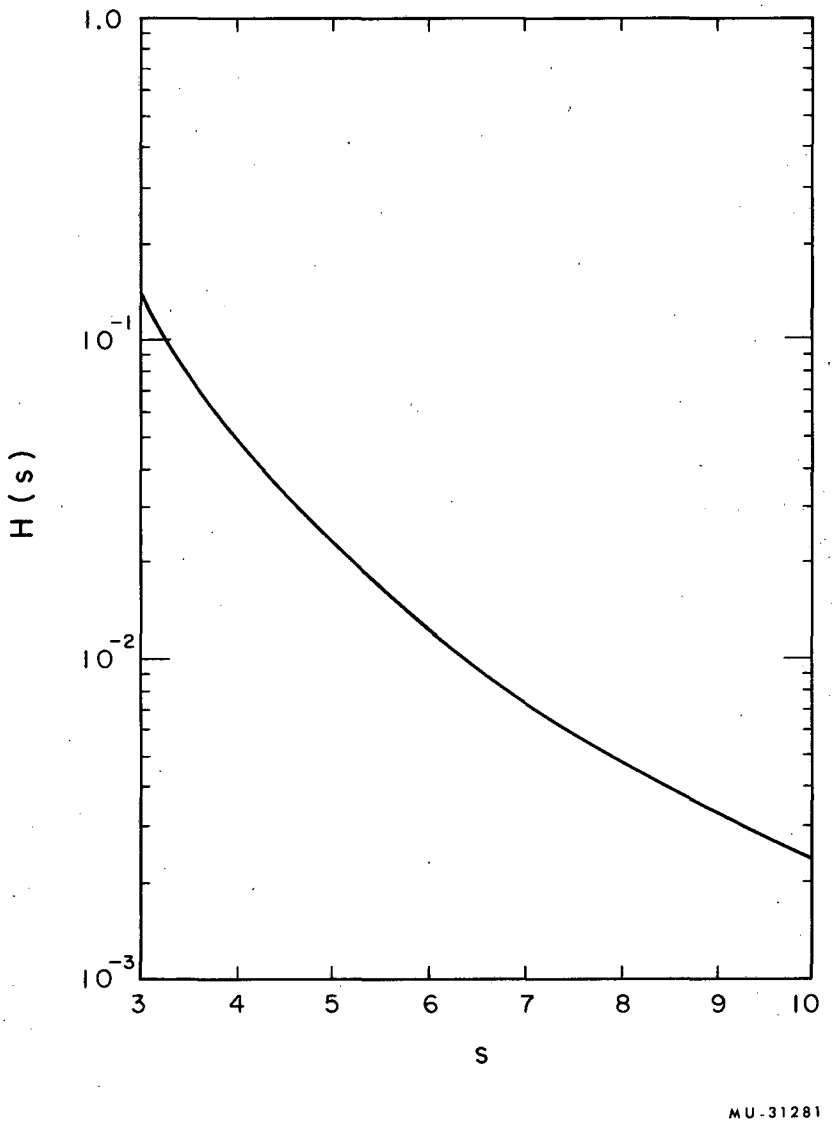

Fig. 8. Plot of H(s) as a function of s.

The coefficients $r_0(p)$, $r_1(p)$, and $r_2(p)$ are always greater than zero, and are functions of the electron density and temperature. Values are tabulated for $10^{10} < N_e < 10^{18}$ cm^{-3}, $250 < T < 64{,}000$ °K, and $2 < p < 10$. Asymptotic forms are also given for higher and lower electron densities. Representative values of r_0 [$\rho(p) > r_0(p)$] for plasmas opaque to the Lyman lines are given in Fig. 9. As expected, equilibrium conditions extend to lower values of principal quantum number as the electron density is increased.

Bates and Kingston also calculate a number p_x which corresponds very closely to our s. They define p_x to be the principal quantum number of the lowest level such that the density of excited atoms in that level is x per cent or less below the equilibrium value. Figure 10 shows lines of constant s and constant p_{30} on an electron density-temperature diagram for an optically thin plasma. The lines of constant s were calculated from Eq. (21). Bates and Kingston's p_{30}, the value of the principal quantum number such that $\rho(p_{30}) = 0.7$, should be a good approximation to what we have called s. Agreement is indeed very satisfactory, considering the approximate nature of the solution.

The disturbing effect of the lack of detailed balance in level s might be expected to perturb the distributions of several levels immediately above the level s. Bates and Kingston's tables of p_x show that for $T > 1000$ °K, the level $p_{30}+1$ or 2 is generally within 10% of the equilibrium value, and $p_{30}+5$ is generally within 1%.

C. Theory of Spectroscopic Measurements

1. Introduction

Various spectroscopic techniques can provide accurate temporal and spatial measurements of the electron or ion density and temperature in a decaying hydrogen plasma. The techniques usually involve measurements of the absolute or relative intensities of line or continuum radiation emitted by a plasma, or measurements of the profiles of the emission lines. Absolute line-intensity measurements provide a means of determining the densities of atoms in the various excited states and, therefore, departures of the system from LTE.

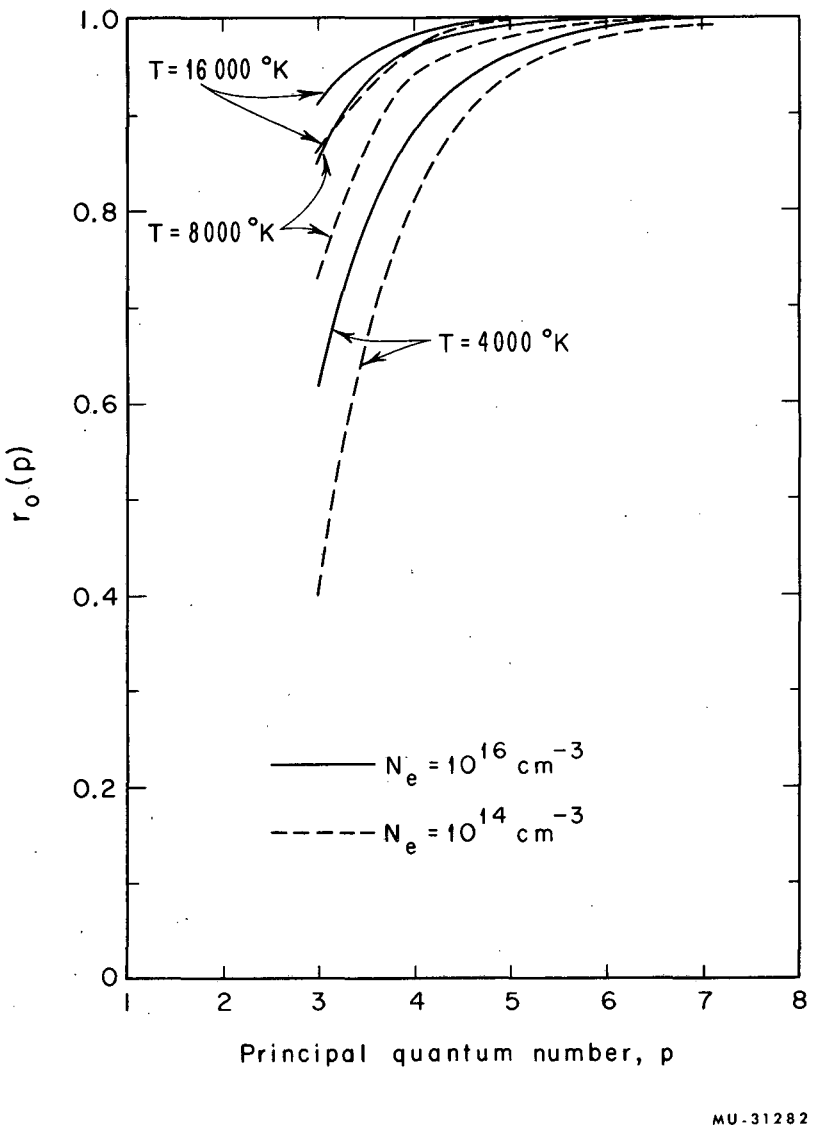

Fig. 9. Plot of r_0 as a function of p for a plasma opaque to L_α, for several temperatures.

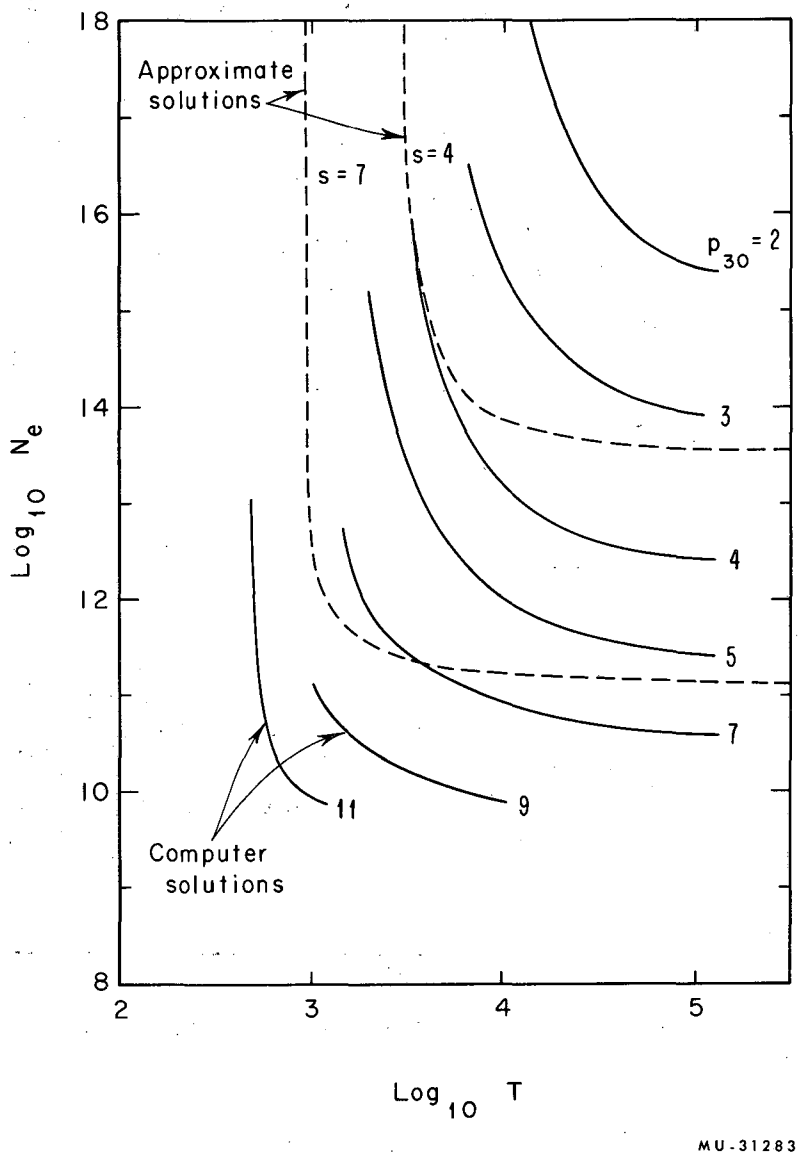

Fig. 10. Electron density-temperature diagram showing lines of constant s and constant p_{30} for an optically thin plasma.

An excellent summary of available spectroscopic techniques and their limitations has been given by Griem[30] and other authors.[31, 32] Only the techniques pertinent to this thesis will be given here. These are (a) temperature measurements by determining the ratio of the intensity of a spectral line to the intensity of the continuum radiation at some wavelength, (b) temperature measurements by determining the ratio of the intensities of the continuum radiation at two wavelengths, (c) electron-density measurements by determining the absolute intensity of either a spectral line or of the continuum radiation at some wavelength, and (d) ion-density measurements by determining the profile of a Stark-broadened emission line.

Figure 11 shows the spectrum of the hydrogen plasma investigated in this thesis. It was taken with a small Hilger quartz-prism spectrograph, and shows features common to the spectra of many hydrogen plasmas. The most obvious lines are those of the hydrogen Balmer series. There is a faint continuum radiation throughout the visible region of the spectrum, and a pronounced recombination continuum beyond the Balmer series limit. Some faint, but sharp, impurity lines due to CuI, AlI, CII, SiII, SiIII, SiIV, OI and OII are also visible. In comparison with them, the Balmer lines are much broadened. These features of the spectrum are discussed quantitatively in the following sections, and methods of determining the electron (ion) density and temperature in the plasma derived.

2. Line and Continuum Radiation Due to the H Atom

If N_n is the density of atoms in the nth quantum level in an optically thin and uniform hydrogen plasma, the energy radiated due to spontaneous transitions from the nth to the pth level is

$$U_{np} = h\nu_{np} A_{np} N_n , \tag{30}$$

where h is Planck's constant, ν_{np} is the frequency of the emitted radiation, and A_{np} is the transition probability for spontaneous emission. We neglect stimulated emission (this will be justified experimentally in the case of the H_β line in our plasma). The transition

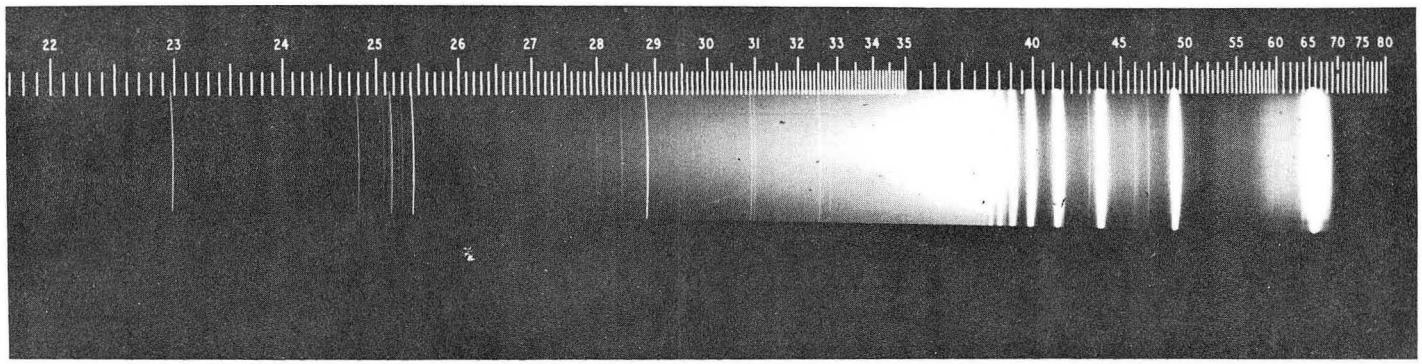

ZN-3832

Fig. 11. Spectrum of the hydrogen plasma.

probabilities A_{np} usually tabulated are averaged over all angular momentum states of a given quantum level, assuming they are populated according to their statistical weights. Bates and Kingston show that this assumption is justified for an optically thin hydrogen plasma with a temperature of 10,000 °K, [13] even for the n = 2 level provided the ion density is at least 10^{13} cm^{-3}. The assumption is even easier to justify if the ion density is higher or if the resonance lines are reabsorbed.

One might question the values of the transition probabilities A_{np}, as they were calculated for a pure Coulomb field and an absence of perturbing effects. Neither assumption is strictly justified if the excited atom is located in a plasma, as Debye shielding effects modify the Coulomb potential, and perturbations exist in the form of electron collisions. Little is known about such effects, but Griem[30] estimates the change in intensity of the H_β line to be only about 1% even with an ion density as high as 10^{17} cm^{-3}.

We assume the upper level of the transition to be in LTE with the free electrons. This assumption may be justified or rejected by consulting Fig. 10. We may then use Saha's equation to calculate N_n in terms of the plasma properties to be measured, N_e, N_i, and T. The generalized Saha's equation may be written[40, 41]

$$\frac{N_i N_e}{N_n} = \frac{2g_i}{g_n} \frac{(2\pi m_e kT)^{3/2}}{h^3} e^{-(\chi_n - \Delta\chi)/kT} \tag{31}$$

where g_i is the statistical weight of the hydrogen ion relative to the atom ($g_i = 1$), g_n is the statistical weight of the atom in quantum state n ($g_n = 2n^2$), k is Boltzmann's constant, m_e is the mass of the electron, and χ_n is the ionization potential from the level n. Evaluating the constant for hydrogen, we have

$$N_n = 4.17 \times 10^{-16} N_i N_e \frac{n^2}{T^{3/2}} e^{+\frac{1}{T}\left[\frac{1.58\times10^5}{n^2} - 3.54\times10^{-7}(N_e/T)^{1/2}\right]} \tag{32}$$

The ionization potential of an atom immersed in a plasma is lower than that of an isolated atom because of Debye shielding effects. We have corrected for this by replacing the ionization potential χ_n in the Saha equation by $\chi_n - \Delta\chi$, where

$$\Delta\chi = \frac{e^2}{\sqrt{2}\,\lambda_D} \text{ ergs.} \tag{33}$$

Here e is the charge of the electron and λ_D is the Debye length. For hydrogen, we have

$$\lambda_D = \left[\frac{kT}{4\pi e^2 N_e}\right]^{1/2} \text{cm.} \tag{34}$$

This is a small correction for the plasma studied in this thesis. Griem[42] has discussed completely this and other corrections involved in the thermodynamics of dense plasmas.

With a knowledge of the geometry of the plasma and the sensitivity of the detector, we may use Eq. (30) to measure the density of excited atoms in the state from which the line originates. If the population of the state is sufficiently close to the equilibrium value, Eq. (31) may be used with Eq. (30) to relate the observed line intensity to the electron density and temperature.

Figure 12 shows the results of computer calculations of

$$W_\ell(4861) \equiv \frac{U_{42}}{N_i N_e} \tag{35}$$

as a function of electron temperature for an electron density of 10^{15} cm^{-3}. This transition produces the H_β line of the hydrogen Balmer series at 4861 Å, a particularly convenient line to observe and the one studied in this thesis. The line intensity is seen to be strong function of the temperature, and is very nearly proportional to the square of the electron density [changing N_e by a factor of 10 changes $W_\ell(4861)$ by less than 10% at T = 5000°K, and less at higher temperatures].

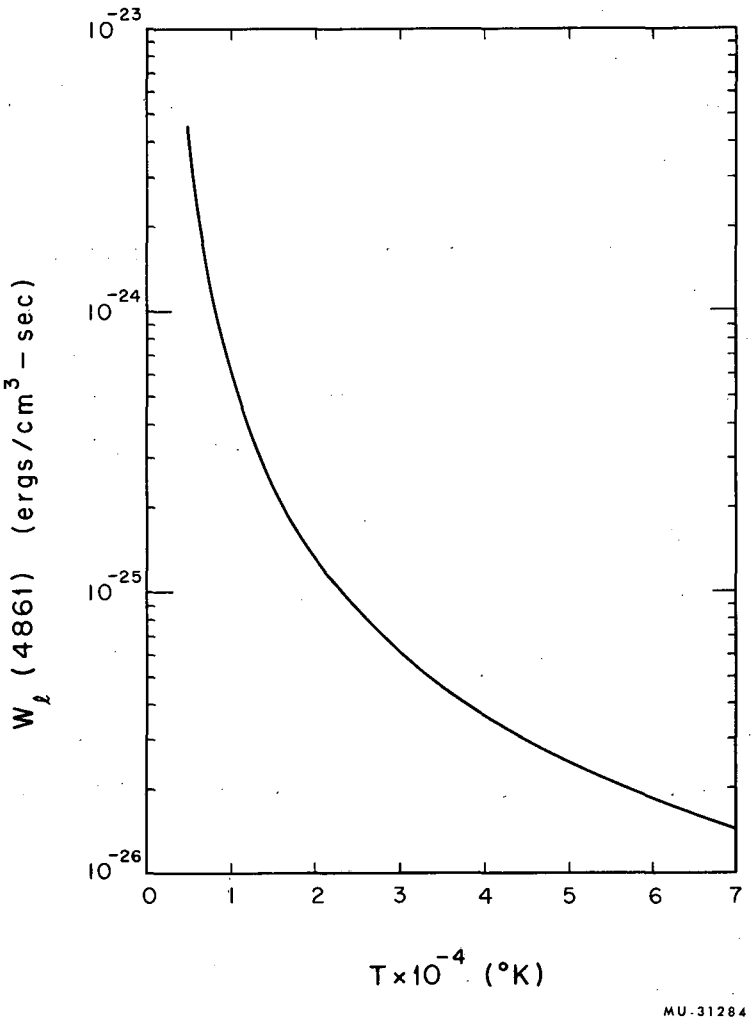

Fig. 12. Normalized H_β line intensity W_ℓ (4861) as a function of temperature.

Several precautions have to be observed in measuring spectral line intensities when the source is a plasma. If the electron (ion) density is 3×10^{15} cm^{-3} -- a typical value for the plasma studied in this thesis -- the H_β line will be broadened by the Stark effect, and will have a width at half-maximum intensity of about 3.4 Å. If one observes the line intensity photometrically, one must then use an exit slit wide enough to pass a bandwidth of at least 50 Å to guarantee that the error caused in the measurement of the total line intensity by failing to observe the light in the far wings of the broadened line be 1% or less.

One must also guarantee that the plasma is optically thin. It is difficult to correct for self-absorption in measuring the intensity of the Balmer lines, as this requires a knowledge of the density of atoms in the $n=2$ level, which is generally far from equilibrium in a recombining plasma. Besides transmission methods, there are at least three ways to determine if a line is partially reabsorbed. If the length of the plasma can be conveniently varied, one can look for a linear dependence of the line intensity on the length of the radiating plasma column. If the line is very strongly reabsorbed, the intensity per unit wavelength at the center of the line approaches that of a black-body at the same temperature as the plasma. One can then measure the intensity per unit wavelength at the center of the line and compare it with the intensity one would observe if the plasma radiated like a black body at the electron temperature. It is possible to observe reabsorption by an analysis of the emission-line profiles. This is difficult, however, unless the profile expected in the absence of reabsorption is accurately known, or the line is very strongly reabsorbed. In the latter case, the line profile is obviously "clipped," and has a nearly flat top.

The continuum radiation emitted by a recombining hydrogen plasma originates from at least three sources: radiative recombination (electron-ion free-bound transitions), Bremsstrahlung (electron-ion free-free transitions), and the H^- continuum (electron-atom free-free and free-bound transitions).

The H^- continuum is only important for $T < 10,000$ °K in the plasma studied in this thesis, and is considered in the next section. In

general, the spectral distribution and intensity of the continuum radiation is most conveniently calculated from the absorption coefficient. For isotropic radiation, the energy radiated per cm^3-sec in a frequency interval $d\nu$ at frequency ν is

$$U_\nu d\nu = 4\pi\epsilon_\nu d\nu , \tag{36}$$

where ϵ_ν is the emission coefficient. The absorption coefficient of the material κ_ν is defined by

$$\frac{dU_\nu}{d\ell} = -\kappa_\nu U_\nu , \tag{37}$$

where ℓ here is length along the optical path of the radiation. In the case of free-free and free-bound transitions, the emission and absorption coefficients are then related by Kirchoff's law (assuming only a Maxwellian energy distribution of the free electrons):

$$\frac{\epsilon_\nu}{\kappa_\nu} = B_\nu(\nu, T) = \frac{2h\nu^3}{c^2} \frac{1}{e^{h\nu/kT} - 1} . \tag{38}$$

The material absorption coefficient κ_ν is related to the atomic absorption coefficient k_ν by

$$\kappa_\nu = N_1(1 - e^{-h\nu/kT})k_\nu . \tag{39}$$

Here k_ν is the absorption coefficient per H atom in the ground state, and is a function only of the properties of the atom, the temperature, and the frequency of the incident radiation. The atomic absorption coefficient k_ν includes contributions from all bound and free states. It is expressed in terms of the ground-state density for convenience. The factor $(1 - e^{-h\nu/kT})$ corrects for stimulated emission. Using Eqs. (36), (38), and (39), we may write the continuum energy radiated per cm^3-sec in $d\nu$ at ν as

$$U_\nu d\nu = \frac{8\pi h\nu^3}{c^2} N_1 e^{-h\nu/kT} k_\nu d\nu . \tag{40}$$

In this application of detailed balancing to relate the absorption of radiation to the emission of radiation, we may assume complete thermal equilibrium and calculate N_1 from Saha's equation, (31). Unsöld[43] gives a classical expression for k_ν:

$$k_\nu = \frac{64\pi^4}{3\sqrt{3}} \frac{m_e e^{10} Z^2}{k^3} \frac{e^{-u_1}}{T^3} \frac{1}{u^3} \left[\sum_{u_n<n}^{4} \frac{e^{u_n}}{n^3} + \frac{e^{u_5}}{2u_1} \right]. \qquad (41)$$

Here Z is the charge on the nucleus (1 for hydrogen), $u = h\nu/kT$, and $u_n = \chi_n/kT$. The first term in the brackets results from summing the contributions from bound states capable of absorbing the incident radiation up to $n=4$ (an arbitrary choice). The second term results from the contributions of the bound states with $n>4$ (an integral approximation to the sum) and free-free absorption (inverse Bremsstrahlung).

Exact quantum-mechanical expressions are similar, except that each term in the bracket in Eq. (41) is multiplied by a quantum-mechanical correction factor $(\bar{g}_{fb})_n$ or $\bar{g}_{ff}$ (for free-bound and free-free transitions, respectively). These are called Gaunt factors, and are approximately 1 for recombining plasmas. The bar denotes averaging over the various angular momentum states. Brussard and van de Hulst[44] in a recent review article give a good discussion of the radiation from free-bound and free-free transitions of the H atom, including Gaunt factors.

The number of bound states of a hydrogen atom in a plasma is reduced because Debye shielding effects produce a non-Coulomb potential. Griem[42] shows that it is consistent with the correction to the ionization potential given by Eq. (33) to assume that the last bound state (having principal quantum number n_{max}) satisfies the equation

$$\chi_{n_{max}} = \Delta\chi . \qquad (42)$$

Therefore, we may as well extend the sum in Eq. (41) to include all bound states. Including Gaunt factors, the atomic hydrogen absorption coefficient becomes (with $Z = 1$), in a form more exact than given by Eq. (41),

$$k_\nu = \frac{64\pi^4}{3\sqrt{3}} \frac{m_e e^{10}}{(kT)^3} \frac{e^{-u_1}}{u^3} \left\{ \sum_{u_n<u}^{u_{n_{max}}} (\bar{g}_{fb})_n \frac{e^{u_n}}{n^3} + \frac{1}{2u_1} \left[\langle \bar{g}_{fb} \rangle (e^{u_{n_{max}+1}} - 1) + \bar{g}_{ff} \right] \right\}. \quad (43)$$

We see from Eqs. (40), (31), and (43) that U_ν is very nearly proportional to $N_i N_e$, and that the frequency dependence is very nearly $e^{-h\nu/kT}$. Computer calculations of U_ν as a function of temperature, using Eqs. (40) and (43), with Gaunt factors taken from the Tables of Karzas and Latter[45] are shown in Fig. 13. An ion density of 10^{15} cm^{-3} was assumed.

From the derivations just given we see that the intensity of any spectral line (assuming the upper state to be in equilibrium with the free electrons) or of the continuum radiation at a given wavelength (assuming a Maxwellian distribution of electron energies) is proportional to $N_i N_e$. The intensities of line and continuum radiations have very different temperature dependences, however. Therefore the ratio of the intensity of a spectral line to the intensity of the continuum radiation at some wavelength is a function of temperature but not of density, and may be used to determine the temperature of the plasma. The same is true of the ratio of the intensities of the continuum radiation at two wavelengths.

The electron (ion) density may be most conveniently determined by an absolute measurement of the intensity per unit wavelength of continuum radiation at a wavelength chosen such that the variation of the intensity with temperature is minimized. Then the density measurements are relatively insensitive to uncertainties in the temperature.

In the experimental work described later in this thesis, simultaneous measurements were made of the intensity of radiation emitted by the plasma at three wavelengths. We will justify the choice of these wavelengths at this point and give theoretical curves of the

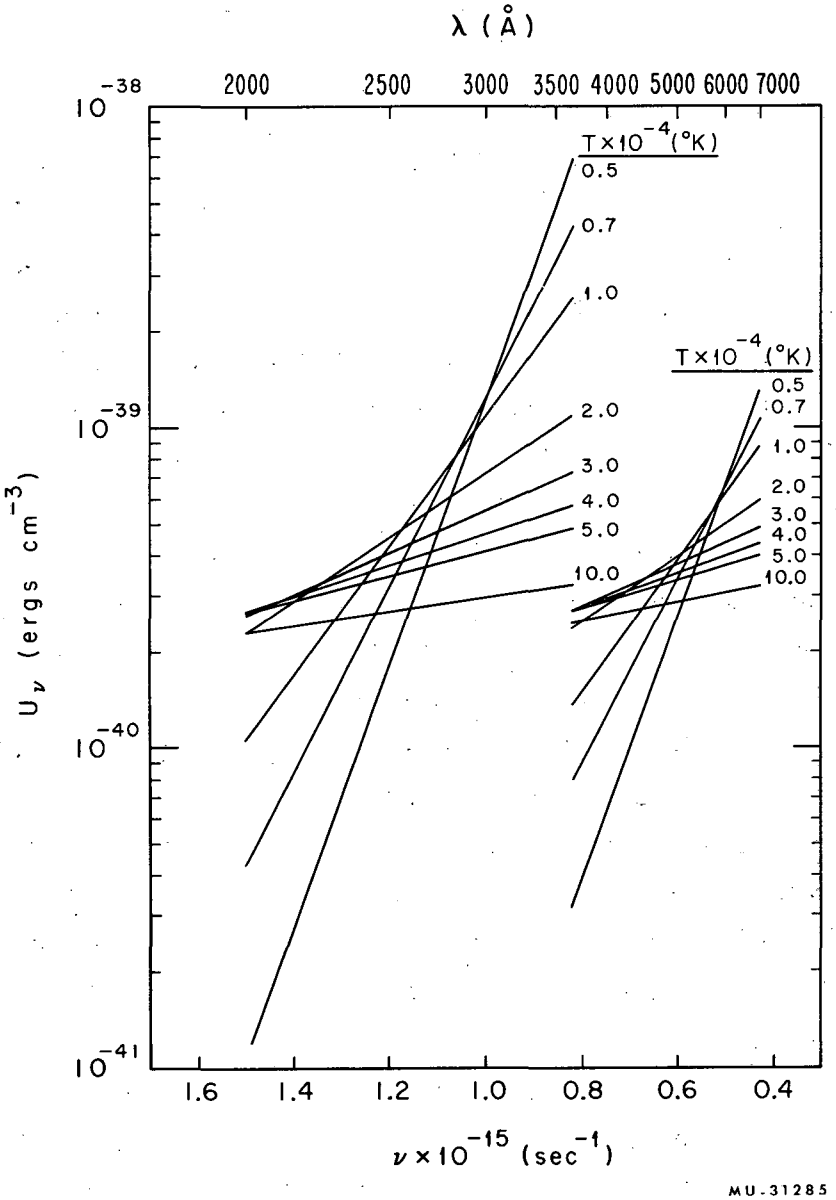

Fig. 13. Normalized continuum intensity U_ν as a function of frequency for several temperatures.

intensities as functions of the plasma parameters, reserving the major part of the experimental details for a later section.

Absolute intensity measurements were made of the H_β line and of the continuum at two wavelengths. The H_β line of the Balmer series was selected for observation because it was at a convenient wavelength for observation with photomultipliers, was not likely to be reabsorbed in the plasma, and because the broadening mechanisms were best understood for this line.

One continuum wavelength was chosen at about 5300 Å because the function

$$W_c(\lambda) = U_\nu \frac{c}{\lambda^2} \tag{44}$$

(assuming a temperature of 10,000 °K, typical of our plasma) has a maximum at this wavelength, making absolute continuum-intensity measurements particularly suitable for density determinations. The wavelength chosen is also far enough from the H_a and H_β lines that the contribution of the wings of these lines to the continuum intensity is less than 1 % for our plasma. The temperature dependence of the continuum intensity for a bandwidth of 1 Å at a wavelength of 5320 Å is shown in Fig. 14 for three electron densities. The actual choice of wavelength depends on the presence of impurity lines in the spectrum.

The second continuum wavelength was chosen at 3225 Å, again to avoid impurity lines, on the short-wavelength side of the Balmer-series limit. The temperature dependence of $W_c(3225)$ is shown in Fig. 15 for two electron densities.

Figures 16, 17, and 18 show $W_\ell(4861)/W_c(5320)$, $W_\ell(4861)/W_c(3225)$, and $W_c(5320)/W_c(3225)$, respectively. Any one of these may be used for temperature measurements. The ratios are completely independent of the ion density. The ratio $W_\ell(4861)/W_c(5320)$ has the strongest temperature dependence, and should provide the most precise measurement of the temperature. The ratio $W_\ell(4861)/W_c(3225)$ is the least dependent on the disturbing effect of the H^- continuum, which is expected to appear at temperatures much below 10,000 °K.

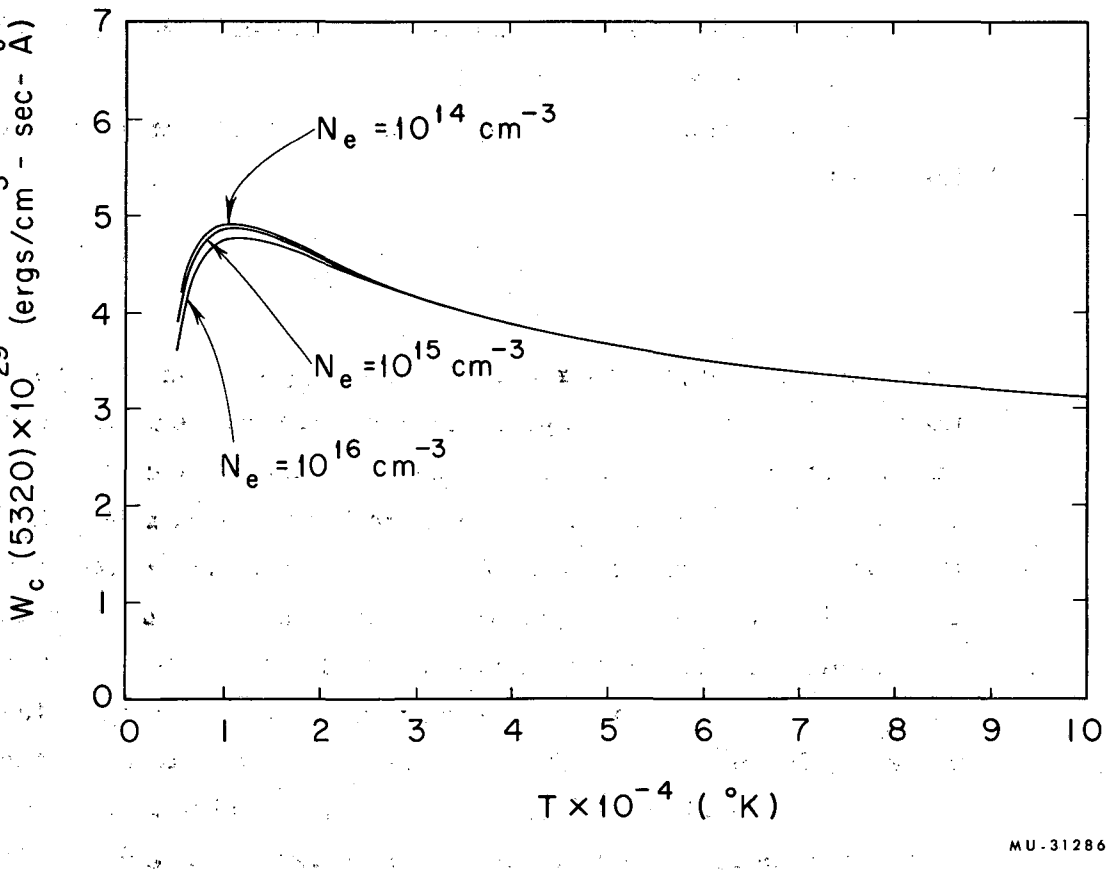

Fig. 14. Normalized continuum intensity $W_c(5320)$ at $\lambda = 5320$ Å as a function of temperature.

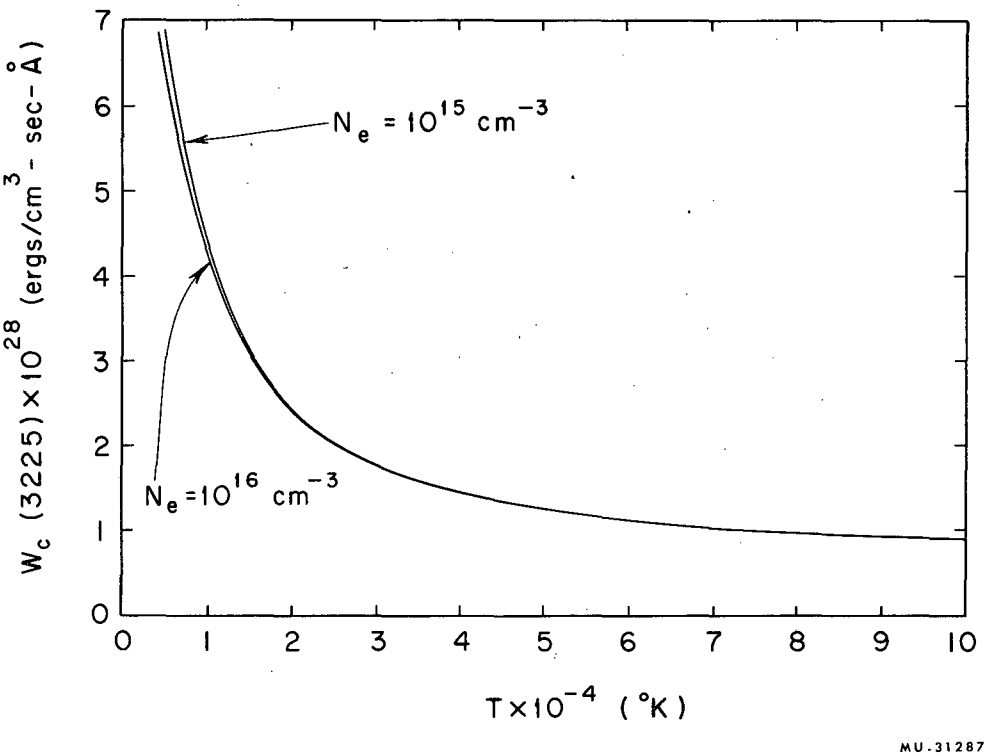

Fig. 15. Normalized continuum intensity $W_c(3225)$ at $\lambda = 3225$ Å as a function of temperature.

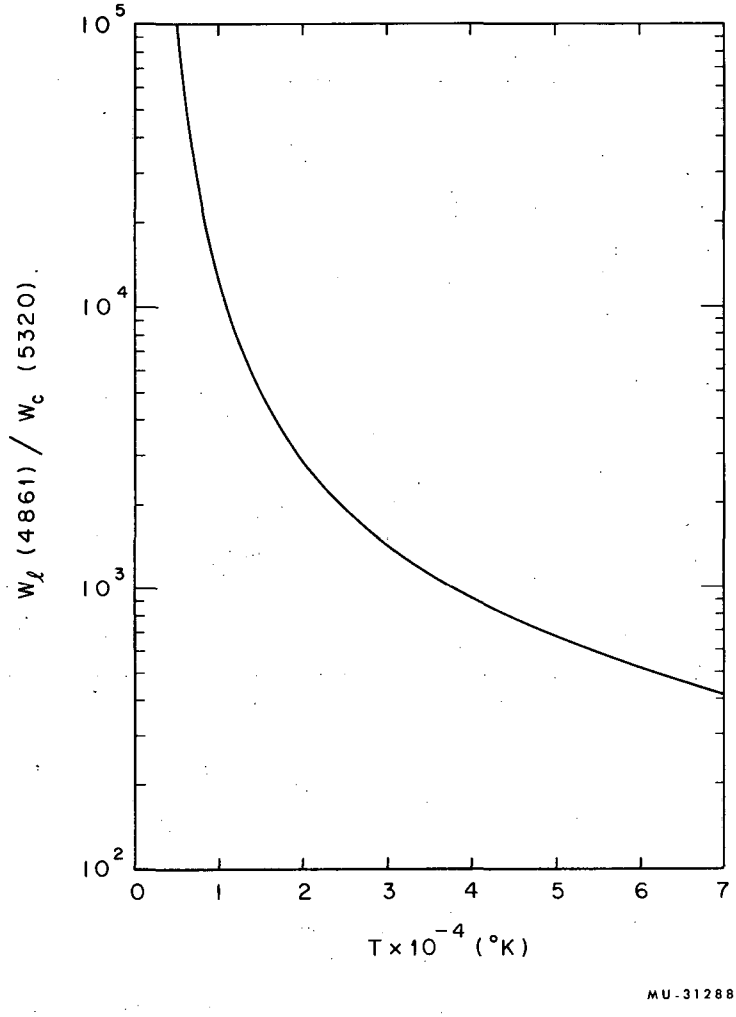

Fig. 16. Plot of $W_\ell(4861) / W_c(5320)$ as a function of temperature.

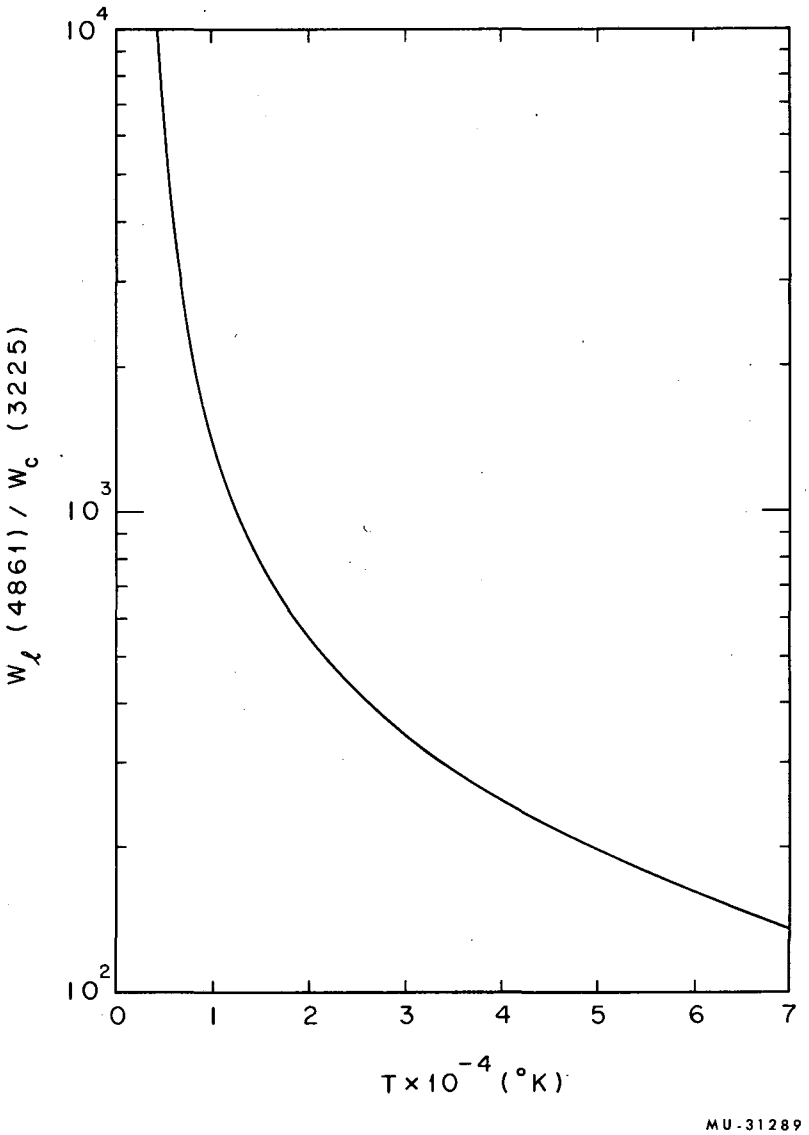

Fig. 17. Plot of $W_\ell(4861) / W_c(3225)$ as a function of temperature.

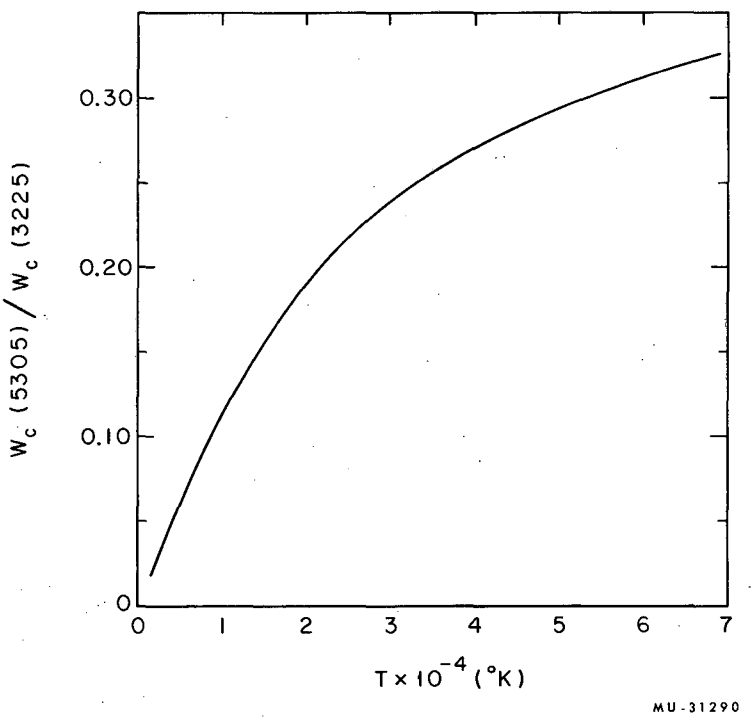

Fig. 18. Plot of $W_C(5320) / W_C(3225)$ as a function of temperature.

The third ratio, $W_c(5320)/W_c(3225)$, has the advantage that it does not depend on the knowledge of the population of an excited state, but depends only on the assumption of a Maxwellian distribution of energies of the free electrons. All three methods were used in temperature determinations in this thesis.

Similarly, if the temperature is known, an absolute intensity measurement at any wavelength will yield the ion density. A measurement of $W_c(5320)$ should yield the most precise value, owing to the particularly weak temperature dependence.

3. Continuum Radiation Due to the H^- Ion

A strong continuum radiation may result in partially ionized hydrogen plasmas from free-free and free-bound transitions of electrons in the residual field of the neutral hydrogen atom. These processes are described by

$$H + e \rightarrow H + e + h\nu \tag{45}$$

and

$$H + e \rightarrow H^- + h\nu \,, \tag{46}$$

with absorption coefficients $k^-_{\nu ff}$ and $k^-_{\nu fb}$, respectively. Using the methods developed in the last section for calculating the emission from a plasma in terms of the absorption coefficient, one can easily calculate the emission at a given wavelength due to these processes. It is convenient to relate this emission to the emission due to H, as calculated in the last section. The H^- continuum intensity is given by

$$W_c^-(\lambda) = \frac{k_\nu^- N_{H^-}}{k_\nu N_1^{eq}} W_c(\lambda) \,, \tag{47}$$

where $W_c^-(\lambda)$ is the emission per unit wavelength due to H^-, $W_c(\lambda)$ is the emission per unit wavelength due to H, k_ν^- is the total absorption coefficient of the H^- ion, N_{H^-} is the number density of H^- ions, and

N_1^{eq} is the number density of H atoms in the ground state, if we assume equilibrium conditions.

Because of the low ionization potential of the H^- ion (χ_{H^-} is only 0.7496 eV), in plasmas with electron temperatures of approximately 1 eV the density of H^- ions will be essentially in thermal equilibrium with the density of H atoms in the ground state. We may therefore use Saha's equation to relate N_{H^-} to the actual density of ground-state neutrals in the plasma, $N_1 = \rho(1) N_1^{eq}$. Equation (47) then becomes

$$W_c^-(\lambda) = \frac{k_\nu^- \rho(1) N_e}{k_\nu S(T)} W_c(\lambda) , \tag{48}$$

where S(T) from Saha's equation is

$$S(T) = \frac{N_1 N_e}{N_{H^-}} = \frac{2g_1}{g_{H^-}} \frac{(2\pi m_e kT)^{3/2}}{h^3} e^{-(\chi_{H^-}/kT)} . \tag{49}$$

The quantity $W_c^-(\lambda)/W_c(\lambda)\rho(1)N_e$ is shown in Fig. 19 as a function of temperature for the two continuum wavelengths 3225 Å and 5320 Å. In this calculation we have used the H^- free-free absorption coefficients of Ohmura and Ohmura[46] and H^- free-bound absorption coefficients of Chandrasekhar.[47]

It is apparent from Fig. 19 that if we assume an electron density of 3×10^{15} cm^{-3}, typical of our plasma, the H^- continuum will be much less than the H continuum at either wavelength, even for $\rho(1) = 1$, provided T is greater than 10,000 °K.

4. Broadening of the Balmer Lines

In a dense recombining hydrogen plasma, the Balmer lines are broadened primarily by the Stark effect. The radiating atom is very likely to find itself in a strong electric field, because of the presence of nearby ions and electrons. The existence of ions can usually be treated in the static approximation, in which the ions are assumed to be fixed during the radiation event. This theory was first developed by Holtsmark,[48] who computed hydrogen line profiles from a

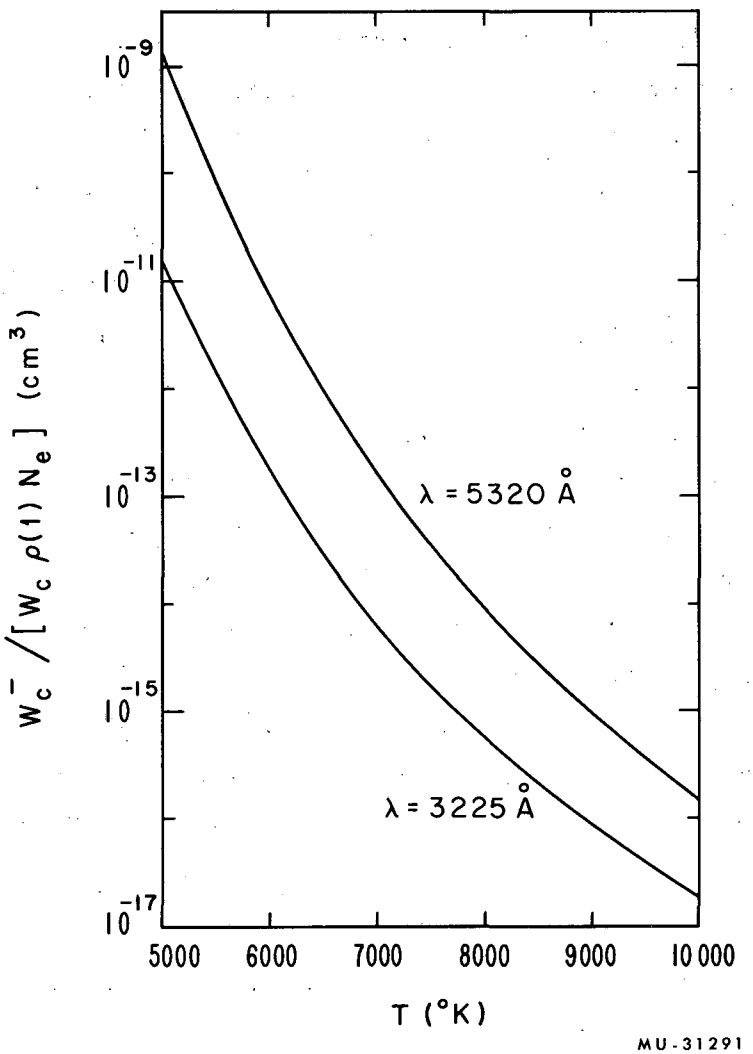

Fig. 19. Normalized ratio of H^- continuum to H continuum $W_c^-/[W_c\rho(1)N_e]$, as a function of temperature for two wavelengths.

field-strength distribution function derived from the "nearest-neighbor" approximation. The recent development of a generalized impact-broadening theory by Baranger[49] and Kolb and Griem[50] has permitted inclusion of important electron-broadening.

Calculations of accurate line profiles, described by Griem et al. are extremely complicated.[51] They have calculated profiles of the first two Lyman lines and the first four Balmer lines for a wide range of plasma properties.[52] More recently, they have published more accurate calculations of the H_β line profile.[53,54] These H_β profiles are expected to have an overall accuracy of about 15%, and agree very well with H_β line profiles recently determined experimentally by Wiese et al.[55]

The Balmer line profiles vary in width roughly as $N_i^{2/3}$ and are not strongly dependent on the temperature. Therefore they provide a useful means of determining the ion density in a hydrogen plasma. By measuring the line profile for a considerable distance on each side of the center of the line and comparing it with theoretical profiles, an accuracy of the order of 20% can be achieved in ion-density measurements.

The only other significant line-broadening mechanism in dense hydrogen plasmas is Doppler broadening. For the H_β line, the half-width in angstroms at half maximum due to Doppler broadening is

$$\Delta\lambda_D = 1.74 \times 10^{-3} \sqrt{T} . \tag{50}$$

The half-width in angstroms due to Stark broadening is approximately

$$\Delta\lambda_S = 7.3 \times 10^{-11} N_i^{2/3} . \tag{51}$$

We are then justified in neglecting Doppler broadening for

$$\frac{\Delta\lambda_D}{\Delta\lambda_S} = 2.4 \times 10^{7} \frac{\sqrt{T}}{N_i^{2/3}} \ll 1 . \tag{52}$$

We are probably safe in neglecting Doppler broadening in ion-density measurements for

$$\frac{\Delta\lambda_D}{\Delta\lambda_S} < 0.2 , \qquad (53)$$

especially if the line profile is observed for a considerable distance from the center of the line. (Doppler broadening affects primarily the central region of a Stark-broadened line.)

III. EXPERIMENTAL APPARATUS AND TECHNIQUES OF MEASUREMENTS

A. Apparatus for Plasma Production

The apparatus used to produce a plasma has been described in several publications,[27, 28, 56, 57] and is reviewed here only briefly. A schematic diagram of the apparatus is shown in Fig. 20. A hydrogen plasma is produced in a cylindrical copper tube 14.6 cm in diameter and 86.4 cm in length, closed at both ends by quartz plates and located in a uniform dc magnetic field of 16 kG. The tube is initially filled with hydrogen gas at a pressure of about 0.1 Torr. A lumped-constant pulse line charged initially to 10 kV is connected by an ignitron switch to a cylindrical molybdenum electrode concentric with the copper cylinder and located in the center of one of the quartz plates. The gas breaks down about 1.5 μsec after application of the high voltage, the current rising to a constant value of 6.7 kA in an additional 3 μsec and ionizing the gas between the electrode and the wall of the tube. This radial current, crossed with the axial magnetic field, exerts an azimuthal force on the plasma, causing the plasma to rotate. A well-defined ionization front develops and proceeds down the tube with a velocity, for the conditions in this experiment, of 4.85 cm/μsec. Such a phenomena has been called a "switch-on ionization wave" or "hydromagnetic ionizing wave," and has been investigated theoretically by Kunkel and Gross.[58]

If the current continues to flow after the ionization wave reaches the end of the tube, prominent spectral lines of impurities appear. The driving current is therefore shorted ("crowbarred") by the "crowbar" ignitron switch shown in Fig. 20 before the ionization front reaches the end of the tube. The voltage across the tube then drops to zero, while the direction of current flow reverses as the energy of rotation of the plasma is dissipated. Oscilloscope traces of the current into the tube and the voltage across the tube as a function of time on a typical shot are shown in Fig. 21.

After about 25 μsec the power input into the plasma is essentially zero, and the plasma begins to cool and decay. It was primarily during the decay period that the spectroscopic measurements were made.

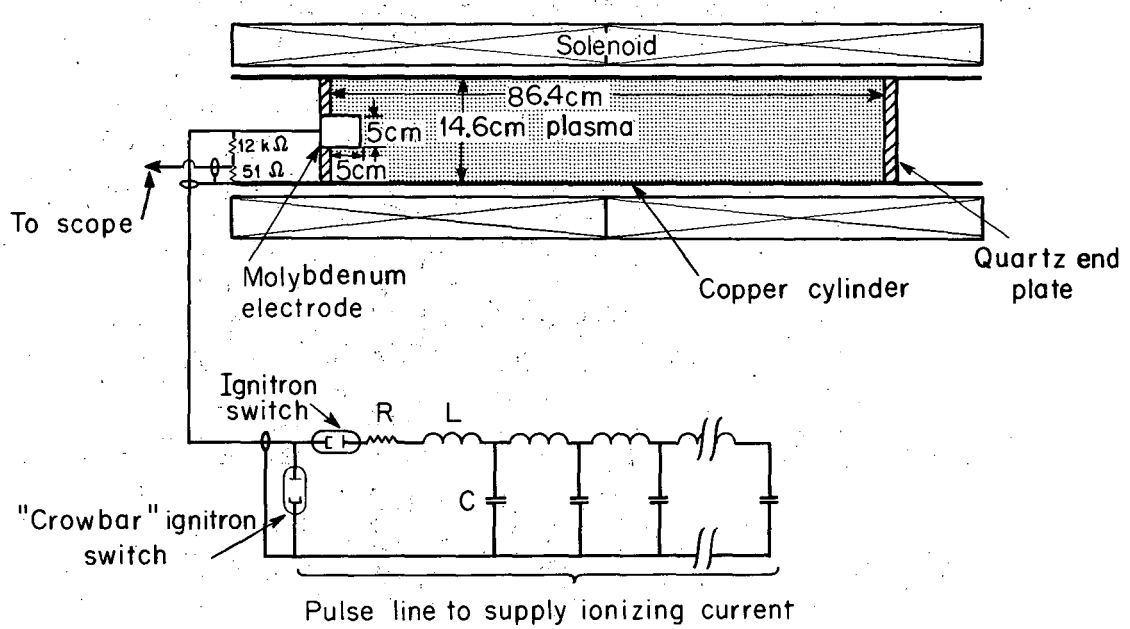

Fig. 20. Schematic diagram of the apparatus used to produce the hydrogen plasma.

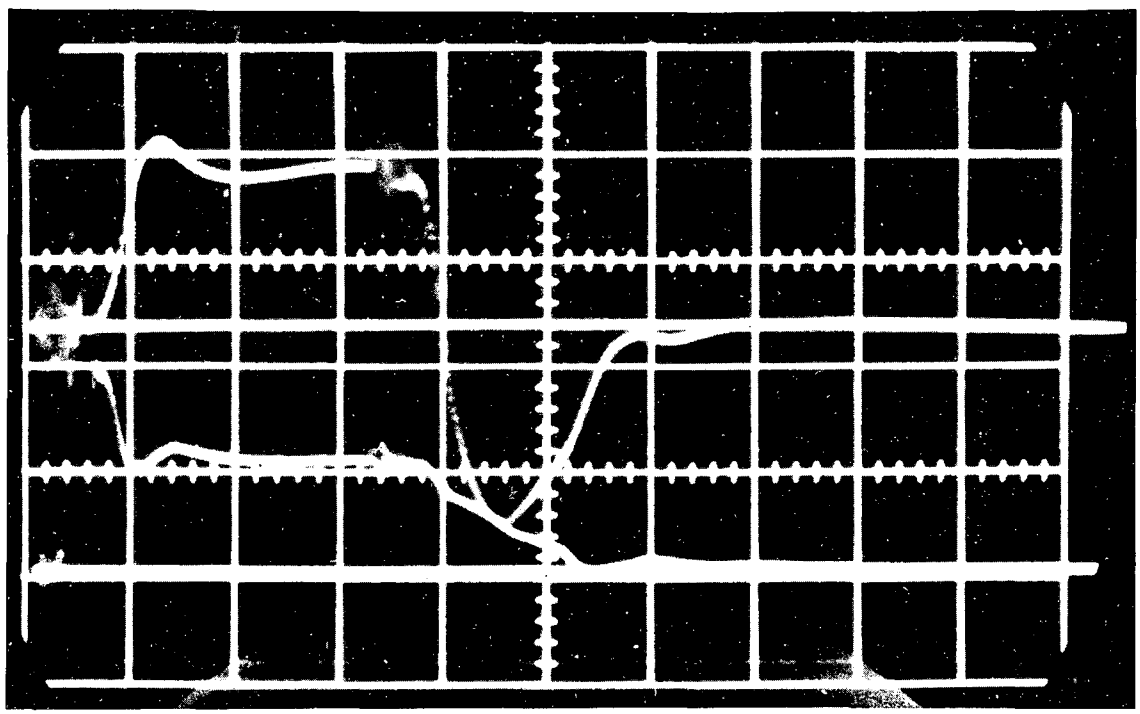

ZN-3830

Fig. 21. Oscilloscope traces of the current into the tube (upper beam; 4770 A/large division) and the voltage across the tube (lower beam; 4710 V/large division) as a function of time on a typical shot. The sweep speed was 5 μ sec/large division.

Wilcox et al. have shown that hydromagnetic "swirls" develop in the plasma after crowbar.[59] These swirls indicate macroscopic motion of a nonuniform plasma, and are obviously undesirable in a study of recombination. Fortunately they may be suppressed by the insertion of a conducting screen in the end of the tube opposite the electrode. The conductor constrains electric fields in the plane perpendicular to the axis of the tube to be zero and prevents motion of the plasma in directions perpendicular to the magnetic field. The decaying plasma then shows no evidence of motion during the decay period. All data in this thesis were taken with such a conducting screen in place.

B. Apparatus for Line- and Continuum-Intensity Measurements

Absolute measurements of the H_β line intensity and the two bands of continuum radiation were made by comparing the brightness of the plasma with the brightness of a carbon arc used as a radiation standard. Figure 22 shows the experimental arrangement. Radiation leaving the plasma through a 3/8-in.-diam hole in the conducting screen (made of 0.005-in.-thick copper "Lektromesh" with 25 lines to the inch) in the end of the tube is reflected by the small mirror and focused by a quartz lens onto the entrance slit of a Jarrell-Ash Model JA-7102 3.4-m plane-grating spectrograph. The system was accurately aligned by using a cathetometer so that the optical axis of the spectrograph was parallel to the axis of the copper tube. There were five holes in the screen, placed at radii of -1.3, 16, 33.5, 50, and 64.5 mm (the tube wall was at 73 mm). The small mirror could be moved on ways in the direction of the arrows, so that light from any of these five holes could be imaged onto the entrance slit of the spectrograph. The aperture at the lens was of such size that the grating of the spectrograph was almost fully illuminated.

Located in the focal plane of the spectrograph were three movable assemblies, each containing an adjustable exit slit and a mounting for a photomultiplier. They could be positioned to select various regions of the spectrum as close together as 400 Å in the first order.

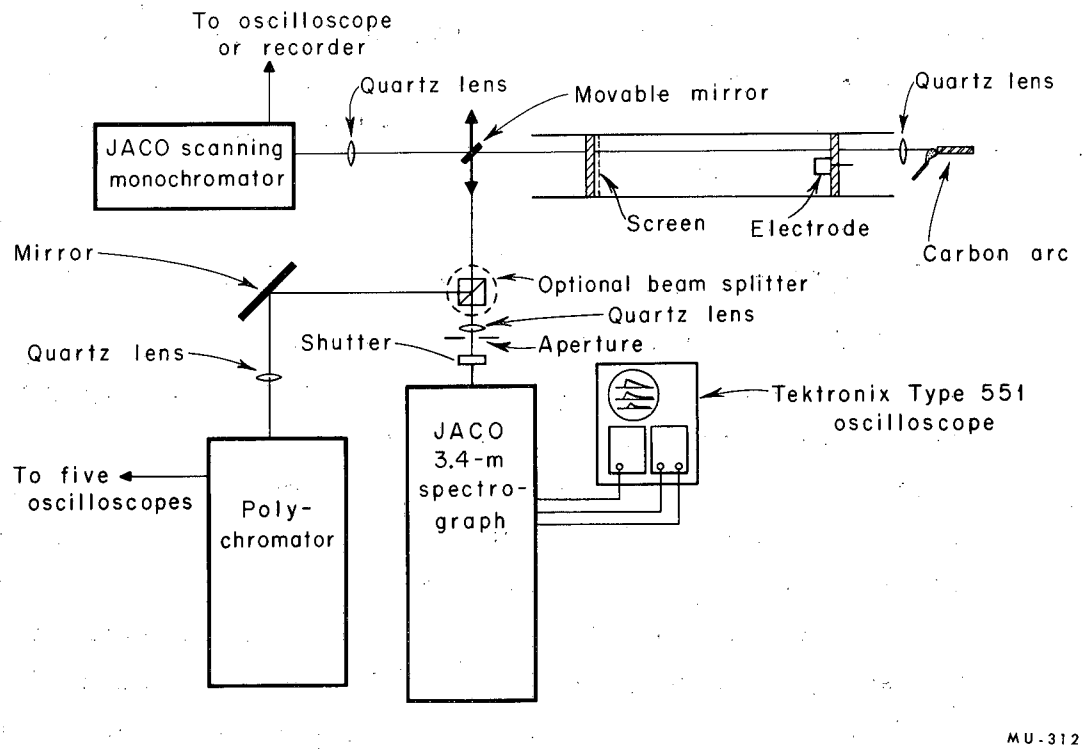

Fig. 22. Schematic diagram of the equipment used in making spectroscopic measurements.

For several reasons, EMI 6255B photomultiplier tubes were selected. The first dynode stage has a very large area available for collecting photoelectrons, because of the "venetian blind" dynode structure. Therefore, the quantum efficiency should vary very little over the central regions of the photocathode,[60] and the sensitivity of the tube should be almost constant across a wide exit slit. The tubes have high gain and very low dark currents. The quartz envelopes permit their use to below 2000 Å. Stability of gain over long periods was essential; these tubes were quite satisfactory in this respect during use. They also show very little tendency to "fatigue," or change gain when illuminated by a steady light.[61, 62] However, they show a slight tendency to change gain with temperature, the coefficient being about -1.3%/°C for blue light.

When observing very weak light signals with the photomultipliers, scattered light within the spectrograph may contribute to the signal. This was eliminated by placing filters in front of the photomultipliers. Interference filters were used in the case of the H_β line and the band of continuum in the visible, and a Corning Type 4-76 uv filter was used with the photomultiplier observing the band of continuum radiation in the uv. As the uv signal was observed in the second order of the diffracted spectrum, this filter also eliminated the overlapping first-order spectrum.

The gain of the tubes was kept constant during the course of an experiment by observing light pulses from an AR-4 argon lamp mounted within the spectrograph and used as a secondary standard. A small pulser connects a delay line charged by a very stable dc high-voltage supply across the lamp at a 60-cycle repetition rate, providing 50-nsec pulses of light from the AR-4 lamp. This device was developed by the Counting Research Group at this laboratory,[63] and has been used by them for similar purposes. The temperature coefficient of the lamp was measured and found to be about +0.1%/°C. Every 15 or 20 minutes during the course of the experiment the lamp was turned on, and the filters in front of the photomultipliers were swung out of the way, permitting an unobstructed view of the lamp by all three

photomultipliers. The peak amplitudes of the signals from the photomultipliers were measured by comparison with a standard reference voltage using a Tektronix Type 551 oscilloscope and a Type Z calibrated differential comparator plug-in unit. If the signal amplitude differed from the previous reading, the voltage on the photomultiplier was adjusted manually to repeat the previous reading. A coaxial switch permitted monitoring each photomultiplier in turn. By using this system, the gain of the tubes could be kept constant to about 1% during the course of an experiment. Without this system of monitoring the gain of the tubes, the gains might change 5 to 10% during the course of a several-hour-long experiment, because of a steady increase in the room temperature. When not in use, the lamp was turned off and the signal lead to the oscilloscope disconnected.

The photomultipliers were shielded against the fringing field of the solenoid by two layers of soft steel tubing and one of mu metal. With the AR-4 lamp as a reference, the change in gain of the tubes when the magnetic field was turned on could be observed, and was minimized by rotating the tubes in their mounts about their longitudinal axes. The small residual gain change, not over 2.5% in any case, was taken into account in the data analysis. These precautions were necessary because the arc could not be made to run properly with the magnetic field on.

In observing the plasma, the signals from the photomultipliers were displayed on two Tektronix Type 551 oscilloscopes used with one Type L and one Type CA dual-beam preamplifier each and photographed on Polaroid film. All three signals were displayed on both oscilloscopes, permitting the same signals to be viewed at different gains and sweep speeds. The time bases of the two oscilloscopes were calibrated by using a Tektronix Type 180A Time-Mark generator. Before each experiment, all preamplifiers were calibrated by using the built-in calibration voltage of one of the oscilloscopes. For more precise reading of the Polaroid pictures of the oscilloscope traces, the signals, which were quite "grassy" in some cases due to the low light levels, were filtered by a simple RC network consisting of a 5.1-kΩ-load

resistor shunted with a 400-pF capacitor. The time constant of this combination was 2 μsec, which was shorter by a factor of 50 than the decay time of any light signal observed from the plasma and so could not introduce significant errors in the measurements. Light signals on three consecutive shots are shown in Fig. 23.

A carbon arc was used as a radiation standard. Euler[64-67] has shown that the anode of a suitably operated carbon arc reaches a temperature of 3995 °K and has an emissivity of about 0.75, which varies slightly with wavelength. Further details concerning the use of a carbon arc as a radiation standard are given in Appendix C. The anode spot of the arc was focused by a second quartz lens onto the hole in the screen at 33.5-mm radius at the end of the tube, and from there by the first lens onto the entrance slit of the spectrograph. Before calibration, the quartz plate supporting the electrode was removed. The light path from the screen to the photomultipliers was then identical, whether the plasma or the arc was being viewed. The transmission of the lens used to image the arc onto the screen must be known; this can be calculated with sufficient accuracy from the transmission and index of refraction of fused quartz. The brightness of the arc image can then be calculated from the temperature and emissivity of the carbon anode, and the brightness of the plasma can be determined in principle by a direct comparison.

Without suitable precautions, however, the brightness of the arc image cannot be compared directly to the brightness of the plasma, since the plasma emits a short pulse of light, and the arc is dc. Furthermore, at some wavelengths there is a great disparity in intensity of light from the arc compared to that from the plasma. To make direct comparisons possible, a shutter was used to obtain a 4-msec pulse of light from the arc with a 200-μsec risetime, and the resistors in the divider string supplying voltages to the last several dynodes of the photomultipliers were shunted with large (up to 1 μF) capacitors to reduce gain changes during a long light pulse. The values of the capacitors were chosen so that the change in gain upon viewing a step of light giving an anode current of 1 mA (which was never exceeded when

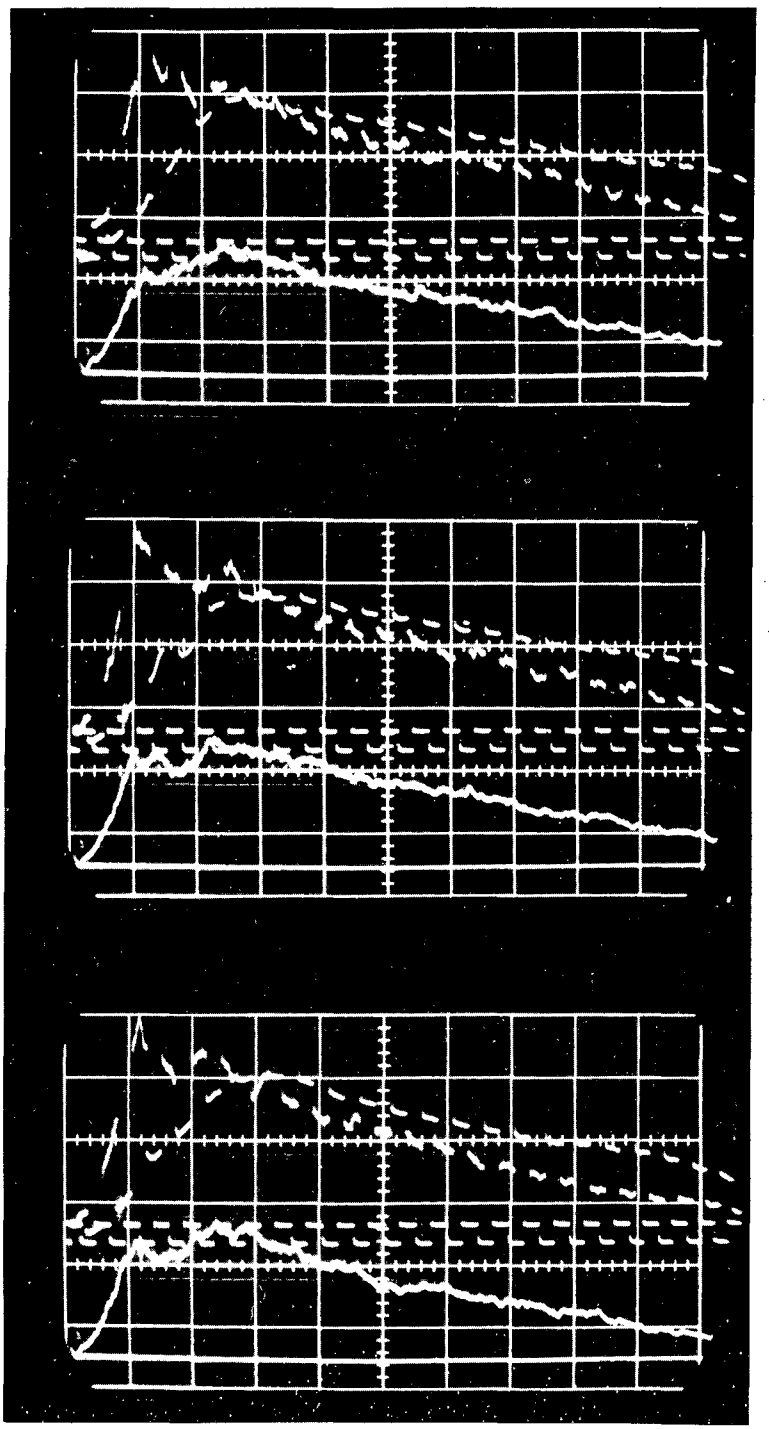

ZN-3831

Fig. 23. Light signals on three consecutive shots. The upper trace shows the continuum intensity at 5305 Å. The middle trace shows the $H\beta$ line intensity. The lower trace shows the continuum intensity at 3225 Å. The sweep speed was 20 μsec/cm.

either the arc or the plasma was viewed) was less than 2%/msec. This was verified experimentally. The gain of the tubes could therefore change by only an insignificant amount during either the duration of the plasma light pulse or the early part of the arc light pulse. The arc is much brighter than the plasma at 5320 Å, necessitating the use of an optical attenuator (a Wratten No. 96, N. D. 1.00 filter, the transmission of which was measured in a separate experiment) to reduce the arc signal to below 1 mA. With the use of this filter, the difference in intensity between the arc signal and the peak intensity of the plasma signal at a given wavelength was never more than a factor of 10. The output of the photomultipliers was determined experimentally to be proportional to the light input to within 5% over a range of three decades in intensity. With all of these precautions, the photomultipliers could be trusted to give valid comparisons of the brightness of the arc to that of the plasma with a maximum error of about 5%.

The short- and long-term stability of the entire system can be determined by repeated measurements of the signals from the arc at the three wavelengths. A series of five or six consecutive measurements of the arc signal shows a fractional rms deviation of about 1% at all wavelengths. This is probably due to actual time variation in brightness of the arc. The long-term stability of the entire system was determined by repeating this type of measurement six times during a period of two weeks. The average intensity (averaged each time over six consecutive shots) showed a fractional rms deviation during the 2-week period of about 3% at all three wavelengths, and showed no indication at all of a drift.

C. Apparatus for Line-Profile Measurements

The profile of the H_β line was determined as a function of time by means of an 18-channel "polychromator." The predecessor of this instrument has been described by Spillman et al.[68] The instrument consists of a Jarrell-Ash Model 82-000 monochromator, modified by the addition of two cylindrical lenses to give greatly increased linear dispersion. Eighteen narrow lucite light pipes in the focal plane slice

the spectral line image and pipe the light to as many 1P21 photomultipliers. The positions of the channels in wavelength may be determined by scanning a narrow spectral line from a Geissler tube across the light pipes, using the grating drive of the monochromator. The relative sensitivities are determined by viewing a continuous source such as the carbon arc or a tungsten lamp with all channels simultaneously. Five Tektronix Type 551 dual-beam oscilloscopes equipped with 2 Type L and 8 Type CA (dual-channel) preamplifiers were used to record the data on Polaroid film.

The Polaroid pictures were read on a semi-automatic data-processing machine developed for use in analysis of bubble-chamber pictures. This machine punched out the coordinates of points on the oscilloscope trace and fiducial marks on IBM cards. The data in this form, together with the spacing and relative sensitivities of the channels, were fed into an IBM 7090 computer, which calculated experimental line profiles as a function of time and selected a matching theoretical profile (using a two-dimensional least-squares fitting procedure). Theoretical calculations of the H_β profiles by Griem et al.[53] were used. The profiles were also plotted and photographed on the cathode-ray-tube output of the IBM 7090.

IV. EXPERIMENTAL RESULTS AND DISCUSSION

A. Choice of Wavelengths for Observation

In selecting regions of the spectrum for observations of the intensity of the continuum relation, the wavelength and bandpass must be chosen such that no lines contribute appreciably to the signals observed, when viewing either the plasma or the arc. Faint line radiation in the spectrum of the plasma may originate from molecular hydrogen or impurities; in the spectrum of the arc, from molecules (C_2 and CN, principally) or impurities in the arc plasma. Spectrographic plates of the arc spectrum taken with the 3.4-m spectrograph showed prominent CN-band radiation extending into the uv to about 3300 Å due to the CN violet system, with bandheads at 3583.9 Å, 3585.9 Å, and 3590.4 Å. The uv continuum wavelength was chosen arbitrarily below this wavelength in an apparently "clean" region of the arc spectrum around 3225 Å. A scan of this region of the arc spectrum with the small Jarrell-Ash Model 82-000 scanning monochromator shown in Fig. 22 verified that there were no lines in the region 3220 to 3230 Å brighter by more than a few per cent than a bandwidth of 0.3 Å of the continuum. Similar results were obtained for a region between 5300 and 5330 Å, and between 4830 and 4890 Å. All these observations were consistent with direct measurements of the intensity of the arc plasma radiation in these regions of the spectrum by viewing the arc first end-on and then side-on. No measurements indicated a contribution of more than 1.5% from the arc plasma to the brightness of the arc within these wavelength limits, by either line or continuum radiation.

Line radiation from the plasma of comparable brightness to the continuum radiation was generally too faint to detect photographically with reasonable exposure times. The regions of the plasma spectrum already shown to be free from extraneous radiation in the case of the arc were scanned by using the small monochromator. The wavelength was changed every third shot. Several very faint and unidentified lines were found in this manner in the regions of the spectrum of interest, but it was possible to avoid them. The region of the spectrum around H_β was not observed. Possible errors in the continuum intensity

measurements due to the presence of faint lines were estimated from a statistical analysis of the data. The wavelengths and bandwidths finally chosen, together with estimates of possible errors caused by faint undetected lines, either in the plasma spectrum or the arc spectrum, are given in Table I.

Table I. Wavelengths and bandwidths used, with estimates of the maximum possible error due to unwanted line radiation from the plasma or from the arc.

Channel	λ (Å)	Bandwidth (Å)	Maximum error due to lines (%)	
			From the plasma	From the arc
1	5305	11.5	3.0	1
2	4861.3	50	--	1
3	3225	4.0	3.5	1

B. Estimate of Longitudinal Uniformity by Side-on Observations

Most of the spectroscopic observations were made by looking into the end of the tube, and so yielded values of electron density and temperature averaged in some sense along the line of sight. It was imperative therefore to make some estimate of the longitudinal uniformity of the plasma. The longitudinal uniformity of this particular plasma was already suspect, as Kunkel and Gross[58] showed that a hydromagnetic ionizing wave of the type used to produce this plasma is compressive and must necessarily be followed by a rarefaction wave.

To investigate the longitudinal uniformity of the plasma, we drilled five 1/2-in.-diam holes in the side of the tube, and sealed them with thin quartz windows. A mirror mounted at an angle of 45 deg on a movable carriage allowed light from any of the five holes to be reflected out to a detector along a line parallel to the axis of the tube. The detector consisted of an RCA 1P21 photomultiplier and an interference filter. To make relative density measurements as a function of axial position, an interference filter having a bandpass of 9 Å

centered at 5305 Å was used. The temperature was already known from preliminary measurements to be about 10,000°K. We see from Fig. 14 that the light intensity at this wavelength should be very nearly proportional to the square of the ion density and roughly independent of temperature. At each window five shots were taken, the intensities averaged at a number of different times, and the square root of the average intensity (corrected for geometrical effects) plotted against axial position. The resulting profiles (which should be proportional to N_i, averaged in some way over the tube diameter) are shown in Figs. 24 and 25.

At 20 μsec the hydromagnetic ionizing wave is still proceeding down the tube. The variation in ion density behind the ionizing wave is of the order of 25%. A sharp jump occurs in the ion density at the end of the tube at 40 μsec, when the ionizing wave strikes the screen. We would expect such a perturbation in the ion density to disappear in roughly the time for an acoustic wave to travel the length of the tube. Calculating the transit time of a sound wave at the prevailing temperature of the plasma early in time, about 15,000 °K, from the formula for the acoustic wave velocity given by Spitzer,[69] we obtain a time of 43 μsec. The nonuniformity of the density has indeed practically disappeared by 80 μsec! After 80 μsec, the density seems to be uniform along the axis to within about 15% .

Temperature measurements as a function of axial position and time are more ambiguous. Measurements similar to those described above were also made looking at the H_β line. One can estimate the temperature variation along the axis by dividing the average (again averaged over five shots) H_β intensity (arbitrary units) at a given time and axial position by the corresponding average intensity at 5305 Å , giving $W_\ell(4861)/W_c(5305)$ in arbitrary units and averaged in some way over the radius. These ratios were then normalized to the ratio obtained by averaging over radius the (absolute) temperature measured from end-on observations (described in the next section), and "temperatures" were derived from the resulting ratios. The absolute values of these "temperatures" are unreliable, and will not be

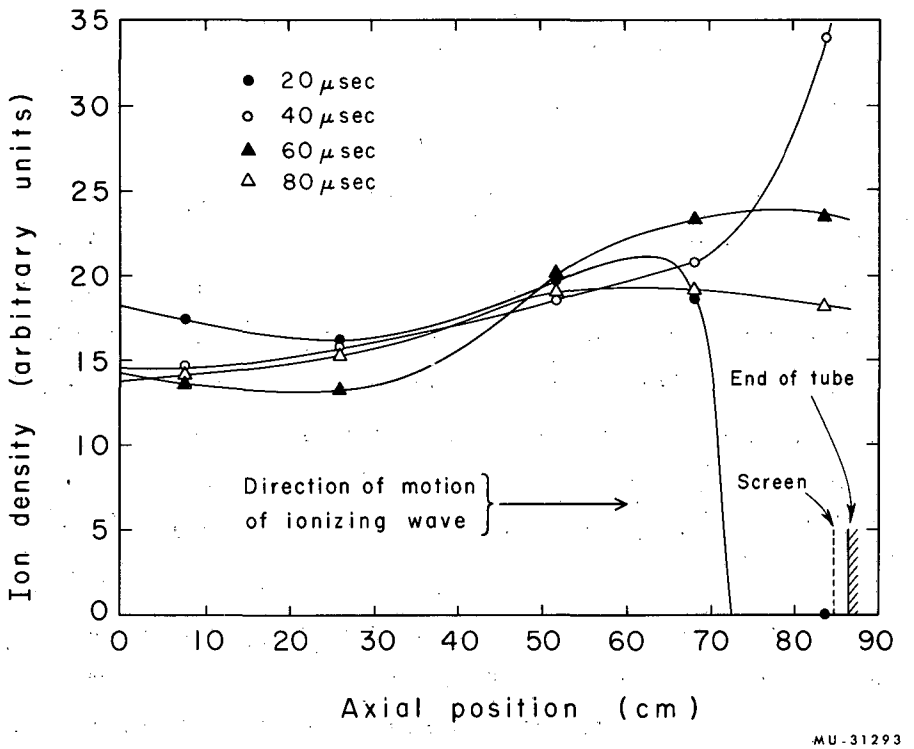

Fig. 24. Ion density (arbitrary units) as a function of axial position at four times.

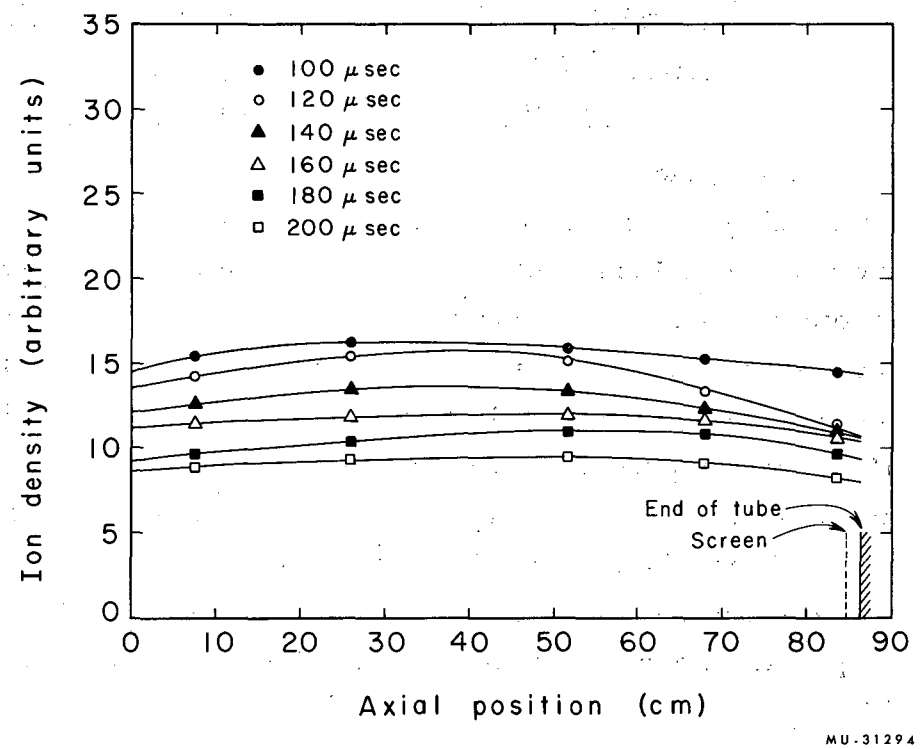

Fig. 25. Ion density (arbitrary units) as a function of axial position at four times.

quoted; however, after 80 μsec, the "temperatures" so derived showed less than 20% variation with length.

These rather crude measurements suggest that the density and temperature of the plasma are probably constant along magnetic field lines to within 20% from 80 to at least 200 μsec.

C. Comparison of the Ion Density as Measured by Stark Broadening of the H_β Line and by the Absolute Intensity of the Continuum at 5320 Å

Using the polychromator, we simultaneously measured the broadening of the H_β line, the absolute intensity of the H_β line, and the absolute intensity of a 5-Å band of continuum centered at 5320 Å (another region checked and found free from line radiation). These measurements were made looking end-on at a radius of 35 mm, using the beam splitter shown in Fig. 22. The H_β line profile at 50, 100, 150, and 200 μsec on a typical shot are shown in Figs. 26, 27, 28, and 29, respectively, together with computer-selected "best fit" theoretical profiles of Griem et al.[53] A temperature of 20,000°K was assumed in the curve fitting. One channel of the polychromator was inoperative; hence only seventeen points are shown on each line profile.

Agreement between the experimental points and the best-fit theoretical profile is generally very good. We have never observed the dip which theoretically should occur in the center of the H_β line profile. It is very likely that the dip is filled in by radiation from low-density regions in the plasma boundary, or is smeared out by Doppler broadening. The curves have not been corrected for Doppler broadening or instrumental broadening, both which are small, however, compared to the Stark broadening. An estimate of reabsorption, based on a comparison of the intensity at the center of the H_β line to the intensity of a black body radiating at the plasma temperature, indicates that the intensity at the center of the line may be reduced as much as 10% due to reabsorption at 200 μsec, and less at earlier times. This small amount of reabsorption, affecting only the center

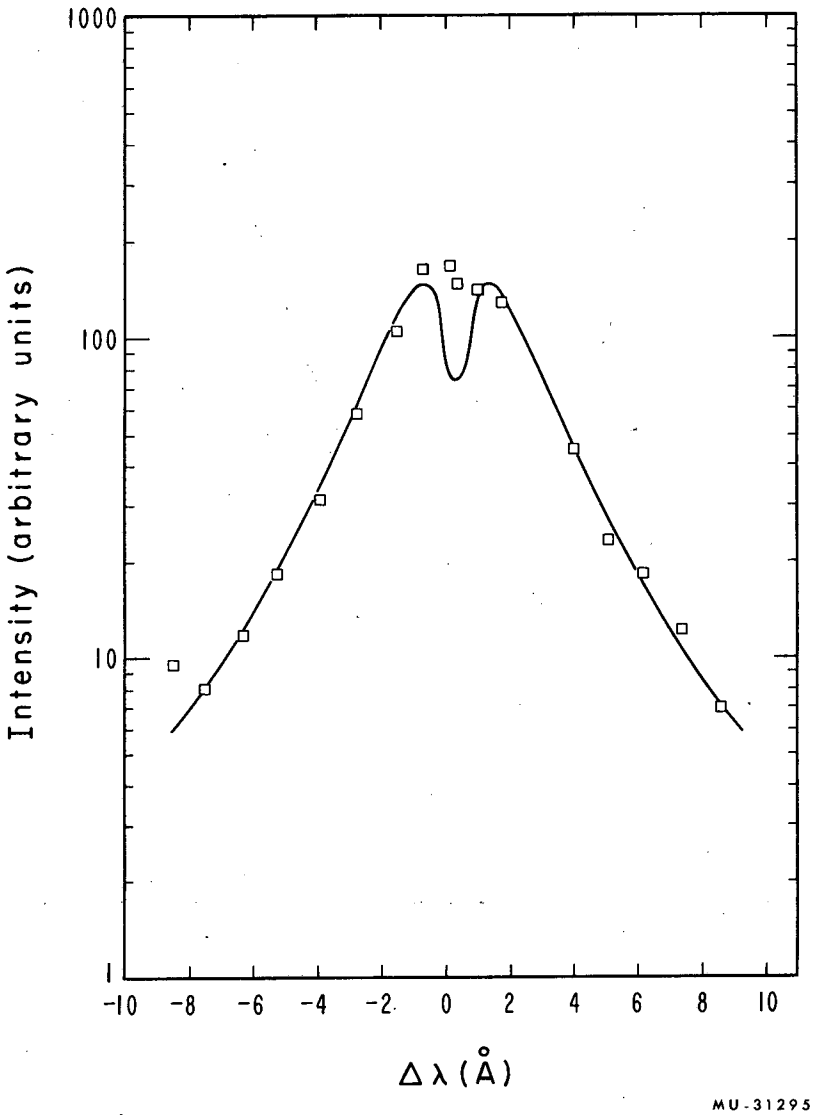

Fig. 26. H_β line profile at 50 μsec on a typical shot. The solid line is a computer-selected "best-fit" theoretical profile.

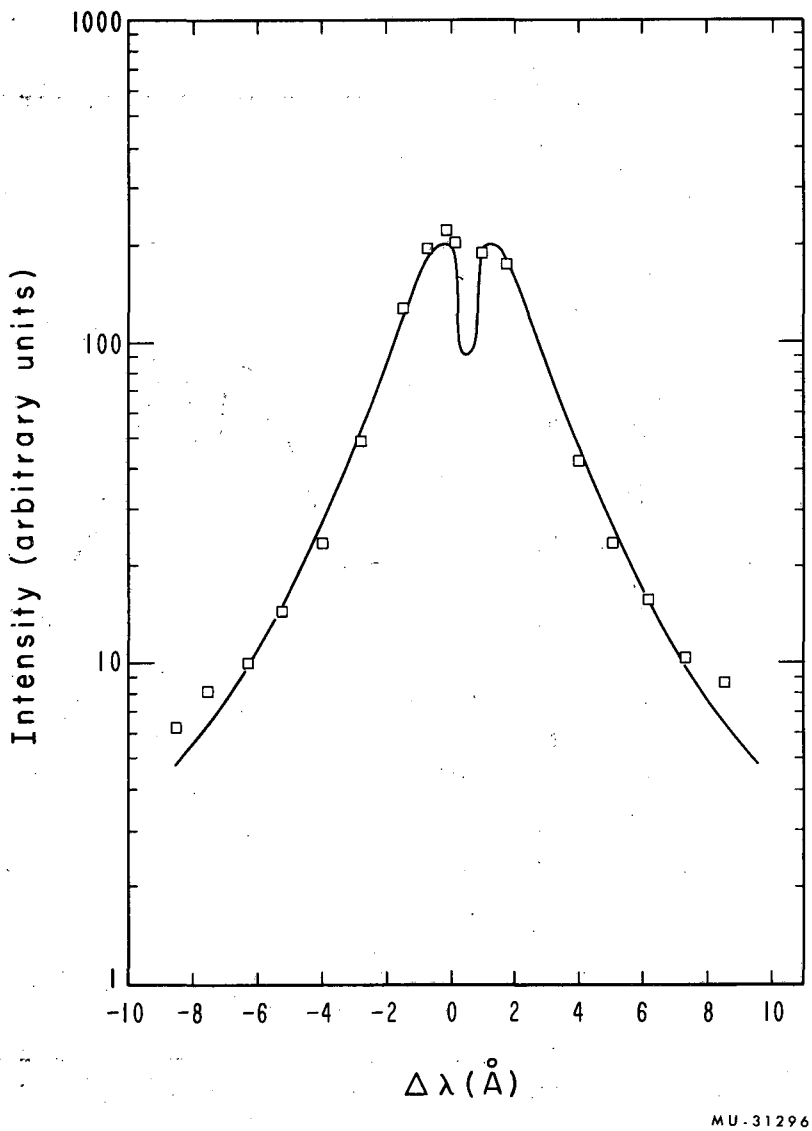

Fig. 27. The H_β line profile at 100 μ sec.

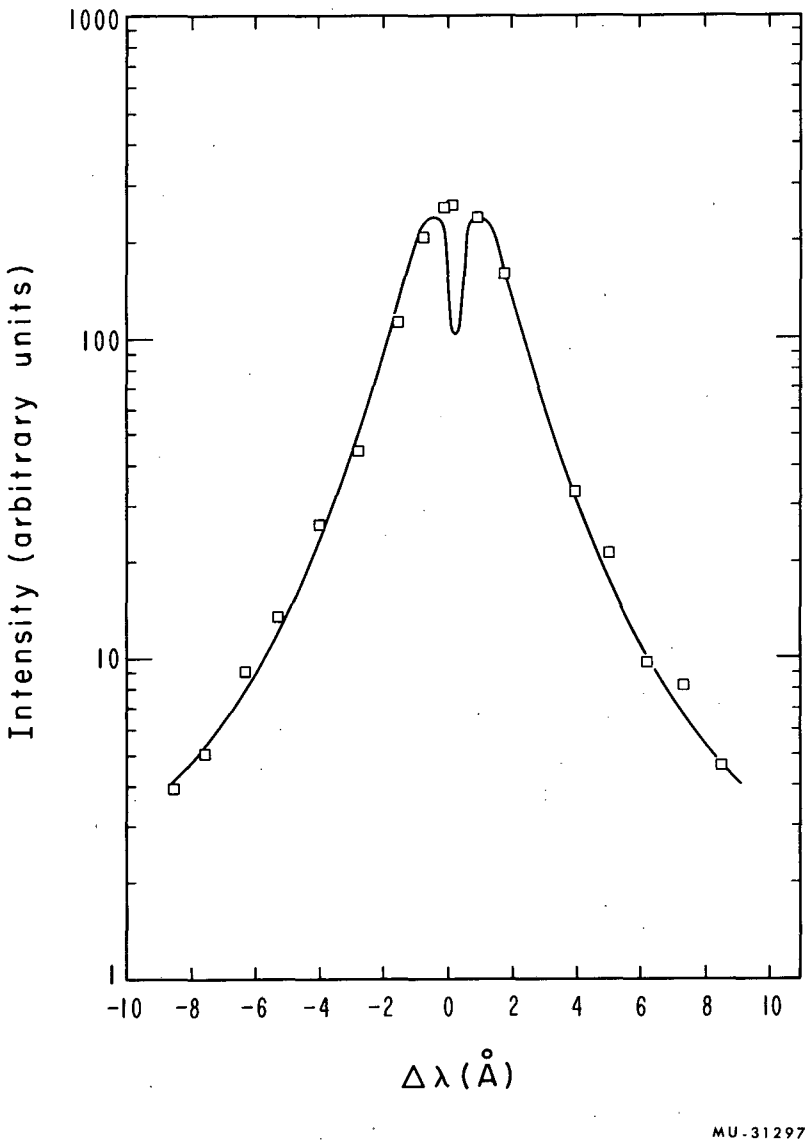

Fig. 28. The H_β line profile at 150 μ sec.

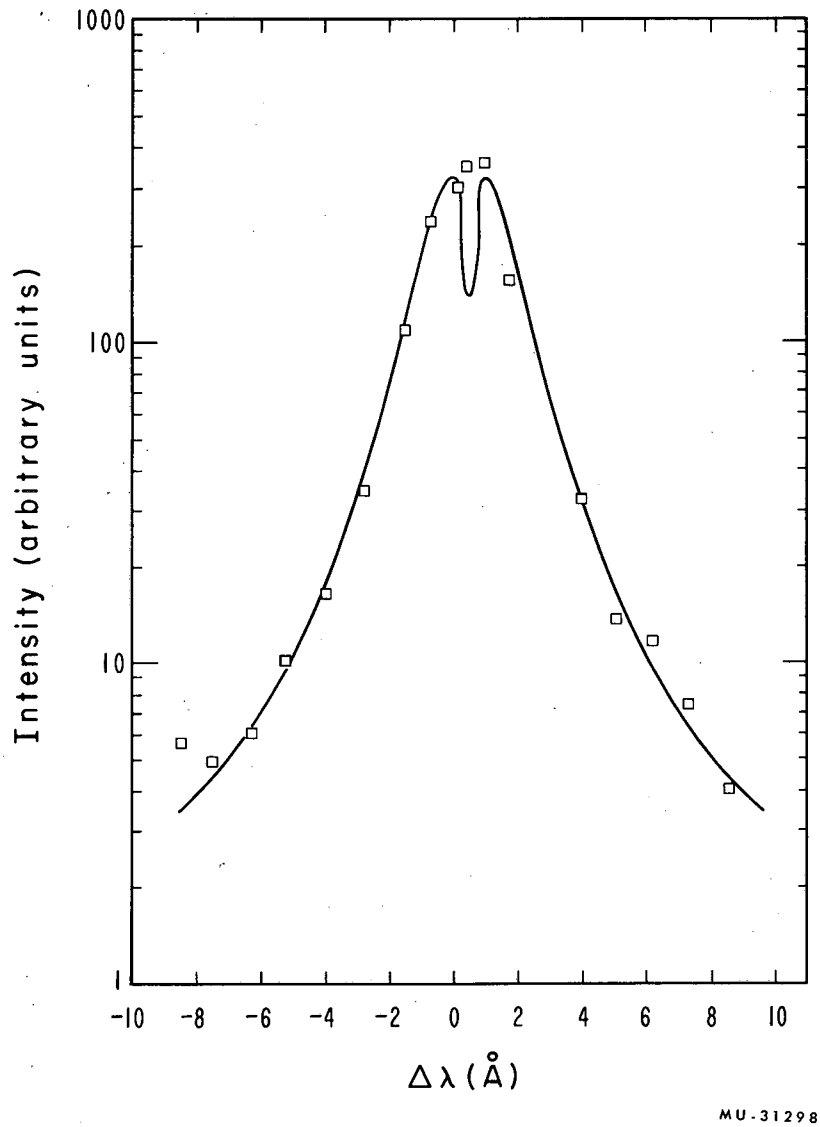

Fig. 29. The H_β line profile at 200 μ sec.

of the line, would have a negligible effect on the value of ion density from the line profiles. The slight axial inhomogeneity present after 80 μsec probably also would have no visible effect on the line profiles.

The temperature as a function of time was calculated on the same shot from the ratio of the H_β line intensity to the intensity of the band of continuum radiation. From these values of the temperature and of the absolute intensity of the continuum radiation at 5320 Å, the ion density was calculated for the same times on the same shot, using Fig. 14 .

Figure 30 shows the ion density measured by the two methods as a function of time for this particular shot, with estimated errors. The values of the ion density determined from the line profiles have been corrected for $T \neq 20{,}000°K$ (about a 10% correction). The two values of ion density agree in each case within the experimental errors. On this and other shots, there seems to be about a 20% discrepancy between the two values of ion density, but this is probably not too significant. A number of refinements of experimental technique, particularly those dealing with the operation of the photomultipliers, were not yet in use when these data were taken. These would affect primarily the absolute line- and continuum-intensity measurements. In fact, the ion densities derived from these polychromator measurements agree almost exactly with the densities derived from more accurate absolute line- and continuum-intensity measurements made 7 months later and reported in the next section. Agreement between the two measurements of the ion density is therefore probably even better than indicated in Fig. 30.

On the basis of this generally satisfactory agreement of the two methods, it was decided to make all further ion-density measurements by absolute continuum-intensity measurements. The ion-density measurements using the polychromator are more nearly foolproof, but are potentially less accurate and require much more data reductions.

D. End-on Measurements of the Electron (Ion) Density as a Function of Time at Different Radii

The electron density and temperature were determined as functions of time at five radii (corresponding to the locations of the holes in

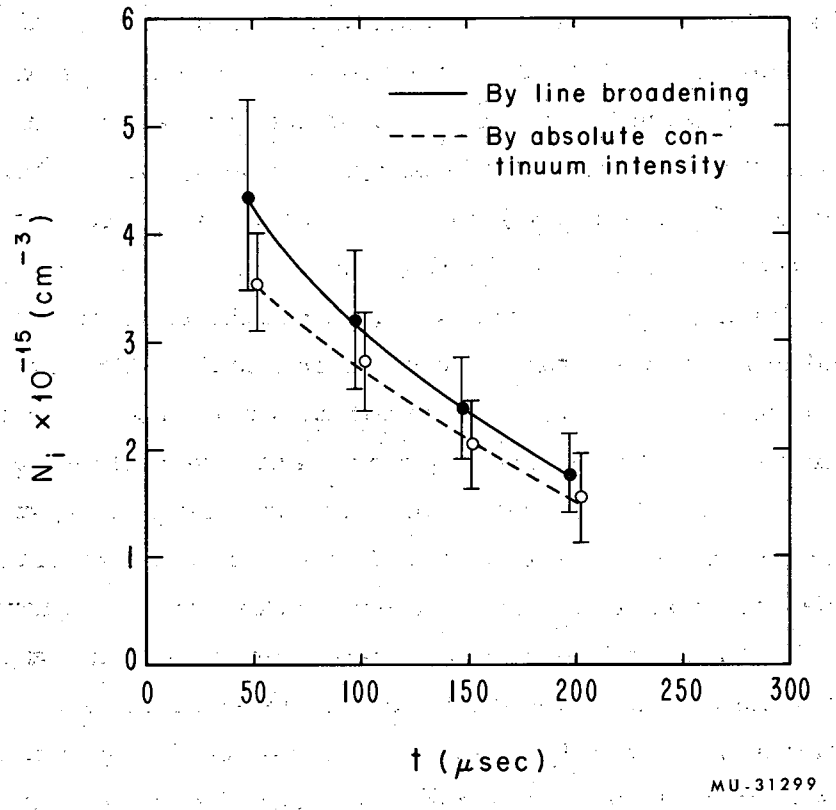

Fig. 30. Ion density as determined by measurements of Stark broadening and absolute continuum intensity on a single shot. Estimated errors (standard deviations) are shown.

the copper screen), from measurements of the absolute intensity of the H_β line and of the two bands of continuum radiation at 5305 Å and 3225 Å listed in Table I. The volume of plasma observed was approximately that of a long tapered truncated prism, parallel to the axis of the tube, and with 1- by 10-mm and 5- by 10-mm bases. At each radius and time, three temperatures were calculated from the three possible different ratios of intensities. We distinguish the three temperatures, for simplicity, by the following notation:

$T(\ell/v)$: the temperature as measured from the ratio of the H_β line intensity to the visible continuum intensity

$T(\ell/uv)$: the temperature as measured from the ratio of the H_β line intensity to the ultraviolet continuum intensity

$T(v/uv)$: the temperature as measured from the ratio of the two continuum intensities.

These temperatures as a function of time at each radius are shown in Fig. 31. Each point is an average of six shots. Agreement between the three temperature measurements at a given time and radius is generally very good, indicating small systematic errors. Considerable discrepancies -- a factor of 2 or more -- exist late in time, however, in the temperature measurements nearest the wall of the tube ($r = 50$ and 64.5 mm). There are three possible reasons for these discrepancies: (1) the population of the upper level of the line may not be in equilibrium with the free electrons, $[\rho(4) < 1]$; (2) the H_β line may be partially reabsorbed, leading to an error in the measurement of the population of the $n = 4$ level; and (3) there may be a significant contribution to the continuum intensity, especially in the visible, because of the H^- ion. Before discussing these possibilities, we can easily estimate the temperature when one or more of these disturbing effects are present by simply plotting the temperature at a given time versus radius, assuming the temperature to be zero at the tube wall, and interpolating. The dashed portions of the curves in Fig. 31 were obtained this way. One may also use the data to find the ion density as a function of time at the five radii. The results are shown in Fig. 32. All points (averages of

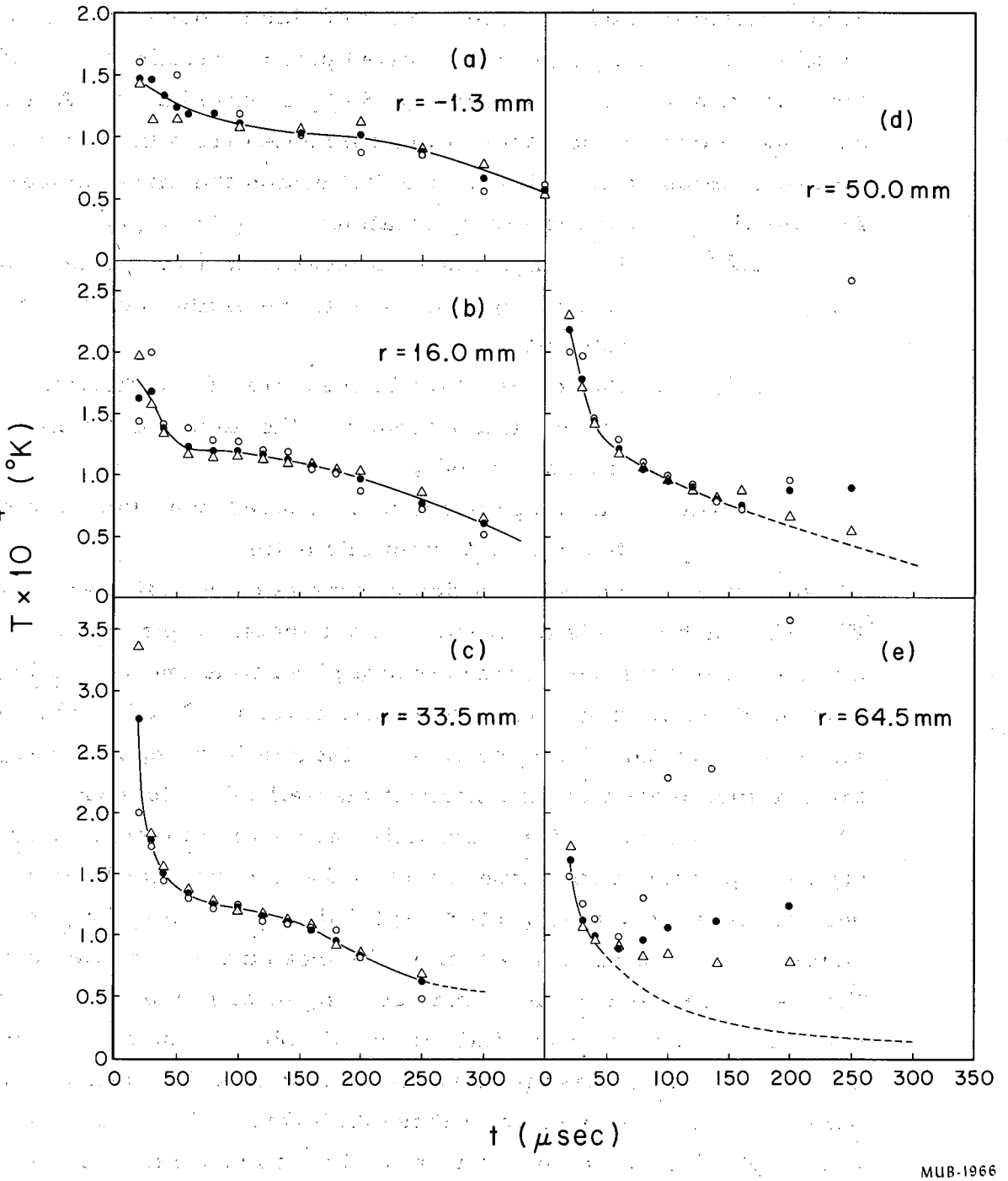

Fig. 31. Three temperature determinations from the three intensity measurements, T(ℓ/v), T(ℓ/uv), and T(v/uv) as a function of time at five radii, looking parallel to the axis of the tube. Each point is an average of six shots.

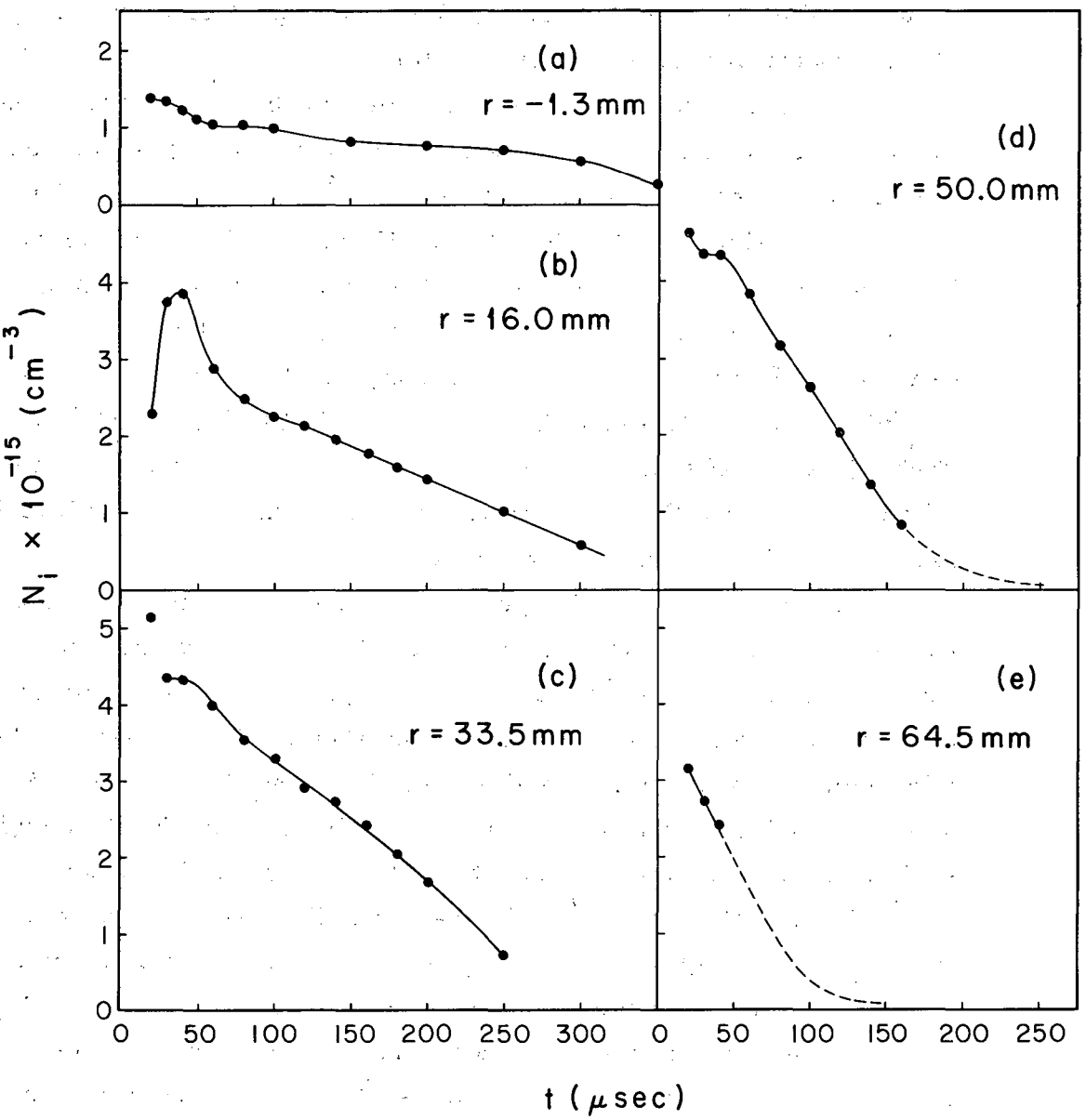

Fig. 32. Ion density (determined from absolute intensity measurements at $\lambda = 5305$ Å) as a function of time at five radii, looking parallel to the axis of the tube. Each point is an average of six shots.

six shots, again) except those late in time in Figs. 32d and e were obtained from measurements of the absolute intensity of the visible continuum radiation. As in Fig. 31, the dashed portions are inferred from other measurements and by interpolation.

We now discuss the discrepancies in the temperature measurements, in particular those shown in Fig. 31e. Using population coefficients calculated by Bates and Kingston,[13] and assuming unfavorable plasma conditions of $T = 4000°K$ and $N_e = 10^{14}$ cm^{-3}, we conclude that in a recombining plasma opaque to the Lyman lines, $\rho(4) \geq 0.8$. This reduction in population of the level from the equilibrium value then causes a 20% error in the line intensity which is reflected as $a \leq 5\%$ in $T(\ell/v)$, and a $< 10\%$ error in $T(\ell/uv)$, with $T(\ell/uv) > T(\ell/v) > T$. $T(v/uv)$ is not affected. As the observed discrepancies are much larger than 5 to 10%, it is unlikely that they are caused primarily by a lack of equilibrium in the $n = 4$ level.

Discrepancies in $T(v/uv)$ can only be explained by the assumption of a source of continuum radiation in addition to that due to the H atom. The most likely candidate is the H^- ion. From Fig. 19 we can estimate the importance of the H^- continuum with respect to the H continuum. Using Fig. 19 and values of T and N_e shown in Figs. 31e and 32e ($r = 64.5$ mm), we estimate that the H^- continuum should become noticeable at this radius (equal to 10 to 20% of the H continuum) between 80 and 100 μsec. The "break" in $T(v/uv)$ actually occurs before this time, at roughly 60 μsec. It is difficult to more accurately estimate the intensity of the H^- continuum, as it depends on T, N_e, and N_1, none of which are known under plasma conditions where the H^- continuum is present. The existence of an additional continuum due to the H^- ion causes all three temperature measurements to be too high, with $T(v/uv) > T(\ell/v) > T(\ell/uv) > T$.

The existence of the H^- continuum also interferes with the electron-density measurements. We can easily set an upper limit on the electron density, however, by calculating it as though the continuum radiation consisted only of the H atom contribution. We see from Fig. 19 that for $T < 5000°K$, the ratio $W_c^-(3225)/W_c(3225)$ is a factor of

100 or more less than the ratio $W_c^-(5305)/W_c(5305)$. We therefore expect that upper limits on the electron density derived from the continuum intensity at the ultraviolet wavelength will be much nearer the correct value than upper limits derived from the visible continuum. Upper limits on the electron density derived this way were used as a guide in extending the curves of electron density versus radius to the tube walls in Figs. 32 d and e.

Using the interpolated values of N_e and T from Figs. 31e and 32e, and the measured line intensity, we can calculate the ratio of the intensity at the center of the line (assuming only Stark broadening) and compare this with the intensity radiated by a black body at the plasma temperature. We find that after about 80 μsec the intensity at the peak of the H_β line becomes larger than the black-body intensity, which means that the line will be strongly reabsorbed. The effect will be to make $T(\ell/uv) > T(\ell/v) > T$.

We conclude, then, that in the cases in Figs. 31d and 31e where $T(\ell/v)$, $T(\ell/uv)$, and $T(v/uv)$ strongly disagree, the discrepancies are caused by both an additional continuum due to the H^- ion and reabsorption of the H_β line. Electron-density measurements at these times are also suspect, because of the H^- continuum. Probably the best estimates of T and N_e under these conditions result from interpolation in radius, if we assume that both T and N_e go to zero at the wall of the tube.

E. Decay Rates and Departures of the State of the Plasma from LTE

Finally, the plasma cooling and decay at a given radial position was studied especially carefully. For this the electron density and temperature were determined as accurately as possible on a single shot from end-on measurements at a radius of 33.5 mm. This radius was chosen because the three temperature measurements, $T(\ell/v)$, $T(\ell/uv)$, and $T(v/uv)$ showed excellent internal agreement (the extreme values from 30 to 200 μsec seldom differed by more than 15%, indicating that errors due to the presence of an H^- continuum or to reabsorption of H_β were small.

A careful estimate was made of the possible experimental errors and their influence on the temperature measurements. This estimate indicated for $T(\ell/v)$, $T(\ell/uv)$, and $T(v/uv)$ fractional standard deviations due to random experimental errors of 0.07, 0.11, and 0.21, respectively, for times between 50 and 200 μsec. The largest errors were due to an estimated 3% uncertainty in the accuracy of the voltage dividers in the input section of the preamplifiers; the next largest errors were due to uncertainties in measuring the transmission of the various filters used and in calculating the brightness of the carbon arc used as a radiation standard. The estimated fractional standard deviation in the weighted mean of the three values of T due to random experimental errors is about 0.06. Systematic error due to uncertainties in the properties of the carbon arc are also possible. Fortunately these have very little effect on the final temperature measurements (see Appendix C).

Every 20 μsec three values of the electron density were calculated from the three absolute-intensity measurements and the weighted mean of T at that time. We call these three values $N_e(v)$, $N_e(uv)$, and $N_e(\ell)$, using the same nomenclature as in the case of the temperature measurements. The estimated experimental errors varied with time; at 100 μsec, the estimated fractional standard deviations in $N_e(v)$, $N_e(uv)$, and $N_e(\ell)$ were 0.05, 0.07, and 0.11, respectively. A weighted average of these three values was then taken at each time, with the estimated fractional standard deviation in the mean due to experimental errors being about 0.05.

The weighted mean values of T and N_e on a typical shot are shown in Figs. 33 and 34, with their estimated errors. The decay coefficient γ [see Eq. (12)] has been determined for the same shot by graphical means from Fig. 34 and is shown in Fig. 35 as a function of time. Only times later than about 80 μsec, when the estimated longitudinal variation from the mean values of the electron density and temperature is 10% or less, were considered.

Also shown in Fig. 35 are theoretical values of γ, calculated from the work of Bates et al.[15, 16] using the observed values of the

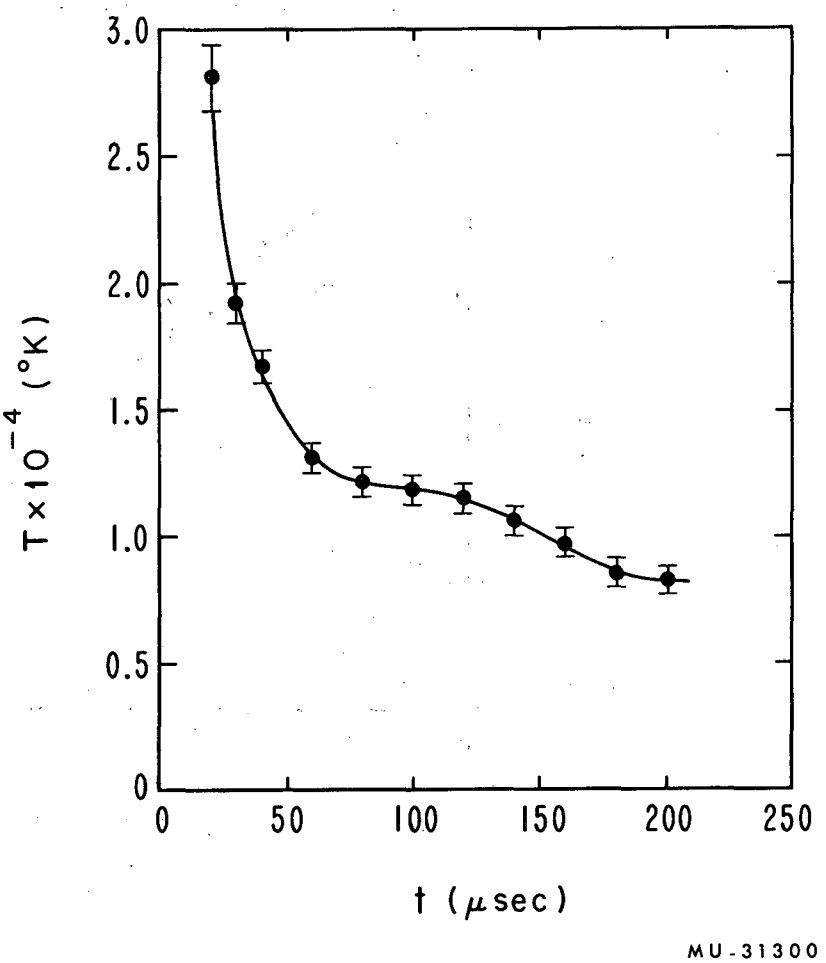

Fig. 33. Weighted mean value of T on a typical shot as a function of time at a radius of 33.5 mm. Estimated errors (standard deviations) are shown.

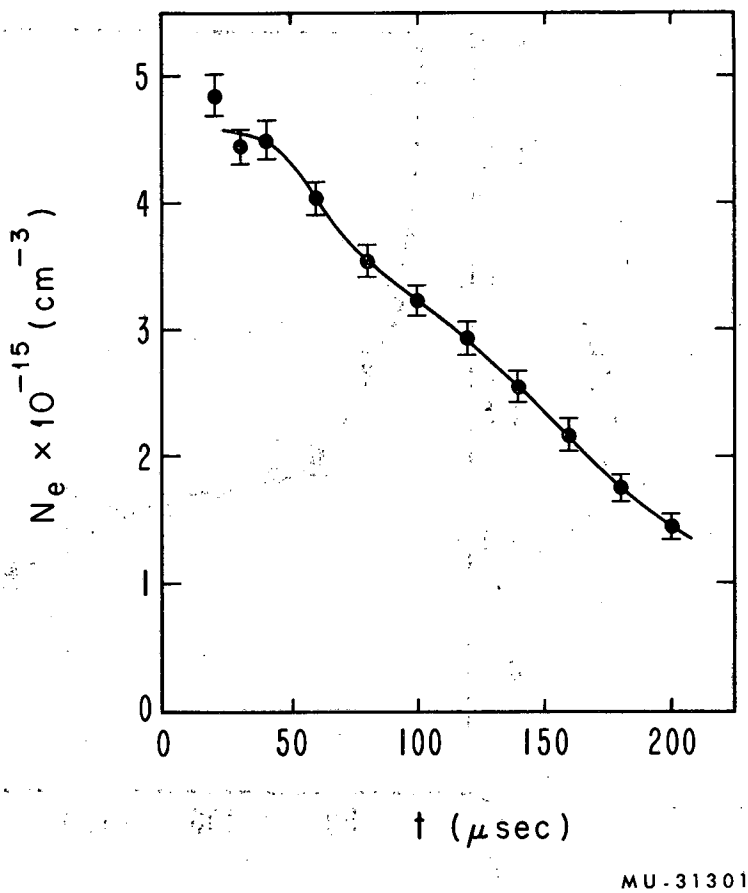

Fig. 34. Weighted mean value of the electron (ion) density on the same shot as in Fig. 33 as a function of time at a radius of 33.5 mm. Estimated errors (standard deviations) are shown.

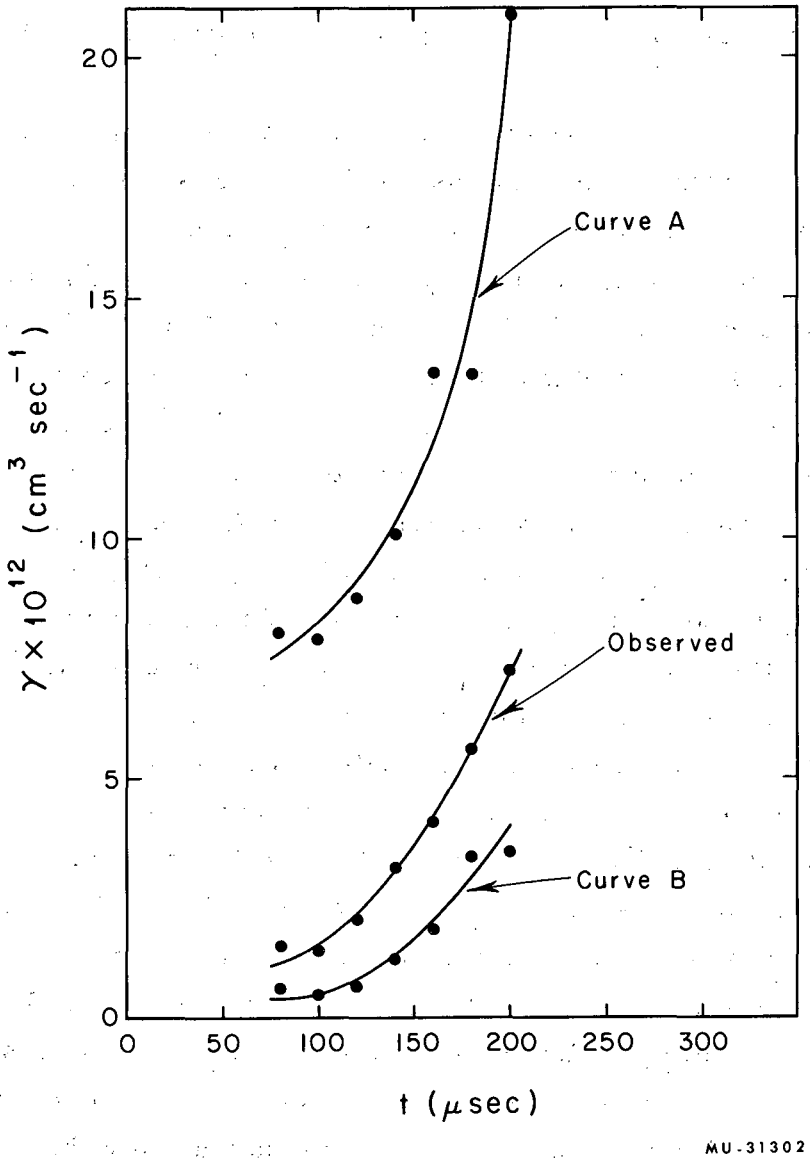

Fig. 35. Observed decay coefficient γ as a function of time, for the same shot shown in Figs. 33 and 34. Theoretical values of γ are also shown, where the plasma is assumed to be optically thin (Curve A) and opaque to lines of the Lyman series (Curve B).

electron density and temperature and assuming that the total particle density remains constant in time. Two cases are shown: in the first, the plasma is assumed to be optically thin (curve A); in the second, the plasma is assumed to be opaque to the lines of the Lyman series (curve B).

The plasma is certainly not completely opaque to the entire Lyman series, as was assumed in the case of curve B, because (1) the lines are broadened, by either Stark or Doppler broadening, and the light in the wings of the lines must escape the plasma with little reabsorption, and (2) the higher members of the Lyman series are broadened so much by the Stark effect that they may not be reabsorbed, even in the center of the line. However, we see from Appendix A that L_α will certainly be strongly reabsorbed in the center of the line. For $p = 1$ the dominant term in the sum $\sum_{p<q} N_q A(q, p)$ on the right of the rate equation, Eq. (11), will be $N_2 A(2, 1)$, namely, the rate of population of the ground state by radiative transitions producing the L_α line. We expect then that even if L_α is the only line in the Lyman series that is reabsorbed, the assumption that all the Lyman lines are reabsorbed will yield a reasonable estimate of the recombination coefficient. Measurements of γ in the recombining plasma investigated in this thesis should therefore fall between the two theoretical curves in Fig. 35, but should be considerably closer to curve B. This is seen to be the case. A plasma-loss mechanism in addition to volume recombination could also explain the relation between the observed γ and the two theoretical values; this possibility will be discussed in a later section.

It is very instructive to plot the electron density versus temperature (which we shall call a "decay curve") for this shot. This is shown in Fig. 36. Also shown is a theoretical curve calculated from Saha's equation (labeled "LTE"), assuming the plasma is always in LTE, and fitted to the early portion of the decay curve, when the plasma apparently is completely ionized. The total particle density for this fit is 4.6×10^{15} cm^{-3}. Only experimental errors are shown; the points before 80 μsec are more uncertain that indicated because of the longitudinal nonuniformities. Apparently the plasma is initially fully ionized,

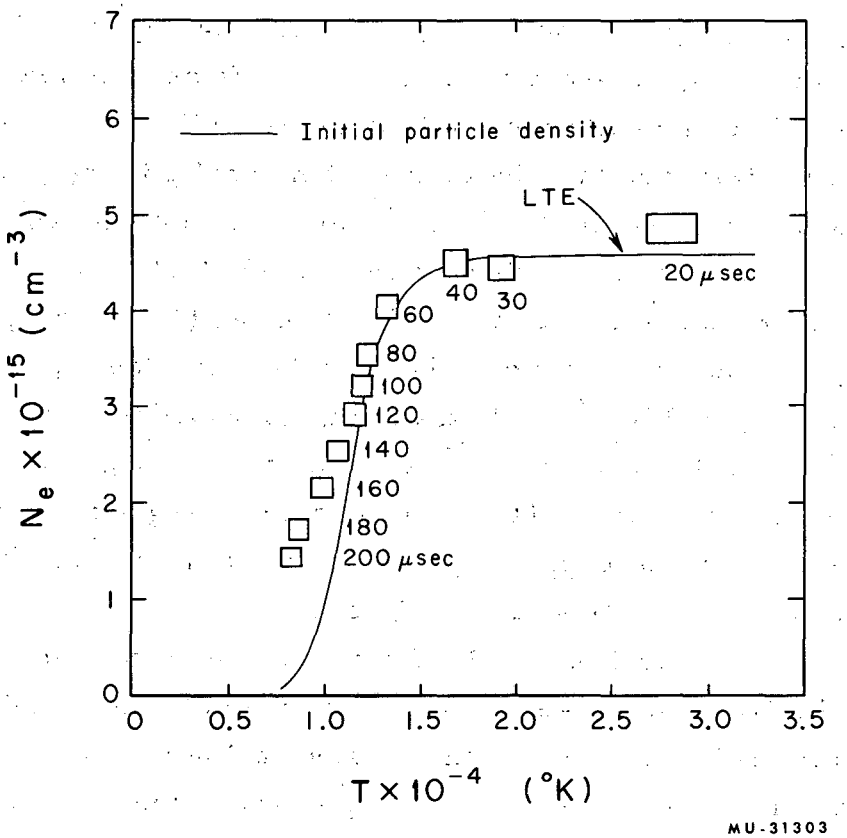

Fig. 36. Decay curve for the shot shown in Figs. 33 to 35. The solid curve labeled LTE was calculated from Saha's equation and was fitted to the early portion of the decay curve.

but with an ion density less than the initial hydrogen-atom density, cools for the first 120 μsec essentially in LTE, and then departs from the equilibrium curve.

We can analyze the decay of the plasma in terms of Eqs. (15) and (16), the rate equations governing the population of levels 1 and 2 for a plasma opaque to the Lyman lines. We first assume $\dot{N}_2 = 0$ in Eq. (16) (a good assumption) and solve that equation for N_2, which now becomes a quasi-steady-state value. We assume that the plasma is initially completely ionized (judging from Fig. 36, a very reasonable assumption) and that the total proton density in the plasma remains constant in time at 4.6×10^{15} cm^{-3} for this shot, allowing us to calculate N_1 by simply subtracting the measured electron density from this number. We can then calculate N_2 from Eq. (16). Using this value for N_2, the observed value of the ion (electron) density, and the values of a_1, P_{21}, and R_1 from Bates et al. appropriate to the observed electron density and temperature,[16] we examine the magnitude of the terms on the right side of Eq. (15). These rates are given in Table II, including also the rate of populating and depopulating the ground state by radiative transitions from the $n = 2$ level.

We see from Table II that, before about 120 μsec, the second and third terms -- essentially the rates of collision-induced transitions from the level $n = 2$ and the corresponding inverse process -- almost cancel. The first term, corresponding to the net rate of populating the ground state due to all other processes, is always small compared with the second. The last term, the rate of populating and depopulating the ground state by emission and absorption of L_α quanta, has no effect on the net recombination rate, as the two rates are assumed to cancel exactly. Before 120 μsec, then, the density of atoms in the ground state should be close to the equilibrium value, as the rates of populating and depopulating the ground state by collisional and radiative processes almost balance in pairs; detailed balance very nearly holds. The plasma during this time is in Region II of Fig. 3.

After 120 μsec, the radiative population and depopulation rates are still assumed to balance, but the temperature is too low for the rate of collisional excitation from the ground state to balance the rate of

Table II. Rates of populating and depopulating the ground state

T (μsec)	Populating and depopulating rates (10^{-19} cm^{-3} sec^{-1})			
	$+ a_1 N_i N_e$	$+ P_{21} N_2 N_e$	$- R_1 N_1 N_e$	$\pm A_{21} N_2$
80	0.25	1.4	1.1	20
100	0.20	1.1	0.87	19
120	0.16	1.4	0.61	25
140	0.13	0.98	0.29	20
160	0.10	0.90	0.10	22
180	0.071	0.98	0.018	30
200	0.048	0.68	0.010	25

collisional deexcitation from the n = 2 level. By 160 μsec, the only important process governing the decay (except for the balancing radiative processes) is the rate of collision-induced transitions from n = 2 to the ground state. The plasma, now in Region I of Fig. 3, recombines at a rate determined by the electron temperature and density, and independent of the density of atoms in the ground state.

We also see from Table II that for the times of interest, the rate of populating and depopulating the ground state by emission and absorption of L_α quanta is always at least a factor of 15 larger than the rate of any other process affecting the population of the ground state. If the plasma is not completely opaque to the Lyman lines, the rate of populating the ground state due to these transitions will slightly exceed the rate of depopulation by the inverse processes. As these rates are so large compared with any other rates, a slight imbalance will noticeably affect the observed decay rate. If the population rate exceeds the depopulation rate by only 5%, the observed decay rate will be approximately doubled. This is probably the reason that the observed γ's shown in Fig. 35 are larger by a factor of two than the theoretical values, for an opaque plasma.

We can also calculate the rate of the observed power loss from the time rate of change of the electron density and temperature, and

compare it with theoretical radiative loss rates computed by Bates and Kingston.[13] Again we find that the observed power loss is between the theoretical losses for optically thick (to Lyman lines) and optically thin plasmas. If about 5% of the radiation in the Lyman series could "leak" out of the plasma without disturbing the distribution of excited states, the observed power loss would be in good agreement with the theoretical loss for a plasma opaque to Lyman lines.

The factor determining the point at which the plasma departs from the equilibrium curve in Fig. 36 is, of course, the temperature at which detailed balance in the collision rates affecting the population of atoms in the ground state fails. In the history of the plasma shown in Fig. 36, this temperature is about 1.2×10^4 °K. Because the rates of collisional processes are such strong functions of temperature, we expect that decay curves for other radii will show similar behavior. Figure 37 shows the average behavior of the decay curves at the five radii (each curve is an average of 6 shots in both density and temperature, from Figs. 31 and 32). The dotted line is the same equilibrium curve as that shown in Fig. 36. All experimental curves begin at 30 μsec (the time the power input into the plasma drops to essentially zero) and end at 200 μsec. The dashed portions indicate circumstances in which the H^- continuum, or reabsorption of H_β, or both, are important. All the decay curves show strongly nonequilibrium behavior for temperatures below 1.2×10^4 °K.

No measurements at any radius ever indicate an ion density as high as the initial particle density, 5.8×10^{15} cm^{-3}, although early in time the plasma at 33.5 mm and 50 mm radius is certainly fully ionized, with an ion density of 4.4×10^{15} cm^{-3}. The plasma at 16 mm and 1.3 mm radius may also be initially fully ionized, with even lower ion densities. It is apparent that some 30% of the hydrogen atoms initially in the tube have been "lost" during the formation of the plasma. Unfortunately one cannot, for any radius or time, calculate with any accuracy the density of neutral particles in the plasma from the observations described in this thesis. Most probably the hydrogen atoms have been displaced radially during the formation of the plasma by the hydromagnetic ionizing wave, and the "lost" particles have accumulated in the

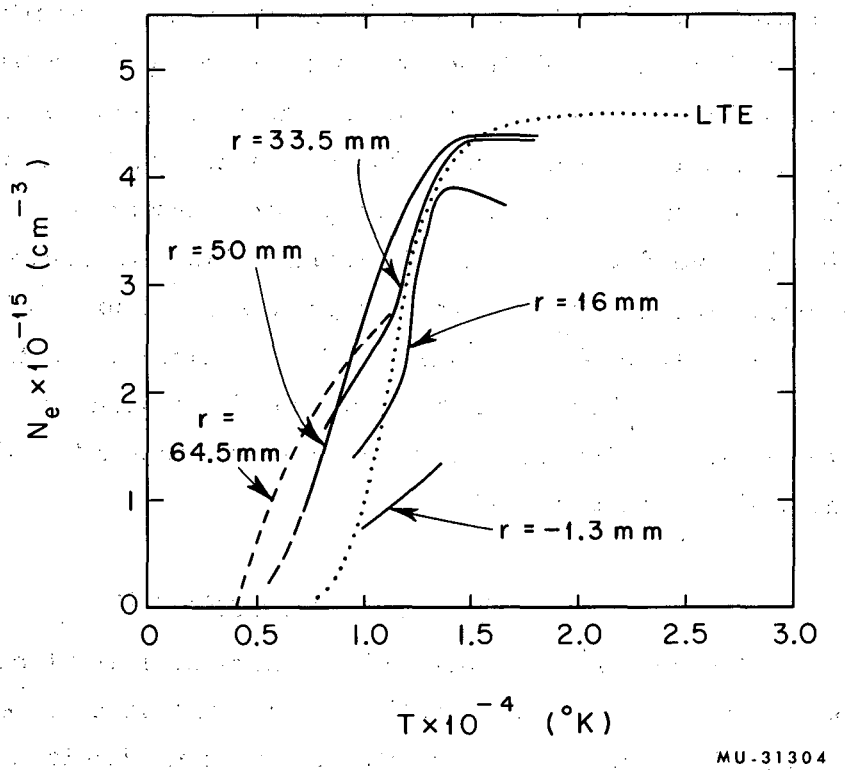

Fig. 37. Average decay curves (each curve is an average of six shots in both density and temperature) for five radii. The dotted line is the same equilibrium curve shown in Fig. 36.

region between 50 mm and the wall (73 mm). The plasma in this region is apparently never fully ionized, so that one cannot even estimate the neutral-atom density by subtracting the observed ion density from the complete ionization value measured initially.

Another possible interpretation of the departure of the decay curves shown in Figs. 36 and 37 from the equilibrium curves is that at the time the "break" occurs the total particle density in the plasma begins to increase with time, the state of the plasma being always close to equilibrium. Such an influx of particles could be caused by the release of absorbed hydrogen from the walls by the passage of the hydromagnetic ionizing wave. We may immediately rule out this possibility. We observe that if the plasma were in thermal equilibrium at 100 μsec at 64.5 mm radius when the temperature is about 5000 °K and the ion density is about 4×10^{14} cm^{-3}, the H^- continuum (from Fig. 19) would be 10^5 to 10^6 times brighter than the H continuum. However, the observed H^- continuum probably does not exceed the H continuum by more than a factor of 10.

F. Mode of Plasma Decay

We have not yet conclusively demonstrated that the plasma disappears by volume recombination. The plasma may be removed by diffusion to the ends or to the walls of the tube. Radial diffusion losses to the walls of the tube were investigated both by space- and time-resolved measurements of temperature and ion density discussed in the last sections, and by direct observations of the plasma during the decay period by a fast framing camera.

The small scanning monochromator shown in Fig. 22 was replaced by a fast Kerr-cell framing camera (Electro-Optical Instruments, Inc., Model No. KFC-600/B), and a sequence of pictures of the decaying plasma was taken. A typical sequence of pictures, taken at 20, 34, 60, 80, 116, and 164 μsec with an exposure time of 1 μsec, is shown in Figs. 38, 39, and 40. Radial profiles of the average values of T and N_e at the same times (derived from Figs. 31 and 32) are shown under the framing camera pictures to the same scale. These pictures were

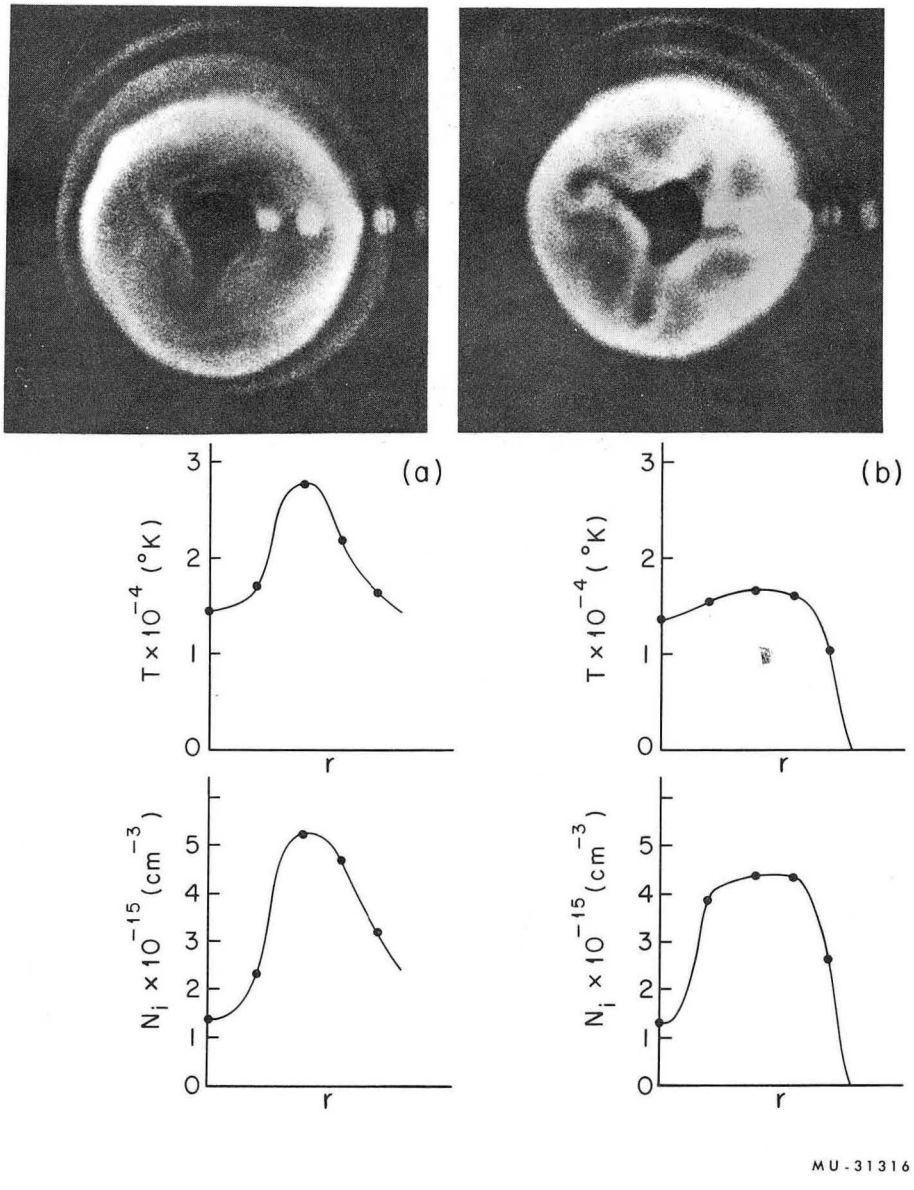

Fig. 38. End-on framing-camera pictures of the plasma at 20 and 34 μ sec. The exposure time was 1 μ sec. Also shown are average profiles of temperature and ion density at these times.

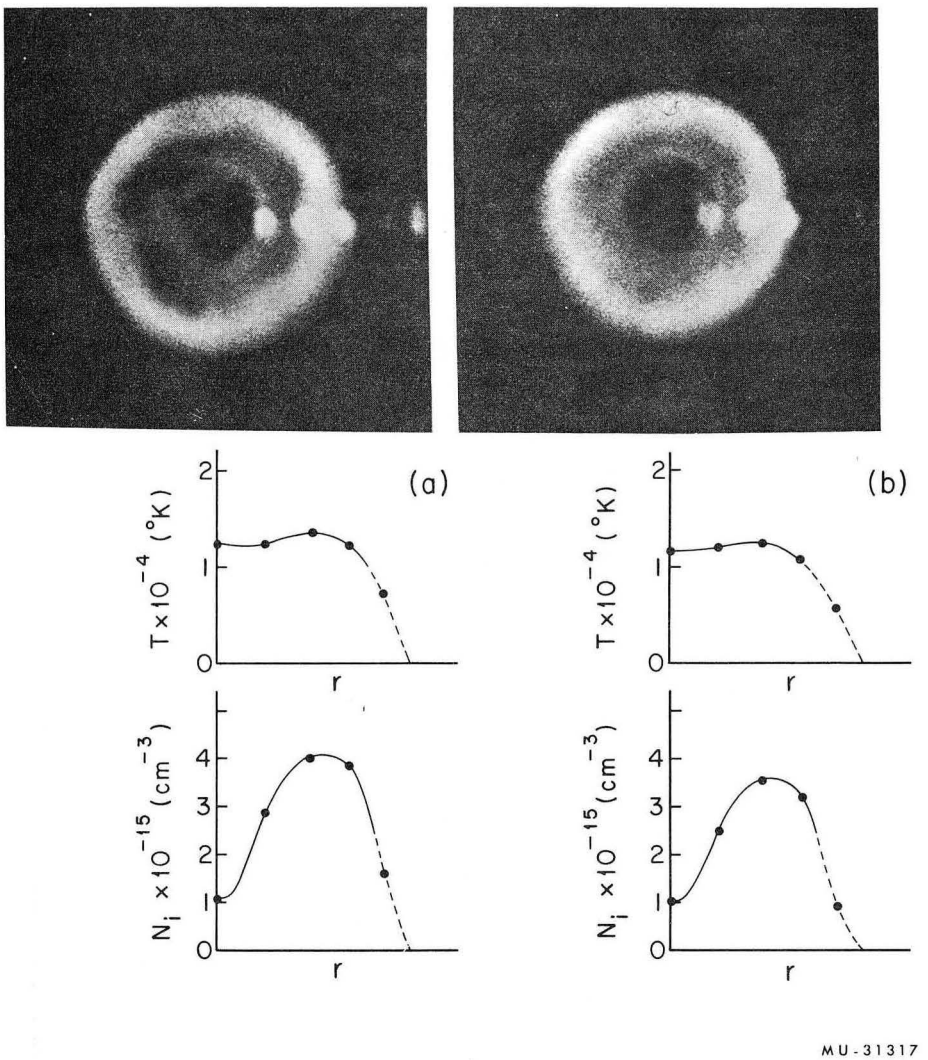

Fig. 39. End-on framing-camera pictures and radial profiles of temperature and density at 60 and 80 μ sec.

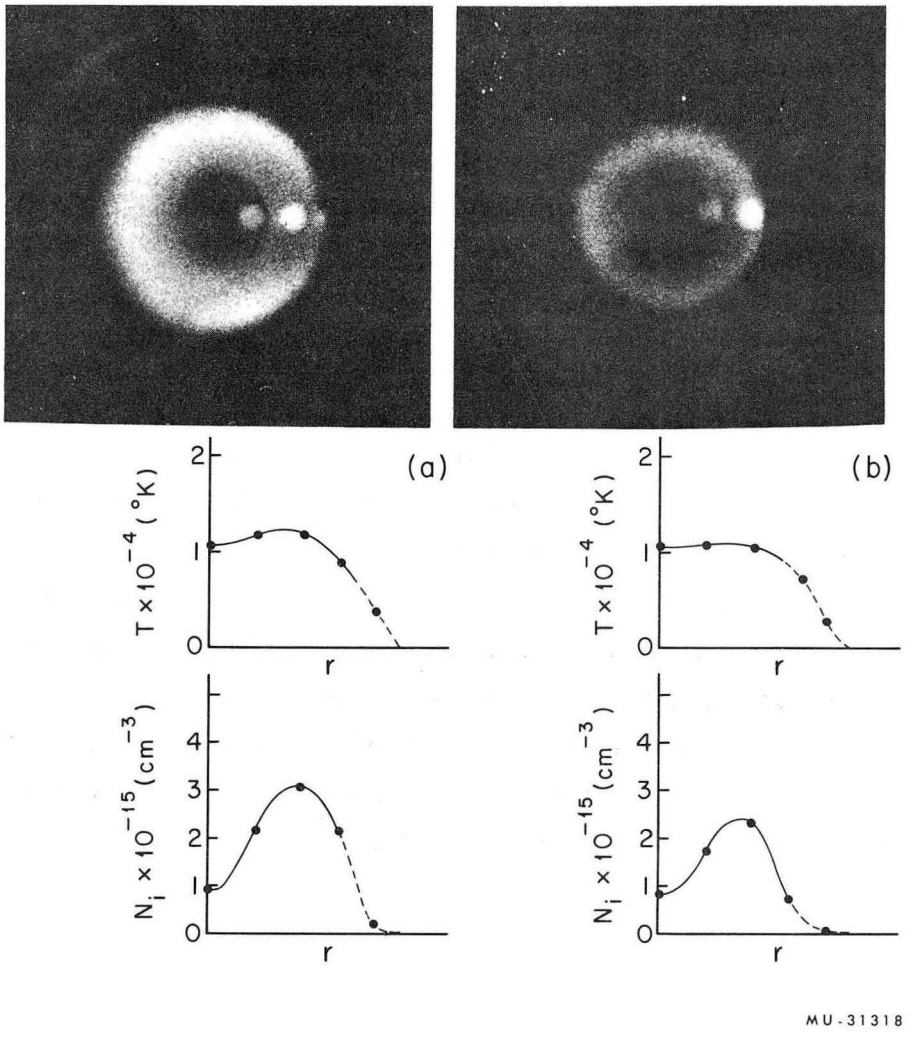

Fig. 40. End-on framing-camera pictures and radial profiles of temperature and density at 116 and 164 μ sec.

taken in visible light; pictures using light only from the H_β line were very similar. The bright spots are the holes in the screen. There is very good agreement between the position of the plasma as determined by the framing camera pictures and the position as determined from the electron density and temperature measurements. Notice that the "hole" in the center of the plasma never does fill in. The magnetic field prevents the plasma from adjacent regions of higher density from diffusing into the center. Figure 41 shows a sequence of 12 pictures taken with a rotating-mirror framing camera, with no screen in the end of the tube. Pronounced "swirls," described in a previous publication,[59] develop in the plasma after crowbar. (Swirls do not develop if a conducting screen is used, as was always the case in the work discussed in this thesis – – see Figs. 38 through 40.) We see also from Fig. 41 that there is negligible diffusion of the plasma across the magnetic field. The structure visible in the plasma at 53 μsec is still distinctly visible at 220 μsec, with no apparent radial motion.

We can easily show theoretically that the plasma cannot decay by classical diffusion across the magnetic field. We assume the plasma to be sufficiently highly ionized that the electrons collide much more frequently with positive ions than with neutral atoms. In that case we can compute drift velocity of the plasma across a strong magnetic field from the formula given by Spitzer[70]

$$v_\perp = - \frac{\eta}{B^2} \nabla p \,, \tag{54}$$

where η is the electrical resistivity in emu, B is the magnetic field strength in gauss, and p is the plasma pressure in dynes cm^{-2}. For η we use the resistivity in ohm-cm transverse to a strong magnetic field[71]

$$\eta = 1.29 \times 10^4 \frac{Z \ell n \Lambda}{T^{3/2}} \,. \tag{55}$$

We take $\ell n \Lambda = 6$ in the expression for η, approximately correct for this plasma, and calculate ∇p from the observed values of T and N_e from Figs. 38 to 40. We find that the plasma should take at least 5 to

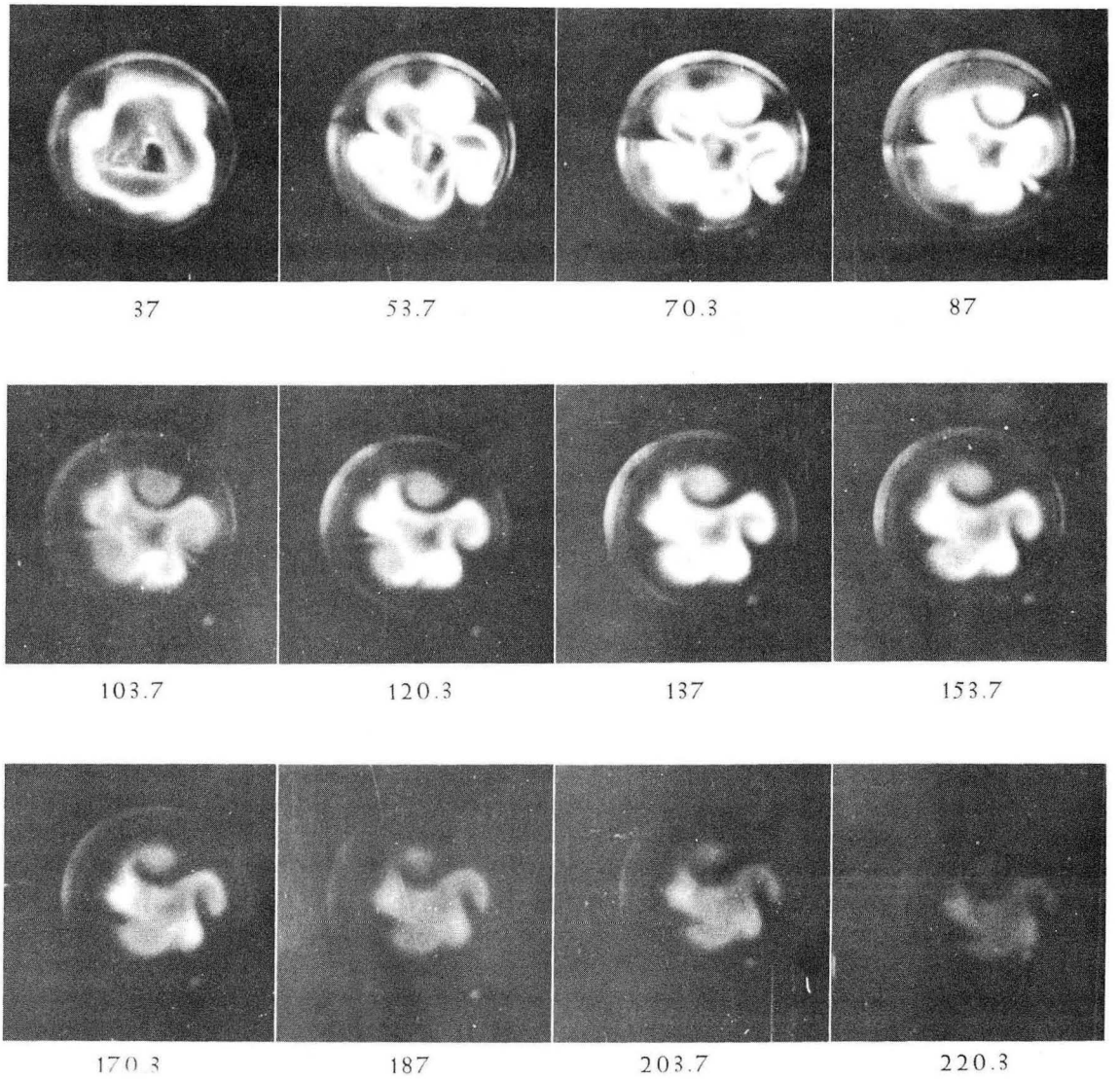

Fig. 41. A sequence of 12 framing-camera pictures showing the development of "swirls" when no conducting screen is used in the end of the tube.

10 msec to drift a distance comparable to the radius of the tube. This diffusion model is unduly pessimistic, as we have completely neglected the presence of neutrals, which must slow down the diffusion by reducing the pressure gradient. As the observed decay times are shorter than these estimated radial-diffusion times by a factor of 50 to 100, we conclude that the plasma is probably not lost by drift to the walls.

We also have direct evidence that the ions do not diffuse through the neutrals along magnetic field lines and recombine at the ends of the tube. First, the axial electron- (ion-) density profiles shown in Figs. 24 and 25 do not approach a cosine distribution late in time, as might be expected if the losses were by diffusion in the lowest mode. Instead, they remain fairly flat after 80 μsec. Second, consider the case late in time, when the plasma is no longer highly ionized. On this model, the ion loss rate is controlled by the diffusion of ions through neutrals. This process is governed by

$$\frac{\partial N_i}{dt} = - \nabla D_a \nabla N_i , \tag{56}$$

which we approximate by

$$\frac{\partial N_i}{dt} = - D_a \nabla^2 N_i . \tag{57}$$

The characteristic decay time for the lowest mode diffusion is

$$\tau \cong \frac{\ell^2}{D_a} , \tag{58}$$

where D_a is the ambipolar diffusion coefficient (twice the ion-diffusion coefficient D_i if the ion and electron temperatures are equal), and ℓ is a characteristic length of the plasma. Evaluating D_i from simple gas kinetic theory for $T = 10{,}000\ ^\circ K$, $N_1 = 3 \times 10^{15}\ cm^{-3}$, and using a value of $6 \times 10^{-15}\ cm^{-2}$ for the charge-exchange cross section,[72] with $\ell = 40$ cm (about half the tube length), we obtain a characteristic decay time of the order of 25 msec. Again this is much longer than the

observed decay time. It is actually a pessimistic estimate, as the observed gradients are not nearly as severe as that implied by Eq. (58).

It is also conceivable that the entire plasma, ions and neutrals together, flows to the ends of the tube in a one-dimensional free expansion and recombines there. The resulting neutral particles would then be required to stick to the quartz endplates or to the copper screen, which seems unlikely. Oblique Kerr-cell pictures of the plasma in a different, but basically similar, device[56] show that the light originates from the volume of the plasma and not from the ends, as might be expected if the plasma were recombining at the ends of the tube. If this mechanism were responsible for the loss of plasma, we would expect to see a rarefaction wave propagating into the plasma from both ends of the tube with a velocity approximately equal to the sound velocity. The sound velocity in a highly ionized hydrogen plasma, with a temperature of 10,000 °K and $\gamma = 5/3$, is about 1.7×10^6 cm sec^{-1}, and the rarefaction wave, if it existed, should reach the center of the tube in about 25 μsec. Figures 25 and 26, which show the longitudinal variation of the electron density at different times, show no indication of such a rarefaction wave.

Since there is no evidence of loss of the plasma by any process involving motion of the plasma either to the walls or to the ends of the tube, and since both the observed decay rate and departures of the state of the plasma from LTE are in good agreement with theory, assuming the plasma to decay by volume recombination, we conclude that volume recombination is the dominant process governing the disappearance of ions from the plasma.

G. Summary of Experimental Results

Simultaneous determinations of the ion (electron) density by measuring the Stark broadening of the H_β line (using the theoretical calculations of Griem et al.) and the absolute intensity of the continuum radiation from the plasma at 5320 Å yielded values that agreed within the experimental errors, estimated to be about 20%. Measurements of the relative intensity of the H_β line and of a band of continuum

radiation at 5305 Å provided estimates of the longitudinal nonuniformities of the electron densities and temperatures: after 80 μsec, the electron density and temperature seem to be independent of axial position to about ±10%. Radial profiles of the electron density and temperature were calculated from end-on observations at five radii for a number of times. These radial profiles agree very well qualitatively with the distribution of light from the decaying plasma, as determined by a sequence of pictures taken with a fast framing camera. The plasma decays by volume recombination; losses by diffusion appear to be negligible. Measurements at one radius of the electron density and temperature as functions of time, and accurate to about 5%, yield decay rates that agree very well (within a factor of two) with theoretical decay rates calculated by Bates et al.,[16] if we assume the plasma to be opaque to the Lyman lines. The discrepancy would be explained if the plasma is almost, but not completely, opaque to the Lyman lines, as is probably the case. The plasma in most of the volume is initially fully ionized. It cools essentially in LTE (local thermodynamic equilibrium) until the temperature drops below about 1.2×10^4 °K. After this time the temperature is too low for detailed balancing of the collisional processes governing the population of the ground state to hold, and the plasma departs from the LTE cooling curve. More accurate measurements of the rate of decay of the plasma and the departure of the state of the plasma from LTE would require a knowledge of the density of neutral atoms in the ground state.

APPENDICES

A. Conditions Under Which a Hydrogen Plasma is Opaque to L_α

Holstein[73] treats the problem of imprisonment of resonance radiation in gases. The half-width of a Doppler-broadened spectral line at half-maximum intensity is

$$\Delta\lambda_D = 3.6 \times 10^{-7} \left(\frac{T}{A}\right)^{1/2} \lambda \qquad (A1)$$

where $\Delta\lambda_D$ is the half-width in Å, λ is the wavelength of the line in Å, T is the temperature in °K, and A is the mass of the particle (hydrogen equals 1). Substituting numbers for L_α, $\Delta\lambda_D$ in Å becomes

$$\Delta\lambda_D = 4.3 \times 10^{-4} \sqrt{T} . \qquad (A2)$$

The only other significant broadening mechanism in dense hydrogen plasmas is Stark broadening. Using results of Stark-broadening calculations of Griem et al.,[52] and assuming only Stark broadening, one can show that the half-width of L_α in Å at half-maximum intensity is

$$\Delta\lambda_s \cong 1.5 \times 10^{-13} N_i^{2/3} . \qquad (A3)$$

Doppler broadening will then predominate provided

$$\frac{\Delta\lambda_D}{\Delta\lambda_s} = 2.9 \times 10^{9} \frac{\sqrt{T}}{N_i^{2/3}} > 1 , \qquad (A4)$$

which will be the case in high-temperature, low-density plasmas. The conditions under which Doppler broadening predominates over Stark broadening for L_α are shown in Fig. 42.

From the work of Holstein[73] we can show that for Doppler broadening, L_α is trapped if the optical depth τ, given (for L_α) by

$$\tau = 5.9 \times 10^{-12} \frac{N_1}{\sqrt{T}} \ell \qquad (A5)$$

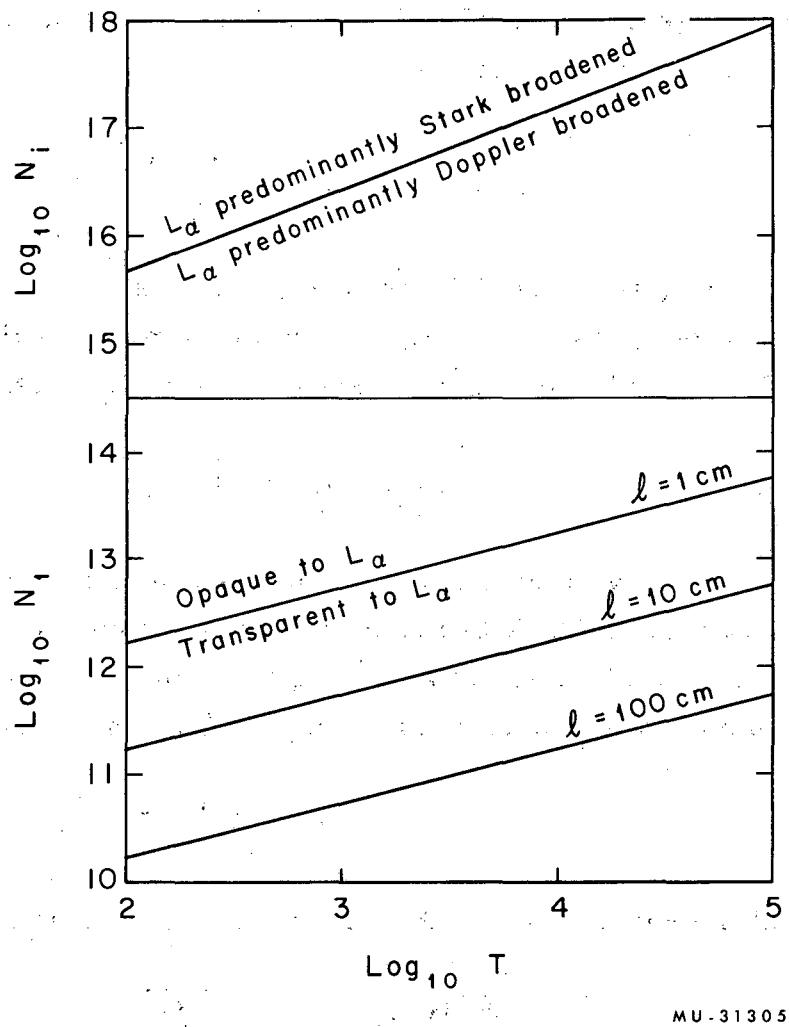

Fig. 42. Electron-density vs temperature diagram, showing conditions under which Doppler broadening predominates over Stark broadening for L_α. Also shown are conditions under which hydrogen plasmas of laboratory dimensions are opaque to L_α.

is greater than one. Here ℓ is a characteristic dimension of the plasma, in cm. Lines of $\tau = 1$ for various values of L are also shown in Fig. 42.

We see that in most highly ionized hydrogen plasmas ($T > 10^4$ °K), the L_a line is predominantly Doppler-broadened. Most highly ionized but recombining hydrogen plasmas of laboratory dimensions are then opaque to L_a, because N_1 is the order of N_i in a recombining plasma.

B. Approximate Solutions of the Rate Equation

For approximately calculating the recombination rate in a dense, highly ionized plasma, several authors have proposed schemes that avoid the necessity of simultaneously solving a set of coupled rate equations.[9,18,19] These approximate solutions hinge on the fact that one can sometimes calculate either the rate at which electrons which will eventually reach the ground state flow into the reservoir of bound electrons by three-body recombinations, or the rate at which electrons "leak" through the lowest level in the reservoir [the level having principal quantum number s, defined in the discussion following Eq. (11)] by either radiative or collisionally induced transitions to lower levels, and eventually to the ground state.

Taking into account three-body recombination, D'Angelo estimated the recombination rate by first estimating the probability that an electron in any given quantum level eventually reaches the ground state (recombines) by a random-walk process, considering only radiative transitions and electron-collisional ionization.[9] This probability is then multiplied by the estimated rate of capture of electrons by three-body recombination into the state. Summing over all states then should give the recombination rate. D'Angelo's values for recombination coefficients, which should apply to plasmas with $10^3 < T < 10^4$ °K and $10^{12} < N_i < 10^{13}$ cm^{-3}, are as expected much larger than the coefficients for radiative recombination alone, but are still lower by as much as a factor of 10 than the values calculated by Bates et al.[15] This discrepancy is caused by the neglect of inelastic and superelastic collisions in calculating the rates of populating the excited states.

This was pointed out by Hinnov and Hirshberg, who proposed two models for calculating recombination rates.[19] Their first model is based on finding a quantum level having principal quantum number r such that the probability per unit time that an electron in this level will be excited to a higher level or to the continuum by electron collisions exactly equals the probability per unit time that the electron will make a transition to lower levels by radiative decay or by superelastic collision. Since these probabilities are all strong functions of the principal quantum number n, essentially all electrons recombining from the continuum into levels with $n > r$ will eventually reach the continuum again, and essentially all electrons recombining into lower levels with $n < r$ will eventually reach the ground state. Assuming no re-excitation or reionization of electrons in the ground state, we then need only calculate the rate of recombination by three-body and radiative processes into the nth level and sum over all levels with $n < r$ to get the total recombination rate. It is relatively easy to determine r if the electron density is high enough that the transition probabilities needed to determine r are due primarily to balancing collisional processes. In that case, r may be estimated simply by the rate of the dominant process -- collisionally induced transitions between adjacent quantum levels. By equating rates one can show that the probabilities per unit time of upward and downward transitions are equal at the level where the equilibrium population of excited states has a minimum in n. This implies that the ionization potential from that level χ_r approximates kT, so that we have

$$r \cong \left(\frac{\chi_1}{kT}\right)^{1/2} , \tag{B1}$$

where χ_1 is the ionization potential from the ground state.

Hinnov and Hirshberg estimate the three-body recombination rate into the nth level from the classical Thomson cross section for ionization, and derive an approximate expression for α in closed form:

$$\alpha \cong 1.1 \times 10^{-8} T^{-9/2} + 3.0 \times 10^{-10} T^{-3/4} . \tag{B2}$$

The first term is due to three-body recombinations; the second, to radiative recombination.

Using densities of excited states calculated by Bates and Kingston,[13] we can estimate (with s for this purpose being defined as the principal quantum number of the lowest level deviating by 30% or less from the equilibrium value) that Hinnov and Hirshberg's approximate solution, Eq. (18), should be valid if the electron density satisfied the inequality

$$N_e < 2.5 \times 10^{-5} T^{4.75} . \qquad \text{(B3)}$$

We also require that there be no re-excitation or reionization of electrons in the ground state by electron collisions, which requires $T < 16{,}000\ ^\circ K$. If all these restrictions are met, Eq. (18) gives values of α that agree within a factor of two with the values obtained from numerical calculations of Bates et al. In this approximate solution, Hinnov and Hirshberg have estimated the rate at which electrons will eventually recombine ("leak") into the reservoir of bound electrons from the continuum. The method is perfectly general; difficulties lie in estimating r.

Byron et al.[18] propose a generalization of Hinnov and Hirshberg's second model, a fairly simple method of calculating the rate at which electrons leak out of the reservoir on their way to the ground state. The electrons already in the reservoir can only proceed downward (toward lower quantum numbers) by two processes, radiative transitions and collisional deexcitation. The rate at which electrons can leave a given level by these two processes depends on the transition probability, the density of atoms in that excited state, and the electron density and temperature. Byron et al. point out that if the plasma properties are kept constant, the rate of depopulation of the nth level by these two process as a function of n has a minimum, and this minimum rate determines the rate at which the plasma recombines. The minimum depopulation rate occurs approximately at the level s. The depopulation rate has a minimum because either radiative decay becomes comparable to

collisional depopulation (the rate of the former decreases with increasing principal quantum number; the rate of the latter increase) or because the rate of collisional depopulation itself has a minimum in n. Using collisional deexcitation cross sections calculated by Gryziński,[38] they then calculate the recombination rate by summing the rates of radiative recombination, radiative transitions from the sth and higher levels, and collisionally induced transitions from the sth to the (s - 1)th levels. The population of the sth level is depressed somewhat below the equilibrium value by the extra loss mechanisms -- this has to be taken into account. They present a sample calculation of the recombination coefficient for a hydrogen plasma with T = 16,000 °K and get excellent agreement with the numerical results of Bates and Kingston.[12] Strictly speaking, the theory must be applied only to plasmas optically thin and cool enough (T < 16,000 °K) so that collisional excitation from the ground state may be neglected.

Byron et al. also point out that in many cases the recombination rate may also be calculated from the electron-energy-balance equation. The electrons gain energy during the recombination process by superelastic collisions with excited atoms, and lose energy to the ions by elastic collisions. Equating the difference in these two rates to the time rate of change of the energy per unit volume of the free electrons then gives the equation for the electron energy balance. Use of this method requires an estimate of the average energy transferred to the second electron by the three-body recombination process, and usually also knowledge of the time rate of change of the electron temperature.

C. The Carbon Arc as a Radiation Standard

Numerous authors have proposed the use of a carbon arc as a radiation standard.[64-67, 74-77] The procedure in using such an arc is as follows: A dc arc is struck between an anode of spectroscopically pure, fine-grained carbon (lampblack) or graphite, about 6 mm in diameter, and a smaller diameter carbon or graphite cathode (the cathode material has very little influence on the operation of the arc). After burning a few minutes, the shape of the ends of the electrodes stabilizes.

As the arc current is then slowly increased, the luminance of the surface of the anode increases until it reaches a maximum value. Further increase in current results in either no change in the luminance of the anode spot, or a slight decrease (depending on operating conditions and anode material). Eventually a current is reached at which the arc begins to burn unstably; the arc "hisses" audibly, and the luminance decreases noticeably.

It is generally agreed that a pyrometric arc (one used as a radiation standard) can be operated very reproducibly. There is some disagreement, however, as to the value of the emissivity of carbon and the true temperature of the anode spot. In an exceedingly thorough series of studies of the pyrometric arc, Euler concludes that the emissivity varies slightly with wavelength, ranging from 0.74 to 0.78 in the visible.[64-67] He also concludes that the true temperature based on measurements by himself and other investigators is 3996 ± 15°K (all temperatures quoted are in the 1948 International Temperature Scale). Null and Lozier[74] maintain that Euler incorrectly determined both the emissivity and the true temperature. They claim that the emissivity is really 0.98 to 0.99, and that the true temperature is very close to 3800°K. It is generally difficult to compare these two conflicting sets of results with those of previous investigators, who did not use the same fine-grained electrodes and may not have run the arc in the same manner.

These disagreements should have no effect in themselves on the use of a pyrometric arc as a radiation standard, as only a knowledge of the spectral distribution of radiance is required. However, the two measurements of the spectral distribution of radiance also disagree. Agreement is perfect at about 6500 Å; at shorter wavelengths, Euler's values of radiance are higher than Null and Lozier's values, the discrepancy reaching about 30% at a wavelength of 3225 Å. It was decided to use the spectral distribution of radiance as measured by Euler in reducing the data presented in this thesis, as he used more measuring instruments and comparison sources than did Null and Lozier, and made more checks for internal consistency.

If the results of Null and Lozier had been used rather than those of Euler in this thesis, agreement between the three different determinations of temperature would no longer be as good as is shown in Fig. 31. For instance, at 33.5-mm radius and 100 μsec, the discrepancies in the three measurements of T would be of the order of 20%, considerably larger than the estimated random experimental errors of 5%. The most precise value, $T(\ell/v)$, is scarcely affected, however. Therefore the weighted mean is changed by only 1 to 2%. The values of $N_e(v)$, $N_e(\ell)$, and $N_e(uv)$ would be reduced by about 1.5, 2, and 15%, respectively, and the weighted mean by about 5%. These small changes would have a negligible result on the final conclusions.

The pyrometric arc used in this thesis was operated, with few exceptions, as nearly as possible as recommended by Euler. The anodes were 6.35-mm-diam Ringsdorff-Werke RWII carbon electrodes. The cathodes were 1/8-in.-diam United Carbon Products Co. grade U-1 (medium) "Ultra Purity" graphite electrodes. The included angle between the electrodes was 120 deg. A well-filtered, full-wave, silicon-diode rectifier provided a source of dc current. Considerable trouble was caused by a persistent tendency of the cathode spot to wander, inducing a similar wandering in the anode spot and fluctuations at about 1 cps in the luminance, even in the center of the anode spot (the only region observed). This was largely eliminated by painting the cathode with a dilute solution of sodium bicarbonate before running. Why the presence of sodium in the arc should stabilize the cathode spot is not known (Euler used copper-covered cathodes, which had the same effect). The addition of sodium seemed to have no effect on the luminance of the arc, but did introduce the prominent absorption lines of sodium.

An oscilloscope proved very useful in monitoring the performance of the arc. The oscilloscope was used at a gain of 0.5 V/cm and a sweep speed of 5 msec/cm to observe the ac component of the voltage across the arc. As the arc current is increased, the point of maximum luminance (the proper operating condition) is marked by the onset of a ripple, at a frequency of about 200 cps, in both the voltage across the arc and the luminance. As the current is further increased, the

frequency and amplitude of the ripple in voltage and luminance both increase, and there is a net decrease in the luminance, as was observed by Null and Lozier,[74] Finkelnburg,[75] and Göing,[76] but not Euler.[67] An arc operating under these conditions emits a soft whistle, which may be heard distinctly. At slightly higher currents -- 10 to 11 A -- the ripple degenerates into random noise, both in voltage and luminance, and the arc begins to hiss. Any wandering of the anode spot is evidenced as a low frequency (~1 cps) ripple on the oscilloscope trace.

An arc operated in this fashion is extremely reproducible. The radiance at any wavelength over a short period of time (e.g., 15 min) shows a fractional rms deviation of about 0.01; over periods of several weeks the fractional rms deviation at any wavelength is less than 0.03.

ACKNOWLEDGMENTS

The author wishes to thank Drs. Wulf Kunkel, Forrest Boley, John Wilcox, and John Stone for their help and encouragement during the course of this work. The interest of Dr. C. M. Van Atta and Mr. William Baker, and the many helpful discussions with Dr. Alan DeSilva, Capt. George Spillman, and Mr. Peter Forman were greatly appreciated. The author is also indebted to Dr. Hans Griem for several enlightening conversations.

This work was done under the auspices of the U. S. Atomic Energy Commission.

REFERENCES

1. Lord Rayleigh, Long Duration of the Balmer Spectrum in Excited Hydrogen, Proc. Roy. Soc. (London) 183A, 26 (1944).
2. J. D. Craggs and J. M. Meek, Afterglow Effects in High-Pressure Gases, Nature 156, 21 (1945).
3. H. Zanstra, Recombination and the Long Duration of the Balmer Spectrum, Proc. Roy. Soc. (London) 186A, 236 (1946).
4. M. N. Chillié, The Hydrogen Emission in Gaseous Nebulae, Monthly Notices Roy. Astron. Soc. 92, 820 (1932).
5. J. D. Craggs and J. M. Meek, The Emission of Light from Spark Discharges, Proc. Roy. Soc. (London) 186A, 241 (1946).
6. J. D. Craggs and W. Hopwood, Ion Concentrations in Spark Channels in Hydrogen, Proc. Phys. Soc. (London) 59, 755 (1947).
7. J. D. Craggs and W. Hopwood, Electron-Ion Recombination in Hydrogen Spark Discharges, Proc. Phys. Soc. (London) 59, 771 (1947).
8. R. G. Fowler and W. R. Atkinson, Electron Recombination in Atomic Hydrogen, Phys. Rev. 113, 1268 (1959).
9. N. D'Angelo, Recombination of Ions and Electrons, Phys. Rev. 121, 505 (1961).
10. R. G. Giovanelli, Hydrogen Atmospheres in the Absence of Thermodynamic Equilibrium, Australian J. Sci. Research A1, 275, 289 (1948).
11. R. A. Smith, Note on Radiationless Transitions Involving Three-Body Collisions, Proc. Cambridge Phil. Soc. 32, 482 (1936).
12. D. R. Bates and A. E. Kingston, Recombination Through Electron-Electron Collisions, Nature 189, 652 (1961).
13. D. R. Bates and A. E. Kingston, Properties of a Decaying Plasma, Planetary and Space Sci. 11, 1 (1963).
14. R. W. P. McWhirter, Rates of Recombination in Hydrogenic Plasmas, Nature 190, 902 (1961).
15. D. R. Bates, A. E. Kingston, and R. W. P. McWhirter, Recombination Between Electrons and Atomic Ions, I. Optically Thin Plasmas, Proc. Roy. Soc. (London), 267A, 297 (1962).

16. D. R. Bates, A. E. Kingston, and R. W. P. McWhirter, Recombination between Electrons and Atomic Ions, II. Optically Thick Plasmas, Proc. Roy. Soc. (London) 270A, 155 (1962).

17. H. E. Stubbs, A. Dalgarno, D. Layser, E. N. Ashley, A. Naqvi, and G. Victor, Study of Recombination Phenomena, Vol. II, Recombination in Plasma, Air Force Special Weapons Center Technical Documentary Report No. AFSWC-TDR-62-11 (1962) (unpublished).

18. S. Byron, R. C. Stabler, and P. I. Bortz, Electron-Ion Recombination by Collisional and Radiative Processes, Phys. Rev. Letters 8, 376 (1962).

19. E. Hinnov and J. G. Hirshberg, Electron-Ion Recombination in Dense Plasmas, Phys. Rev. 125, 795 (1962).

20. G. Elwert, Über die Ionisations- und Rekombinationsprozesse in einem Plasma und die Ionisations formel der Sonnenkorona, Z. Naturforsch. 7a, 432 (1952).

21. G. Elwert, Verallgemeinerte Ionisationsformel eines Plasmas, ibid. 7a, 702 (1952).

22. G. Elwert, Die Weiche Röntgenstrahlung der ungestörten Sonnenkorona, ibid. 9a, 637 (1954).

23. E. M. Dewan, Generalization of the Saha Equation, Air Research and Development Command Report ERD-CRRD-TM-60-114 (1960) (unpublished).

24. H.-W. Drawin, Ionization and Recombination in a Hydrogen-, Helium-, and Lithium Plasma under Steady State Conditions, EUR-CEA-FC-200 (1963) (unpublished).

25. R. W. P. McWhirter, W. G. Griffin, and T. J. L. Jones, The Interpretation in Terms of Atomic Collision Processes of a Measurement of the Absolute Intensities of some of the Balmer Spectral Lines as Emitted by a Deuterium Discharge in Zeta, Proceedings of the Fourth International Conference on Ionization Phenomena in Gases (North-Holland Publishing co., Amsterdam, Holland, 1960) Vol. II, p. 833.

26. J. A. Harrison and J. D. Craggs, Excitation in a Low Pressure Electrodeless Discharge, J. Electronics and Control 4, 289 (1958).

27. J. M. Wilcox, F. I. Boley, and A. W. DeSilva, Experimental Study of Alfvén-Wave Properties, Phys. Fluids 3, 15 (1960).

28. J. M. Wilcox, A. W. DeSilvia, and W. S. Cooper III, Experiments on Alfvén-Wave Propagation, Phys. Fluids 4, 1506 (1961).

29. W. S. Cooper III, A. W. DeSilva, and J. M. Wilcox, Ion Density Measurements in a Decaying Hydrogen Plasma, Lawrence Radiation Laboratory Report UCRL-9509, March 1, 1961 (unpublished).

30. H. R. Griem, Plasma Spectroscopy, Proceedings of the Fifth International Conference on Ionization Phenomena in Gases, (North-Holland Publishing Co., Amsterdam, Holland, 1962), Vol. II, p. 1857.

31. H.-W. Drawin, Spectroscopical Measurements on Cold and Hot Plasmas, Euratom Internal Report No. 101, May, 1961 (unpublished).

32. A. N. Zaidel', G. M. Malyshev, and E. Ya. Shreider, Spectroscopic Diagnostic Techniques for Hot Plasmas, Soviet Phy.--Tech. Phys. 6, 93 (1961).

33. D. R. Bates (editor), Atomic and Molecular Processes (Academic Press, New York, 1962), Chap. 7.

34. Lyman Spitzer, Jr., Physics of Fully Ionized Gases (Second Edition, Interscience Publishers, Inc., New York, 1962), Chap. 5.

35. M. J. Seaton, Radiative Recombination of Hydrogenic Ions, Monthly Notices Roy. Astron. Soc. 119, 81 (1959).

36. A. Burgess, the Hydrogen Recombination Spectrum, Monthly Notices Roy. Astron. Soc. 118, 447 (1958).

37. The numerical results of Stubbs et al., contained in Vol. I of Ref. 17, may be more accurate, but they are calssified and were not available to the author.

38. Michał Gryziński, Classical Theory of Electronic and Ionic Inelastic Collisions, Phys. Rev. 115, 374 (1959).

39. H. R. Griem, Validity of Local Thermal Equilibrium in Plasma Spectroscopy, University of Maryland, 1963 (unpublished).

40. A. Unsöld, Physik der Sternatmosphären, (Springer-Verlag, Berlin, 1955) pp. 80-83.

41. W. Finkelnburg and H. Maecker, Elektrische Bögen und Thermischen Plasma, Handbuch der Physik (Springer-Verlag, Berlin, 1956), Vol. XXII, p. 254.

42. H. R. Griem, High-Density Corrections in Plasma Spectroscopy, Phys. Rev. 128, 997 (1962).

43. See Ref. 40, p. 169.

44. P. J. Brussaard and H. C. van de Hulst, Approximation Formulas for Nonrelativistic Bremsstrahlung and Average Gaunt Factors for a Maxwellian Electron Gas, Rev. Mod. Phys. 34, 507 (1962).

45. W. J. Karzas and R. Latter, Hydrogenic Bound-Free Gaunt Factors, Rand Corporation Research Memorandum RM-2091-AEC (15 Jan., 1958); Free-Free Gaunt Factors, Rand Corporation Research Memorandum RM-2010-AEC (Nov. 8, 1957); Astrophys. J., Supplement Series 6, 167 (1961).

46. T. Ohmura and H. Ohmura, Free-Free Absorption Coefficient of the Negative Hydrogen Ion, Astrophys. J. 131, 8 (1960).

47. S. Chandrasekhar, On the Continuous Absorption Coefficient of the Negative Hydrogen Ion IV, Astrophys. J. 128, 114 (1958).

48. J. Holtsmark, Über die Verbreiterung von Spektrallinien, Ann. Physik 58, 577 (1919).

49. M. Baranger, Problem of Overlapping Lines in the Theory of Pressure Broadening, Phys. Rev. 111, 494 (1958).

50. A. C. Kolb and H. Griem, Theory of Line Broadening in Multiplet Spectra, Phys. Rev. 111, 514 (1958).

51. H. R. Griem, A. C. Kolb, and K. Y. Shen, Stark Broadening of Hydrogen Lines in a Plasma, Phys. Rev. 116, 4 (1959).

52. H. R. Griem, A. C. Kolb, and K. Y. Shen, Stark Broadening of Hydrogen Lines in Plasma, U. S. Naval Research Laboratory Report 5455, March 4, 1960.

53. H. R. Griem, A. C. Kolb, and K. Y. Shen, Stark Profile Calculations for the H_β Line of Hydrogen, Astronphys. J. 135, 272 (1962).

54. H. R. Griem, A. C. Kolb, and K. Y. Shen, Stark Broadening of Hydrogen and Hydrogenic Neutral and Ionized Helium Lines in a Plasma, U. S. Naval Research Laboratory Report 5805, August 3, 1962.

55. W. L. Wiese, D. R. Paquette, and J. E. Solarski, Profiles of Stark-Broadened Balmer Lines in a Hydrogen Plasma, Phys. Rev. 129, 1225 (1963).

56. J. M. Wilcox, W. R. Baker, F. I. Boley, W. S. Cooper III, A. W. DeSilva, and G. R. Spillman, Devices for Generating Highly Ionized Hydrogen Plasma, J. Nuclear Eng. Part C, 4, 337 (1962).

57. A. W. DeSilva, Experimental Study of Hydromagnetic Waves in Plasma (Ph. D. Thesis), Lawrence Radiation Laboratory Report UCRL-9601, March 17, 1961 (unpublished).

58. W. B. Kunkel and R. A. Gross, Hydromagnetic Ionizing Waves, in Plasma Dynamics (Proceedings of the Sixth Lockheed Symposium on Magnetohydrodynamics) (Stanford University Press, Stanford, Calif., 1962).

59. J. M. Wilcox, W. S. Cooper III, A. W. DeSilva, G. R. Spillman, and F. I. Boley, Swirls Produced in a "Crowbarred" Rotating Plasma, J. Appl. Phys. 33, 2714 (1962).

60. J. Sharpe, Photoelectric Cells and Photomultipliers, Electronic Technology, June and July, 1961, p. 2.

61. D. F. Covell and B. A. Euler, Gain Shift vs Counting Rate in Certain Multiplier Phototubes, U. S. Naval Radiological Defense Laboratory Report TR-521, 8 June 1961 (unpublished).

62. A subsidiary experiment verified that these particular tubes were less subject to fatigue than any other tubes tested.

63. Q. A. Kerns and R. F. Tusting, Constant-Amplitude Light-Flash Generator for Gain Stabilization of Photosensitive Systems, in Proceedings of the Conference on Instrument Techniques in Nuclear Pulse Analysis, Monterey, Calif., April 29 – May 3, 1963 (to be published).

64. J. Euler, Der Graphitbogen als spektralphotometrisches Strahldichtenormal im Gebiet von 0,25 bis 1,8 μ, Ann. Phys. 11, 203 (1953).

65. J. Euler, Über den Vergleich zwischen Graphitbogen und UV-Standard, ibid. 14, 145 (1954).

66. J. Euler, Die Axiale Temperaturverteilung im Inneren der Anode des Kohlebogens und das Wärmeleitvermögen von Graphit bei hohen Temperaturen, ibid. 18, 345 (1956).

67. J. Euler, Der Grafit-Kohlebogen als Strahldichtestandard, Sitzber. Heidelberg. Akad. Wiss. Math. Naturw. Kl. Abhandl. 4, 418 (1956/57).

68. G. R. Spillman, W. S. Cooper III, and J. M. Wilcox, Nine-Channel Polychromator for Observation of Time-Dependent Spectral Line Profiles, Appl. Optics 2, 205 (1963).

69. See Ref. 34, p. 58.

70. See Ref. 34, p. 43.

71. See Ref. 34, p. 143.

72. J. M. Wilcox, A. W. DeSilva, W. S. Cooper III, and F. I. Boley, Experiments on Alfvén-Wave Propagation, in Radiation and Waves in Plasmas (Proceedings of the Fifth Lockheed Symposium on Magnetohydrodynamics) (Stanford University Press, Stanford, Calif., 1961), p. 148.

73. T. Holstein, Imprisonment of Resonance Radiation in Gases, Phys. Rev. 72, 1212 (1947); ibid. II, 83, 1159 (1951).

74. M. R. Null and W. W. Lozier, Carbon Arc as a Radiation Standard, J. Opt. Soc. Am. 52, 1156 (1962).

75. W. Finkelnburg, Höchstromkohlebögen (Springer-Verlag, Berlin, 1948), p. 95.

76. W. Göing, Bestimmung der radialen Temperaturverteilung von Hg-Höchstdruckbögen aus den Kuppenstrahldichten selbstumgekehrte Linien, Z. Phys. 131, 603 (1952).

77. H. G. MacPherson, The Carbon Arc as a Radiation Standard, in Temperature – – Its Measurement and Control in Science and Industry (Reinhold Publishing Corporation, New York, 1941), pp. 1141-1149.